Geochronological constraints on the Trans-Hudsonian tectono-metamorphic evolution of the pre-Athabasca basement within the Wollaston-Mudjatik Transition Zone, Saskatchewan

Pauline Jeanneret, Philippe Goncalves, Cyril Durand, Marc Poujol, Pierre Trap, Didier Marquer, David Quirt, Patrick Ledru

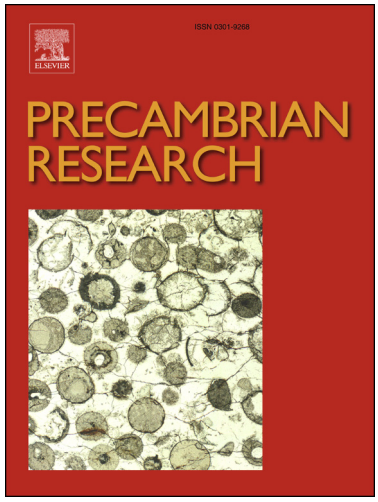

Geochronological constraints on the Trans-Hudsonian tectono-metamorphic evolution of the pre-Athabasca basement within the Wollaston-Mudjatik Transition Zone, Saskatchewan

Pauline Jeanneret, Philippe Goncalves, Cyril Durand, Marc Poujol, Pierre Trap, Didier Marquer, David Quirt, Patrick Ledru

PII: S0301-9268(17)30272-3
DOI: http://dx.doi.org/10.1016/j.precamres.2017.07.019
Reference: PRECAM 4829

To appear in: *Precambrian Research*

Received Date: 20 May 2017
Revised Date: 3 July 2017
Accepted Date: 18 July 2017

Please cite this article as: P. Jeanneret, P. Goncalves, C. Durand, M. Poujol, P. Trap, D. Marquer, D. Quirt, P. Ledru, Geochronological constraints on the Trans-Hudsonian tectono-metamorphic evolution of the pre-Athabasca basement within the Wollaston-Mudjatik Transition Zone, Saskatchewan, *Precambrian Research* (2017), doi: http://dx.doi.org/10.1016/j.precamres.2017.07.019

Geochronological constraints on the Trans-Hudsonian tectono-metamorphic evolution of the pre-Athabasca basement within the Wollaston-Mudjatik Transition Zone, Saskatchewan

Pauline Jeanneret[1-2] *, Philippe Goncalves[1], Cyril Durand[3], Marc Poujol[4], Pierre Trap[1], Didier Marquer[1], David Quirt [5]and Patrick Ledru[5].

[1] Laboratoire Chrono-environnement, UMR CNRS 6249, Université de Bourgogne-Franche-Comté, 16 route de Gray, 25000 Besançon, France.

[2] Department of Earth Sciences, Uppsala University, Villavägen 16, 752 36 Uppsala, Sweden

[3] EA 4515 Laboratoire Génie Civil et géo-Environnement, Université de Lille 1, 59655 Villeneuve d'Ascq, France

[4] Géosciences Rennes, UMR CNRS 6118, OSUR, Université de Rennes 1, 35042 Rennes Cedex, France

[5] AREVA Resources Canada Inc. 817-45th St West, Saskatoon, S7K 3X5, CANADA.

*Corresponding author: Pauline Jeanneret (pauline.jeanneret@geo.uu.se)

Highlights

- Accurate and continuous P-T-D-t path for the Wollaston-Mudjatik Transition Zone.
- The first tectono-metamorphic event (M1-D1) took place between ca.1840 and 1813 Ma
- The second tectono-metamorphic event (M2-D2) took place between ca.1813 and 1770 Ma
- Multistage genetic model for Uranium-enriched pegmatite based on this P-T-D-t evolution

Abstract

The Hudsonian Pressure-Temperature- Deformation-time- (P-T-D-t) evolution of the pre-Athabasca crystalline basement (>~1700 Ma) of the Wollaston-Mudjatik Transition Zone (WMTZ) highlights two major tectono-metamorphic events M1-D1 and M2-D2. The ages of these two event have been obtained by in-situ LA-ICPMS U-Th-Pb dating of monazite from Grt-Crd bearing pelitic gneiss and U-Pb analyses performed on zircons from pegmatites, using both exposed basement and drill cores from the Wolly–McClean exploration drilling project. The M1-D1 event, interpreted as the burial of the thinned Hearne margin via southward thrusting to pressures varying from 10 to 6 kbar, occurred between ca.1840 and 1813 Ma. The M2-D2 event, producing the northeast structural trend of the WMTZ, was formed in a sinistral transpressional tectonic regime during the late stage of the Hudsonian oblique collision between ca. 1813 and 1770 Ma. Thermobarometric estimates on the M2–D2 assemblages show that the entire studied area was reequilibrated at about 5 kbar and 750–825 °C. Trans-hudsonian pegmatites are viewed as the main proto-ore of the uranium-rich Athabasca unconformity-type deposits. Formation, transfer and differenciation of these Trans-hudsonian pegmatites are replaced in this P-T-D-t evolution. During the 1840-1813 Ma M1-D1 partial melting event, the first batches of melt produced in the deep crust are the most likely enriched in uranium. Then, these melts were transferred upwards to the upper crustal levels owing to the development of crustal scale steeply-dipping D2 shear zones, and finally were differentiated to form uranium-enriched pegmatites between 1813 and 1770 Ma. Some monazite and zircon grains within retrogressed migmatites recorded a later event at ca. 1720 Ma, interpreted as the terminal cooling event down to 300-400 °C responsible for partial retrogression of metamorphic assemblages. This age provides new insights into the timing of the onset of the Athabasca sedimentation that should therefore be at least 1710 Ma old or younger.

Keywords:

LA-ICP-MS monazite and zircon geochronology, P-T-D-t evolution, Trans-Hudson Orogen, Wollaston-Mudjatik Transition Zone, Uranium-enriched pegmatites.

1. Introduction

Although the Athabasca and Beaverlodge regions from the northern Saskatchewan in Canada are well known as uraniferous provinces and uranium has been mined there for over 65 years, the primary source of uranium in the Athabasca unconformity-type deposits is still contentious (Jefferson et al., 2007b, 2007c). Two potential sources have been suggested: 1) the uranium was primarily derived, during brine percolation, from altered detrital U-bearing accessory minerals that were present in the Athabasca sedimentary rocks themselves, such as apatite, zircon, and monazite (Fayek and Kyser, 1997; Hoeve and Sibbald, 1978; Kotzer and Kyser, 1995; among others) ; 2) the primary source of uranium was primarily derived from the underlying sub-Athabasca igneous and metamorphic basement, including Hudsonian (ca. 1850–1700 Ma) granites and granitic pegmatites, through destabilization of uraninite (Mercadier et al., 2013) and/or U-bearing accessory minerals (e.g., monazite or zircon; Hecht and Cuney, 2000). Monazite and zircon grains show some evidence of significant alteration by percolating basinal brines around U deposits and there are numerous occurrences in the eastern Athabasca region of uranium-enriched Hudsonian granites and granitic pegmatites (ca. 1810–1760 Ma), that contain up to 130 ppm U (Beck, 1969; Harper, 1987; Madore et al., 2000; Ray, 1975; Thomas, 1978, 1979, 1980), in particular near the southeastern margin of the Athabasca Basin. Uranium-enriched pegmatites are present in the vicinity of many unconformity-related uranium deposits, such as Moore Lakes (Annesley et al., 2000), McLean Lake, and P-Patch (Key Lake area: Madore et al., 2000). The Karin Lake-Foster Lake-Kulyk Lake and Fraser-Lakes areas contain uraninite and monazite mineralization in pegmatites and may have similar analogues in the western Wollaston Domain and the Wollaston-Mudjatik Transition Zone basement rocks present below the eastern Athabasca Basin (Fig.1).

Because of these examples, exploration and research activities have been carried out on these pegmatites and leucogranites as a potential source of uranium for the Athabasca unconformity-type deposits, although the debate continues over the method by which U was transferred from the basement rocks to the deposit sites (Alexandre et al., 2005; Annesley and Madore, 1999; Annesley et al., 2000; Boiron et al., 2010; Cloutier et al., 2009; Cuney, 2009; Hecht and Cuney, 2000; Jefferson et

al., 2007a; Madore et al., 2000; ; McKechnie et al., 2012a, 2012b, 2013; McKeough and Lentz, 2011; McKeough et al., 2010, 2013; Mercadier et al., 2010, 2013; Quirt, 1997; and Richard et al., 2010).

Two types of mineralization in granite/pegmatite have been identified and documented (McFarlane and McKeough, 2013; McKeough et al., 2010; Mercadier et al., 2013): magmatic uraninite in granitic pegmatites and leucogranites, and higher-grade micrometric to pluricentimetric high-temperature uraninite in veins. The most common are the uranium oxide-bearing granitic rocks formed by partial melting of mostly Wollaston Group metasedimentary rocks during the peak thermal event of the Trans-Hudson Orogen (THO; Mercadier et al., 2013). The origin of the vein-type uranium remains unclear, but their high thorium and rare earth element (REE) contents suggest a high-temperature process associated with Ca and/or Na metasomatism (Annesley et al., 2010; Mercadier et al., 2011a, 2013; Rand et al., 2009; Thomas, 1980). Within the granitic pegmatite type occurrences, McKechnie et al. (2012a, 2013) highlighted two groups of radioactive granitic pegmatites present in the Fraser Lakes area (Fig.1): uranium-and thorium-enriched pegmatites (Group-A), and thorium- and LREE-enriched and U-depleted pegmatites (Group-B). Group A intrusions are interpreted to have crystallized in their present position between 1850 and 1800 Ma (McKechnie et al., 2012a). Reliable primary magmatic ages for Group B intrusions have not been obtained yet but based on the similarities of their intrusive contacts, these rocks were probably intruded at roughly the same time as Group A rocks (McKechnie et al., 2013).

Deciphering the origin of the pegmatites, their age(s), and their link(s) to the Trans-Hudsonian tectonic and metamorphic evolution is therefore critical in order to understand the mechanisms that led to the orogenic redistribution of uranium and the formation of uranium-enriched pegmatites in the middle crust during the THO.

While there is a wealth of geochronological data in the studied area, most of the data regarding the Trans-Hudsonian tectono-metamorphic evolution of the WMTZ comes from intrusive granites and pegmatites and the timing of the deformation and metamorphic phases remain indirectly constrained. Although these data are valuable, they are insufficient to determine accurately the age of the two tectono-metamorphic events M1-D1 and M2-D2 defined by Jeanneret et al. (2016).

The M1-D1 event, is interpreted as the burial of the thinned Hearne margin via southward thrusting to pressures varying from 10 to 6 kbar. The M2-D2 event, producing the northeast structural trend of the WMTZ, was formed in a sinistral transpressional tectonic regime, at about 5 kbar and 750–825 °C, during the late stage of the Hudsonian oblique collision.

These age constraints will shed some light on the geodynamic setting of the WMTZ prior to the deposition of the Athabasca Basin and subsequent formation of the high-grade unconformity-type uranium deposits. Indeed, This manuscript provided a accurate chronology of the Pressure-Temperature-Deformation evolution established in Jeanneret et al. (2016). Time is the key parameter that is determined by in-situ LA-ICP-MS monazite dating performed in-context (polished thin-sections) on garnet-cordierite-bearing metapelitic paragneisses that have been used by Jeanneret et al. (2016) to constrain the tectono-metamorphic evolution of the studied areas. LA-ICP-MS geochronological analyses on zircon separated from pegmatites sampled from well-constrained structural settings were also used to enhance the data set. The choice of samples to date is based on the field relationships, tectonic setting, and their petrological characteristics. The main outcome of this multidisciplinary approach, was establishing a P-T-D-t path that provides a full understanding of the WMTZ tectono-metamorphic evolutionary history during which the behaviour of uranium-bearing mineral phases are changing in time. This work represents a valuable and important contribution to both our knowledge and our understanding of unconformity-type uranium deposits in northern Saskatchewan and worldwide

2. Geological setting

2.1 The Trans-Hudson Orogen in central Canada

Along the northern boundary of the Archean Superior Province, the THO is a major Paleoproterozoic orogenic belt that extends southwestward from Greenland to the Baffin Island through central Canada (Nunavut, Manitoba and Saskatchewan), to the northcentral United States (Hoffman, 1990). In this section, only the western part of the THO located in central Canada is discussed (Fig.1). The

beginning of the Trans-Hudson orogeny at ca. 1920–1890 Ma), was characterized by a phase of amalgamation of the Hearne and Rae cratons, also referred to as the composite Western Churchill Province, concurrent with oceanic arc formation within the Manikewan Ocean (Ansdell, 2005; Corrigan, 2012; Corrigan et al., 2005, 2009). The next major phase involved accretion of juvenile crust associated with the closure of the Manikewan Ocean (Corrigan et al., 2009): (i) accretion of the La Ronge–Lynn Lake arcs to the southeastern Hearne Craton margin between ca. 1880-1865Ma (Bickford et al., 1990, 1994; Corrigan et al., 2005), (ii) voluminous magmatic accretion along the southeastern margin of the western Churchill Province related to the ca. 1865–1845 Ma Wathaman Orogeny (Corrigan et al., 2005; Thériault et al., 2001), and (iii) micro-continent accretion at ca. 1840-1830 Ma, as the Sask Craton collided with the Flin Flon–Glennie Complex (Ashton et al., 2005). The final stage of the THO corresponds to the final closure of the Manikewan ocean and the continental collision between the Hearne margin with the accreted juvenile arc complex and the northern Superior craton margin, between 1830 and 1800 Ma (Corrigan et al., 2009). This final stage was followed by a late-collisional event from 1800 to1760 Ma, which is characterized by strike-slip deformation and emplacement of undeformed pegmatites and aplites (Bickford et al., 2005; Culshaw and Clarke, 2009; Schneider et al., 2007).

The THO includes two major domains, the Reindeer Zone and the Hearne Province from south/south-east to north/north-west (also referred to as the Cree Lake Zone in Corrigan et al., 2005). The Reindeer Zone, formed during the closure of the Manikewan Ocean (Lewry and Collerson, 1990), consists of three major belts that were accreted on the Hearne margin between 1920 and 1850 Ma: the Flin Flon - Glennie Complex, the La Ronge - Lynn Lake Arcs, and the Rottenstone Domain (Fig.1). Although each domain has individual lithology groups and different tectono-metamorphic evolutions, they share similar features. The next major accretionary event in the Reindeer Zone consisted in the arrival of the Sask Craton and amalgamation of the latter with the Flin-Flon-Glennie complex via a south-vergent thrust system, at ca. 1840 Ma (Ashton et al., 2005). The buried Sask Craton has been imaged seismically (Hajnal et al., 2005) and can be observed within three small windows in the Glennie Domain. The Reindeer Zone and the Archean Hearne craton margin are separated by the Wathaman Batholith, a major continental-arc complex (Fumerton et al., 1984) that was emplaced between 1860-

1850 Ma, and intruded the Archean rocks of the northwestern Hearne margin (Peter Lake Domain) and the southeastern previously-accreted Paleoproterozoic Reindeer Zone (La Ronge domain) (Corrigan et al., 2005; Kyser and Stauffer, 1995; Lewry et al., 1994).

2.2 Wollaston Domain, Mudjatik Domain and the WMTZ

The crystalline basement adjacent to, and underlying, the eastern part of the Athabasca Basin in northern Saskatchewan consists of complexly deformed and strongly metamorphosed igneous and supracrustal rocks (Fig. 2). These crystalline basement rocks are unconformably overlain by the undeformed lower Paleoproterozoic to Mesoproterozoic Athabasca Group that consists mainly of sandstone with minor siltstone and conglomerate. The rocks at the vicinity of the sub-Athabasca unconformity, both sandstone and basement, host numerous high-grade unconformity-type uranium deposits. These deposits are related to sandstone-basement fluid interactions that were constrained broadly by structural corridors containing brittle reactivated faults and Wollaston Group graphitic pelitic gneiss (Hoeve et al., 1980; Hoeve and Quirt, 1984; Jefferson et al., 2007a; Quirt, 2003; among numerous others). The Wollaston and Mudjatik domains belong to the Hearne Province which consists of Archean rocks and their Paleoproterozoic passive margin sediments that have been reworked during the collision stage of the THO. The Wollaston Domain corresponds to a northeast-trending fold and thrust belt where supracrustal Paleoproterozoic sediments are dominant, whereas the Mudjatik Domain is a northeast-trending, shear-bounded belt in which Archean basement is dominant (Annesley et al., 1997a) (Fig. 2). Both domains, separated by the north-east-trending Wollaston Mudjatik Transition Zone (WMTZ) (Fig.2), were subjected to a complex polyphased deformation and metamorphism accompanied by metaluminous to peraluminous magmatism during the ca. 1800 Ma continent–continent collision of the THO (Annesley et al., 1997a, 1997b, 1999, 2005; Jeanneret et al., 2016; Lewry and Sibbald, 1977, 1980; Madore and Annesley, 1993; Madore et al., 1999a, 1999b; Orrell et al., 1999).

2.2.1 Lithological units

The Archean basement is best exposed in the Mudjatik Domain (MD) and within structural domes in the Wollaston Domain (WD) and consists of 2730 to 2700 Ma felsic to tonalitic gneisses (Annesley et al., 1997b; Harper and Van Breemen, 2004) intruded by 2640 -2580 Ma old Neoarchean granites (Annesley et al., 1997b, 1999b; Ansdell et al., 2000; Hamilton and Delaney, 2000; Harper et al., 2006; Rayner et al., 2005).

The Paleoproterozoic supracrustal Wollaston Group, overlying the Archean basement, can be divided into three main sequences: the Lower, Middle, and Upper (Annesley et al., 2005; Harper et al., 2005a, 2006; Lewry and Sibbald, 1977; Sibbald, 1983; Tran 2001; Yeo and Delaney, 2007). In the portion of the WMTZ that is discussed in this contribution, only the Lower and Middle sequences are exposed. These sequences of the Wollaston Group were deposited between 2100 and ca. 1850 Ma (Tran et al., 2008). The Lower sequence consists of a Quartzite-Amphibolite succession (QA) and rare "banded iron formation" (Harper et al., 2005a). In the Middle sequence, two main lithological units have been distinguished: 1) a basal unit that consists of quartzo-feldspathic psammitic to pelitic gneisses, representing 70-80% of the metasedimentary rocks occurring in the WD (Annesley et al., 2005), with garnet, cordierite, sillimanite, Ti-rich biotite, Ti-rich tourmaline, and local enrichments in graphite; and 2) calc-pelitic to calc-silicate rocks, with respect to the gneisses description.

2.2.2 Metamorphism and deformation

The Paleoproterozoic tectono-metamorphic evolution of the pre-Athabasca basement within the Wollaston-Mudjatik Transition Zone has recently been revisited by Jeanneret et al. (2016). The finite ductile strain pattern results from the superimposition of two distinct tectono-metamorphic events M1-D1 and M2-D2 (Fig. 2). M1-D1 is associated with the development of a gently dipping foliation striking N090°-100° and to a northeastward increase of peak pressures from 6 kbar in the Wolly-McClean exploration drilling project area to 10 kbar in the Cochrane River area (Fig.2). This north-eastward increase in peak pressure, trending perpendicular to the S1 foliation, is consistent with the observation of kyanite in the Charcoal Lake area (north-east of Cochrane River; Fig.2; Card et al., 2006a, 2006b, 2006c), that could require pressures higher than 10 kbar at 800° C.

Jeanneret et al. (2016) suggested that the M1 regional metamorphic event was related to the burial of the supracrustal Wollaston Group rocks toward a maximum depth of ~35 km and 750-825° C through nappe stacking and under-thrusting during a north-south convergence of the Superior Province and the western Churchill Craton. During the early collision stage of the Trans-Hudson Orogen, this tectono-metamorphic event generated a thrust stacking wedge in which Mudjatik Domain Archean gneisses structurally alternate with Paleoproterozoic Wollaston Group metasediments. The second regional tectono-metamorphic event M2-D2 was responsible for the exhumation of M1 rocks during an isothermal decompression event, which led to the formation of cordierite-bearing M2 assemblages at 4.5-5.5 kbar and 750-825° C (Fig. 2). This metamorphic event was coeval with the folding of the S1 foliation by F2 up-right folds, the development of steeply-dipping N40° S2 foliation axial plane of the F2 folds and the formation of sinistral shear zones (Fig.2). All of these structures formed progressively in the same sinistral transpressional tectonic regime with NE–SW-directed strike-slip shearing during a bulk north – south horizontal shortening (Jeanneret et al., 2016). The M2-D2 event is interpreted as the result of the transition from a continental collision to oblique collision of the Superior Province and Sask Craton with the Churchill Craton during the final collision of the Trans-Hudson Orogeny.

3. Geochronological investigations of the WMTZ: state of the art

U–Pb dating studies on zircon, monazite, titanite, and xenotime from this region have been carried out on a large variety of lithologies: (*i*) Archean basement rocks (tonalitic–trondhjemitic gneisses, migmatitic tonalitic gneisses and granitic– granodioritic gneisses) *(ii)* Wollaston Group rocks (migmatitic garnet-cordierite-pelitic gneisses, quartzite and granodioritic gneisses), (*iii*) Trans-Hudsonian intrusive peraluminous leucogranites and pegmatites (including grey granite suite), and (iv) tholeiitic to calc-alkaline granitoids and associated gabbroids (including Sandy Islands Gabbro Complex - SIGC) . A synthesis of these geochronological results is represented in Figure 3. Previously published U–Pb zircon analyses of the granitic and tonalitic basement gneisses from the Mudjatik Domain and within structural domes in the Wollaston Domain have yielded ages ranging

from ca. 2726 to 2706 Ma (Annesley et al., 1997b; Harper and Van Breemen, 2004) and may locally be as old as 2780 Ma (Annesley et al., 1999b). A single Rb-Sr age of ca. 2600 Ma was obtained from granitic gneiss of the Shaganappie Island inlier (Chandler, 1978) which is comparable to the *ca*. 2640 to 2580 Ma granitic rocks from the eastern Wollaston Domain (Annesley et al. 1997b, 1999b; Ansdell et al., 2000; Hamilton and Delaney, 2000; Harper et al. 2006; Rayner et al. 2005). In the Wollaston Lake area, Archean source rocks are also well represented in the detrital zircon populations in a number of the Wollaston Group metasedimentary lithologies.

The timing of regional metamorphic events associated with the Paleoproterozoic THO crustal thickening has been constrained by U-Pb dating on zircon, monazite, and titanite, mostly obtained from granites and pegmatites (Ansdell and Norman, 1995; Gordon et al., 1990; Machado et al., 1999; Norman et al., 1995; Schneider et al., 2007; plus numerous data in Saskatchewan and Manitoba provincial reports and Geological Survey of Canada reports). A large number of intrusive rocks have been dated, yielding zircon U-Pb ages ranging from 1840 to 1795 Ma (Annesley et al., 1992, 1997b), which corresponds to the main period of Hudson granite emplacement throughout the Western Churchill Province (Peterson et al., 2000, 2002; Van Breemen et al., 2005). Magmatic zircon and monazite ages show several episodes of magma generation, one at ca. 1835 Ma and the other at ca.1815 Ma. The oldest leucogranites and granitic pegmatites belong to the grey granite suite dated at ca. 1840-1835 Ma (Annesley et al.,1997b, 2005). This magmatic event was followed by the emplacement of gabbro (Sandy Islands Gabbro Complex) and basic dykes at ca. 1830- 1820 Ma (Annesley et al., 1995a; Annesley et al.,1997b), the emplacement of porphyritic calc-alkaline granites between 1824-1812 Ma, and the emplacement of more common and younger peraluminous leucogranites and associated granitic pegmatite at ca. 1820–1800 Ma (Annesley et al., 1997c). Metamorphic accessory minerals (monazite and titanite) from intrusive rocks yield U-Pb ages ranging from 1810 to 1770 Ma. The oldest ages at ca. 1810 Ma are consistent with the U-Pb ages for granite emplacement and peak metamorphism, while the younger ages at ca 1770 Ma have been interpreted as late orogenic cooling ages (Annesley et al., 1992, 1997; Annesley and Madore, 1994; Chakungal et al., 2004; McKeough et al., 2013; Schneider et al., 2007) or as the age of a late Hudsonian thermotectonic event of wide regional significance (Fig. 3; Annesley et al., 1992, 1997; Annesley and Madore, 1994).

However, a late Hudsonian thermotectonic event is favoured because the ca. 1770 Ma age is comparable with ages obtained from the THO-related Kivalliq Igneous Suite (Peterson et al., 2015; eg. Nueltin granite; Pitz Formation volcanics) occuring in Nunavut ~200 km to the northeast of the studied area. This significant thermal event is also recorded and well constrained by the ca. 1780-1760 Ma ages of undeformed pegmatitic bodies that intrude the migmatitic tonalitic gneisses and garnet-cordierite-pelitic gneisses (Annesley et al., 1997c; Bickford et al., 2005; Chiarenzelli, 1989; Chiarenzelli et al., 1998).

Some of the granitic pegmatites and leucogranites are uranium-enriched, such as those at Fraser Lakes that contain either Th-rich magmatic uraninite or low-Th uraninite in veins (Mercadier et al., 2013). U-Pb isotope ages, obtained on the vein type uranium mineralization, range from 1805 to 1774 Ma, suggesting that the primary mineralization event was at 1805 Ma, followed by a high-temperature dissolution/precipitation event at 1774 Ma (Mercadier et al., 2013). A relatively young date (1713 Ma) was also obtained on magmatic uraninite, although Mercadier et al. (2013) interprets this date to a late isotopic resetting. These ages are consistent with the 1807 Ma monazite ages reported for similar uranium-enriched granitic pegmatitic material at Karin Lake (Fig.1) (McKeough and Lentz, 2011).

Two pegmatite subtypes have been distinguished within the uranium-enriched Fraser Lakes granitic pegmatites (McKechnie et al., 2013): uranium-and thorium-enriched (Group A), and thorium- and LREE-enriched and U-depleted (Group B). Group A pegmatites are interpreted to represent an early melt phase (Mercadier et al., 2013). Electron microprobe U-Th-Pb chemical ages obtained on uraninite from the Group A pegmatites range between 1850 and 1800 Ma (McKechnie et al., 2012a); comparable to the U–Pb zircon and monazite ages (1820–1760 Ma) determined for the main pulse of leucogranites and pegmatites within the Wollaston Domain (Annesley et al., 2005), and to the 1805-1774 Ma age range obtained by Mercadier et al. (2013). Although electron microprobe U–Th–Pb chemical age dating of monazite from the (Group-B) pegmatites yielded cryptic older ages of 2200-2100 Ma, McKechnie et al. (2012a), based on the similarities of their intrusive contacts, suggested that these rocks were intruded at roughly the same time as Group A rocks. In the basement exposed to the south-east of the Athabasca Basin, McFarlane and McKeough (2013) have also dated uranium-enriched pegmatites by LA-ICP-MS U–Pb dating of monazite. These monazites grain yielded an age

of 1830 ± 5 Ma from Kulyk Lake and an age of 1774 ± 3 Ma from Yellow Lake (McKeough et al., 2013).

The Wollaston Group, mostly formed by anatectic garnet- and cordierite-bearing pelitic to psammopelitic gneisses, has yielded monazite ages ranging from 1820 to 1800 Ma and younger titanite ages at ca. 1780 Ma (Annesley et al., 1992, 1997; Schneider et al., 2007). These ages are consistent with those classically interpreted as the Trans-Hudson peak metamorphism. However, Schneider et al. (2007) demonstrated that total-Pb EMPA analyses of monazite grains from this pelitic material have a more complex history with at least two intra-crystalline age domains at ca. 1760 Ma and and ca. 1725 Ma. Moreover, a Hearne Province augen gneiss (Birch Lake area) dated by Orrell et al. (1999) at ca. 2600 Ma by U–Pb on zircon, also produced an age of ca. 1769 Ma by U-Pb ID-TIMS analyses on titanite consistent with the ca. 1760 Ma EMP ages (Schneider et al., 2007). The waning stage of the Trans-Hudson Orogeny was represented by the exhumation and post-peak metamorphism cooling at ca. 1730 Ma (Alexander et al., 2009; Durocher et al., 2001; Schneider et al., 2007), as suggested by $^{40}Ar/^{39}Ar$ ages of 1735 to 1720 Ma obtained on mica and amphibole by Kyser et al. (2000). The formation of the Athabasca Basin, which was initiated by the development of a series of fault-bounded precursor basins across parts of the Hearne Province also around 1730 Ma (Evans and Bingham, 1973), was followed by the deposition of the Athabasca Group sediments, perhaps around 1720 Ma (Cumming et al., 1987; Cumming and Krstic, 1992; Rayner et al., 2003). However, a younger biotite Rb-Sr age of 1711 ± 8 Ma (Worden et al., 1985) appears to represent a retrogression phase of the THO. Schneider et al. (2007) also obtained younger (1740-1720 Ma) $^{40}Ar/^{39}Ar$ biotite ages from the Southern part of the Wollaston Domain. These geochronological data document a younger and lower temperature (~350°C) event, or simply prolonged cooling from the previous high-temperature metamorphic event. However, through $^{40}Ar/^{39}Ar$ dating of muscovite from unaltered host rocks of the basement hosted deposits at McArthur River and Dawn Lake, Alexander et al. (2009) also obtained an $^{40}Ar/^{39}Ar$ age of 1731± 18 Ma (weighted mean). This age is important as it suggests that there was a regional thermal event in the crystalline basement at around 1730-1710 Ma. Given that previous geochronological interpretations have suggested that the Athabasca sedimentation had started

by this time, these age data rather indicate that the onset of sediment deposition should occurred ca. 1710 Ma or later.

The oldest ages of the various Athabasca Group formations are only weakly constrained by a few dates. Diagenetic apatite cement from the Fair Point Formation provides poorly-constrained U-Pb dates in the range 1700-1650 Ma (Cumming et al., 1987). Zircons in tuffaceous layers in the Wolverine Point Formation indicate deposition at 1644 ± 13 Ma (U-Pb SHRIMP; Rainbird et al., 2007), consistent with ages of 1640-1620 Ma for associated fluorapatite cement in the tuffaceous material (Rainbird et al., 2003b). The depositional age of the Douglas Formation, higher in the stratigraphic column, is 1541 ± 13 Ma through Re-Os pyrite dating (Creaser and Stasiuk, 2007).

Diagenetic events that occurred within the Athabasca Basin are marked by dates obtained on various materials, such as apatite and illite. The 1640-1620 Ma apatite ages obtained by Rainbird et al (2003b) and the 1675-1620 Ma ages from $^{40}Ar/^{39}Ar$ dating of illite and chlorite (Alexander et al., 2003, 2009) are suggestive of a regional hydrothermal event at that time that may be related to the 1644 Ma depositional age of the Wolverine Point Formation.

Geochronological investigations on the unconformity-type deposits have been carried out since the 1970s using various techniques (Alexandre et al., 2009; Cumming and Krstic, 1992; Hoeve and Quirt, 1984; among numerous summaries). Recent works using ion probe (SIMS) U-Pb dating of uraninite yields upper intercept ages of 1519 ± 22 Ma for the sandstone-hosted deposit at McArthur River and 1467 ± 47 Ma for the sandstone-hosted deposit at Cigar Lake (Fayek et al., 2002a, 2002b), These ages are consistent with previous ID-TIMS U-Pb upper intercept ages of 1521 ± 8 Ma of (McGill et al., 1993) and LA-ICP-MS U-Pb dating of uraninite from McArthur River that yielded a similar maximum age of 1540 ± 19 Ma (Alexandre et al., 2009). McGill et al. (1993) also report a younger age for McArthur River at 1348 ± 16, interpreted as the age of a remobilization event.

The latest intrusive activity in the Athabasca region is characterized by the emplacement of mafic dykes that cross-cut the Athabasca Group sediments. The Mackenzie diabase dyke swarm comprises a series of northwest-trending diabase dykes (Fahrig and West, 1986; Hulbert et al., 1993; Quirt, 1993) that have a U-Pb age of 1267 ± 2 Ma (LeCheminant and Heaman, 1989). The Moore Lakes Complex,

located in the southeast corner of the Athabasca Basin, consists of several gabbro/diabase sills dated at 1108.8 ± 2.4 Ma (U-Pb baddeleyite; Macdougall and Heaman, 2002).

4. Sampling and Methodology

Five samples of garnet-cordierite-bearing pelitic gneiss and three samples of pegmatite were selected from two outcrops within the WMTZ (Wollaston Lake and Cochrane River) and from three drill cores (Wolly-McClean exploration project area; see Fig.2 and Table 1 for location). Monazite grains from the five pelitic gneiss samples (13W022C, 12W008, TC34, LS70, MC15A) were selected, examined in context in polished thin-sections, and analyzed using in-situ isotopic analysis by LA-ICP-MS. Prior to the analysis, the presence and location of the monazite grains was determined using a scanning electron microscope (SEM) to highlight their distribution at the thin-section scale and their settings with respect to the structural fabrics defined by Jeanneret et al. (2016). Each of the monazite grain was then characterized in terms of petrography (matrix grain or inclusion, presence/absence of inclusions, overgrowths) and chemical zonings. This textural information is critical for an accurate interpretation of the in-situ LA-ICP-MS dates (e.g. Dumond et al., 2015; Goncalves et al., 2004; Williams et al., 2006). Electron microprobe (EMP) X-ray compositional maps of yttrium, thorium, uranium, and calcium, were obtained on selected grains to identify and characterize the internal zonation patterns in each grain.

Zircon grains were separated from the three pegmatitic samples from the Wollaston Lake (12W002a, 12W002b) and the Cochrane River (13W042) areas. As the goal of this contribution is to better constrain the age of metamorphism and deformation in the WMTZ, the selection of these pegmatite samples was guided by their relationship with the deformed host gneisses. Mineral separation was done by conventional techniques, including crushing, sieving, and magnetic and heavy-liquid methods. Zircon crystals were randomly handpicked from heavy mineral concentrations, regardless of their size, clarity, color, or morphology, with the goal of producing a final age distribution that accurately reflects the true distribution of zircon ages in each sample. Selected grains were mounted in epoxy resin and polished. Before analysis, the polished mounts were photographed and imaged by

SEM, using the MIMENTO platform in Besançon or at the University of Lille 1, France. Back-scattered electron (BSE) images were used to visualize the internal structure of the zircon grains. Points for isotopic analysis were selected on several zircon grains to include all the texturally distinct domains identified in the BSE imaging.

U-Th/Pb geochronology of monazite and zircon was conducted using Laser Ablation - Inductively Coupled Plasma Mass Spectrometry (LA-ICP-MS) at Géosciences Rennes, France, using an ESI NWR193UC Excimer laser coupled to an Agilent 7700x quadripole ICP-MS. Detailed operating and instrumental conditions can be found in Ballouard et al. (2015) and in supplementary Table S1. Ablation spot diameters of 10 µm and 25 µm, with repetition rates of 3 Hz and 4 Hz, were used for monazite and zircon, respectively. Data were corrected for U-Pb and Th-Pb fractionation and for the mass bias by standard bracketing with repeated measurements of the GJ-1 zircon (Jackson et al., 2004) or the Moacyr monazite standards (Gasquet et al., 2010). Repeated analyses of the Plešovice zircon (Sláma et al., 2008) or the Manangoutry monazite (Paquette and Tiepolo, 2007) standards, treated as unknowns, were used to control the reproducibility and accuracy of the data corrections (supplementary Table S1).. Data reduction was carried out with the GLITTER software package developed by Macquarie Research Ltd. (Van Achterbergh et al., 2001). Concordia ages and diagrams were generated using Isoplot (Ludwig, 2008). All errors given in Table 2 and Table 3 are listed at one sigma, but where data are combined for regression analysis or to calculate weighted means, ages are quoted at 2sigma absolute.

5. Results

5.1 Petrography and structural setting of the garnet-cordierite-bearing pelitic gneiss samples

5.1.1 Sample 13W022C

This sample is a garnet-cordierite-bearing pelitic gneiss taken from the south shore of the Cochrane River. Structurally, this sample belongs to one of the D2 high strain zone (Fig.2) with a peak

metamorphic assemblage M1, at 8.5 to 11 kbar and 775-825°C, defined by Jeanneret et al. (2016). This M1 assemblage consists of garnet porphyroblasts, sillimanite, biotite and quartz. Cordierite is a M2-D2 retrograde phase that developed at 5 to 6.5 kbar and 815-825°C that forms either coronas developed at the expense of M1-D1 garnet or large porphyroblasts containing sillimanite needles, ilmenite, and spinel inclusions that are elongated parallel to the S2 foliation (Jeanneret et al., 2016). Hercynite ± corundum is also present within the S2 foliation and is locally, in quartz-undersaturated domains, contemporaneous with cordierite.

Monazite grains in this sample can occur as minute inclusions in M1 garnet porphyroblasts (Fig.4). The monazite inclusions in garnet are small (<40 µm), rounded to sub-rounded and weakly zoned (Fig.5). Monazite grains armored by garnet are of a particular importance, as garnet tends to shield the monazite from interaction with fluid and potential recrystallization (Braun et al., 1998; Foster et al., 2000; Kydonakis et al., 2016; Montel et al., 2000; Simpson et al., 2000; Stern and Berman, 2000; Terry et al., 2000).

5.1.2 Sample 12W008

This sample is a garnet-cordierite-bearing pelitic gneiss from the western part of Wollaston Lake (Fig.2, Fig.6). This sample belongs to the main D2 high strain zone (Fig. 2). Garnet occurs as centimeter- to millimeter-size peritectic porphyroclasts that are interpreted to be part of the M1 peak metamorphic assemblage estimated at 7 to 8.5 kbar and 750-800°C (Jeanneret et al. 2016; Fig.2, Fig.6). Garnet contains inclusions of biotite, feldspar, and ilmenite, and a S2 foliation defined by the preferred orientation of biotite and sillimanite that wrap around the M1 garnet porphyroclasts (Fig.7). M2 retrograde cordierite is mostly present within the pressure shadows of M1 peritectic garnets and was formed at about 5 kbar and 750-800°C (Jeanneret et al., 2016; Fig.2). This pelitic gneiss contains abundant euhedral monazite crystals that range in size from 50 to 150 µm (Fig.7). They are located and aligned within the biotite-sillimanite S2 foliation (Fig.7A). Some elongated grains also contain micron-scale euhedral sillimanite inclusions that are also aligned with the S2 foliation (monazite 8 and 1, Fig.7A, B and C) suggesting that their crystallization was coeval with the development of the M2-D2 assemblage.

5.1.3 Sample TC34

This garnet-cordierite-bearing paragneiss is a drill core sample (Fig.6B) from the northern part of Wolly-McClean exploration project area, situated on the west side of the WMTZ. It belongs to the westernmost D2 high strain zone of the studied region (Fig.2). This rock contains porphyroblasts of garnet, cordierite and feldspar, with biotite-sillimanite-rich layers and accessory phases (ilmenite and pyrite), that are interpreted as a M1 assemblage (Fig.7D). From this sample, the M1-D1 conditions have been estimated at 6 to 7 kbar and a temperature of 750-800°C (Jeanneret et al., 2016). Garnet and cordierite in this sample are in equilibrium, without any evidence for retrogression. The sample is characterized by the presence of a millimeter-scale D2 high strain zone that is significantly enriched in sillimanite and depleted in garnet with respect to D2 low strain domains (Fig.7D). It contains abundant rounded to sub-rounded monazite grains that range in size from 80 to 160 µm (Fig.7D, E and F). In the D2 high strain zones, monazite grains are either absent or almost completely dissolved (Monazite 31 – Fig.7D and E), while in the host-rock that has undergone a lower strain, monazite crystals are still preserved (Monazite 28 - Fig.7D and F, Fig.8A). Monazite grains are weakly zoned and some them exhibit core-rim zonation, with a low-Y contents core surrounded by high-Y contents rims (Fig.8A). Grains that do not exhibit any zonation have Y contents that are consistent with those of the monazite rims. All the analyzed monazite grains were taken from the lower-strain regions.

.1.4 Sample LS70

This drill core sample also comes from the same westernmost D2 high strain (Fig.2). LS70 share the same petrological and structural features of sample TC34 (Fig.6C): a M1 peak metamorphic assemblage estimated at 5.5kbar and 850°C that consists of garnet, cordierite, biotite, sillimanite, and melt, and a D2 high strain zone enriched in sillimanite (Fig.9A; Jeanneret et al., 2016). As for TC34, in the centimeter-scale D2 high strain zone, monazite crystals are almost absent or smaller than 70 µm in length (Monazite 2 - Fig.9A and B), whereas the very low strain zone contains abundant monazite rounded to sub-rounded grains that range in size from 80 to 180 µm (Monazite 42 - Fig.9A and C). Some of these grains also exhibit core-rim zonation with a Y-poor core surrounded by Y-rich rims (Fig.8B).

5.1.5 Sample MC15A

This psammopelitic gneiss drill core sample was taken from the southern part of the Wolly-McClean exploration project area (Fig.2), within the main D2 high strain zone defined by Jeanneret et al. (2016), where several uranium deposits have been mined. Although this sample is strongly retrogressed to cordierite and phyllosilicates, a former M1 peak metamorphic assemblage is inferred and consists of garnet-biotite-sillimanite-graphite and melt. The M2 retrogression is characterized by the complete breakdown of garnet into cordierite, which is itself altered into a fine-grained assemblage of phyllosilicates (Fig.9D). The retrogression is also associated with an intense chloritization of biotite and the crystallization of abundant sulfide minerals (chalcopyrite and pyrite). Monazite grains are abundant in this sample and range in size from 80 to 200 μm (Fig.9D). They occur either as anhedral grains (Monazite 2 - Fig.9D and E) or as euhedral grains (Monazite 7 - Fig.9Dand F) in the retrogressed matrix. Euhedral grains are zoned with Y-rich cores surrounded by Y-poor rims (Monazite 8, Fig.8C) and are aligned with the S2 foliation defined by biotite/chlorite. Anhedral grains (Monazite 2, Fig.9D and E) are located in the biotite, chlorite, and graphite domains. Monazite grains embedded in chloritized biotite, contain inclusions of chlorite. Some monazite grains are surrounded by late pyrite, chalcopyrite, apatite, and anatase, and have fractures filled with chalcopyrite. All these micro-textural observations suggest that monazite was recrystallized contemporaneously with the late retrogression that is characterized by the formation of chlorite and sulfide minerals.

5.2 Petrography and structural setting of the pegmatitic samples

5.2.1 Sample 13W042

This sample is a pink pegmatite taken from an outcrop on the north shore of the Cochrane River (Fig.2). Structurally, this pink pegmatite is a vertical dike trending NE that intrudes tonalitic gneiss of the Archean basement (Fig.6D). It is located along the axial plane of an upright F2 fold and is therefore interpreted to be coeval with the D2 event. The sample consists of quartz, K- feldspar, plagioclase, and biotite, with subordinate apatite and zircon (Fig.10A and B). Zircon grains are subhedral to euhedral, elongated and are 250 to 350 μm in length (Fig.11A). BSE images reveal core-rim zonation (Fig.11A– Zr19 and Zr23), with the cores being rich in minute inclusions of monazite.

Cores show either an oscillatory magmatic zoning or patchy zonations that are always associated with the monazite inclusions. The rims appear to be homogeneous and contain abundant radial fractures (Fig.11A).

5.2.2 Samples 12W002a and 12W002b

These samples are from a single outcrop that hosts, respectively, a leucocratic pegmatite and a pink pegmatite intruding the Archean basement exposed to the north of Crozier Island in the western part of Wollaston Lake (Fig.2). These samples are located in the margin of the main D2 high strain zone where D1 structures are still preserved. On this outcrop (Fig. 6E), three generations of pegmatite have been distinguished: (1) leucocratic pegmatite (12W002a) in continuous layers that range in width from a few millimeters to tens of centimeters and are parallel to the S1 foliation ; (2) pink pegmatite (12W002b), that forms coarse-grained layers that are at least 10 centimeters in width, crosscut at a low angle the S1 foliation and leucocratic pegmatite 12W002a ; and (3) pink pegmatite that is parallel to the axial plane of F2 folds. This last generation, which is contemporaneous with the D2 folding, appears to be similar from a structural point of view to sample 13W042. Both pegmatites 12W002a an 12W002b are folded by F2 folds with steeply-dipping axial planes that trend ~ N030. Field relationships therefore suggest that pegmatite 12w002a is syn-D1 while pegmatite 12W002b is post-S1 and pre F2 folding.

12W002a is composed of variable amounts of quartz, weakly-altered K-feldspar, plagioclase and biotite, with subordinate apatite, and zircon (Fig.10C). In this sample, zircon crystals are subhedral to euhedral, elongated, and range in length from 200 to 300 µm. BSE images reveal a core-rim zonation with rounded homogenous core surrounded by a large euhedral rim containing abundant radial cracks and a fine oscillatory magmatic zoning (Fig.11B). The oscillatory-zoned rim is sometimes truncated and overgrown by another narrow unzoned rim (overgrowth) that may be metamorphic in origin (Fig.11B– Zr7).

12W002b is composed of quartz, plagioclase, altered K-feldspar, and chloritized biotite, with subordinate apatite and zircon (Fig.10D). Zircon grains are subhedral to euhedral, elongated to rounded, and range in length from 150 to 300 µm. BSE images reveal that some zircon grains show a preserved primary oscillatory magmatic zoning which has been partly affected by a fluid-mediated

alteration phase, as suggested by the formation of embayment and other corrosion features (Fig.11C-Zr26). These fluid-mediated alteration phases are characterized by calcium enrichment according to the compositional maps obtained on zircon grains. Some grains show homogeneous domains in BSE that might correspond to the recrystallized rims after fluid-related alteration (Fig.11C – Zr1and Zr19).

5.3 U-Th-Pb geochronology of monazite

For sample 13W022C, from the Cochrane River area, twelve U-Th-Pb analyses have been obtained on seven monazite grains (Table 2). All the grains are included in M1 garnet porphyroblasts and are not affected by fractures. In a $^{206}Pb/^{238}U$ versus $^{208}Pb/^{232}Th$ Concordia diagram, they all plot in a concordant to sub concordant position and define a concordia date of 1813 ± 11 Ma (MSWD = 0.73) if the four most discordant data are excluded (Fig.12A). This date, obtained from monazite inclusion in garnet, is interpreted as the age of the M1 peak pressure-assemblage associated with the D1 phase of deformation.

For sample 12W008, located in the main D2 high strain zone in the western side of the Wollaston Lake, fifteen U-Th-Pb analyses have been obtained on 6 monazite grains. All the analyzed grains are located in the matrix and aligned with the S2 crd-bio-sill foliation (Table 2). Analytical points are slightly discordant but a concordia date of 1781 ± 11 Ma (MSWD = 0.92) can be calculated if the seven most discordant data are excluded (Fig. 12B).

For the Wolly-McClean exploration project area, two samples coming from the same D2 high strain zone have been dated: TC34 and LS70. In sample TC34, thirteen U-Th-Pb data have been obtained on seven monazite grains aligned with the foliation (Table 2). Analytical points are slightly discordant but a concordia date of 1779 ± 10 Ma (MSWD = 0.66) can be calculated if the two most discordant data are excluded (Fig. 12C). In sample LS70, twenty-two U-Th-Pb analyses have been obtained on eleven monazite grains aligned with the foliation (Table 2). Analytical points are slightly discordant but a concordia date of 1774 ± 8 Ma (MSWD = 0.79) can be calculated if the four most discordant data are excluded (Fig.12D). Although some grains are chemically zoned, there are no clear relationships between the obtained dates and the chemical domains. A weighted mean $^{208}Pb/^{232}Th$ date of 1779 Ma

is common and found in all analyzed grains aligned with the S2 crd-bio-sill foliation. This date is regarded as the age of the second tectono-metamorphic event M2-D2.

In the strongly retrogressed sample MC15A, sixteen U-Th-Pb analyses have been obtained on nine monazite grains (Table 2). Ten data have been obtained on Y-rich cores and five on Y-poor rims. U-Th-Pb data show two distinct concordant populations that allow to calculate two concordia dates at 1787 ± 10 Ma on Y-rich cores and unzoned Y-poor grains (MSWD=0.48) and 1718 ± 12 Ma on Y-poor rims (MSWD=0.65) (Fig. 12E). The oldest date (ca. 1790 Ma) obtained from monazite cores commonly aligned with the biotite S2 foliation is interpreted as the age of the M2-D2 event in good agreement with the previous sample (12W008, TC34 and LS70). The youngest date of ca. 1720 Ma is recorded mostly from monazite rims that may contain inclusions of chlorite and embayment within biotite or monazite surrounded by sulfides. This younger date is regarded as the age of a late retrogression during post-peak metamorphism cooling.

5.4 U-Pb geochronology on zircon

In the pegmatite 13W042, located in a F2 axial plane, thirty-five analyses were performed on seventeen grains (Table 3). During the course of the analyses, several zircon grains showed the presence of common Pb, but no correction was applied. Furthermore, minute inclusions of monazite in some of the cores have been ablated. These particular analyses have been excluded.

Due to the complexity of the zircon grains and the variation in individual apparent ages, a different approach has been adopted to interpret the zircon data in this sample. Individual apparent $^{207}Pb/^{206}Pb$ ages have been plotted in a relative probability diagram and formed a single cluster based on age distribution (Fig. 13B). This cluster yields a weighted mean date of 1784 ± 13 Ma. In the concordia diagram (Fig. 13A), the entire data set plots roughly on a discordia line with an upper intercept of 1783±7 Ma (MSWD = 7.2), in agreement with the mean $^{207}Pb/^{206}Pb$ date of 1784 ± 13 Ma (Fig. 13A). The 13W042 pink pegmatite being located along a F2 axial plane and this emplacement being coeval with the D2 event, the date of 1783 ± 7 Ma, identical to the weighted mean age of 1779 ± 10 Ma

found for the monazite and consistent with the age of the peak of second metamorphic event corresponding to the emplacement of the 13W042 pegmatite.

In the pegmatite 12W002a, that defines the S1 foliation, thirty-six analyses were performed on fifteen grains and plotted in the U-Pb Concordia diagram. Analyses with a degree of concordance greater than 99% and lower than 101% have been plotted in brown (Fig13C and D). Individual apparent $^{207}Pb/^{206}Pb$ ages have been plotted in a relative probability diagram and formed two main clusters based on age distribution (Fig.13D). The concordant apparent ages range from Mesoarchean to Neoarchean. The oldest Mesoarchean dates are interpreted as inherited while the youngest Neoarchean date of ca. 2750 Ma could either be interpreted as the age of the development of the S1 foliation or as an inherited age if we assume that the S1 foliation is Paleoproterozoic.

The pegmatite 12W002b is defined as a post-S1 and pre-F2 folding. Twenty-nine analyses were performed on fifteen grains. The age spectrum is completely different when compared to the neighbor white pegmatite 12W002a (Fig.13C and D), since only Paleoproterozoic apparent ages have been obtained, without any Archean inheritance. Seven data have been obtained on unaltered cores preserving occasionally and locally magmatic oscillary zoning and twenty-two on the homogeneous recrystallized rims that are interpreted as being formed during fluid-assisted alteration. In the concordia diagram (Fig. 13E), seven analyses from the cores plots roughly on a discordia line with an upper intercept of 1770±9 Ma (MSWD = 2.2). This date of ca. 1770 Ma obtained on unaltered core is also consistent with the age of the M2-D2 event obtained on monazite from garnet-bearing paragneiss and the pegmatite 13W042 emplaced in F2 axial plane. Consequently, we conclude that the 12W002b pegmatite was emplaced during the M2-D2 event. The analyses performed on the altered phase are, for most of them, highly discordant (Fig.13 F). This discordance can be attributed to the combination of a non-negligible amount of common lead together with complex and variable Pb loss, possibly linked to the alteration. Three data, however, including one concordant within error allow to calculate a poorly constrain upper intercept date of 1753 ± 26 Ma (MSWD=1.8) which is comparable within error with the age obtained on the non altered phase (1770 Ma).6. Discussion

The age dataset obtained from monazite and zircon coming from deformed migmatitic paragneiss and pegmatites, respectively, are used to define the timing of the tectonic-metamorphic events that have taken place into the WMTZ and to discuss the likely geodynamic evolution of this part of the THO at around 1810 - 1780 Ma. Multiple grains of monazite, from garnet-bearing migmatitic metapelites, were identified in thin section, but only grains that could be texturally linked to synkinematic and/or synmetamorphic growth during M1-D1, M2-D2 events and the later retrogression, were selected for dating in order to reconstruct the most accurate and continuous Hudsonian P–T–D-t path in the WMTZ (Fig.14). Zircon ages carried out from pegmatites with a well-defined structural setting are also used to strengthen the P-T-D-t. The ultimate goal is to place the episodes of pegmatite formation that have been previously defined on this P-T-D-t evolution, with a special interest for the mineralized uraninite-bearing pegmatites that are believed to be the proto-ore of the giant U unconformity-type deposits of the Athabasca Basin.

6.1 Timing of S1 foliation and Synkinematic M1- Garnet Growth

In the WMTZ, the earliest paleoproterozoic regional tectono-metamorphic event M1-D1 is characterized by the development of near east-west-trending and shallow dipping S1 foliation together with a high-grade metamorphism that lead to the development of a garnet-bearing assemblage and to the partial melting in meta-pelites of the Wollaston Supergroup. The P-T-D-t conditions of this early stage have been poorly documented in the literature due to the strong overprint of the later M2-D2 north-east -oriented regional sinistral transpression. Jeanneret et al. (2016) have estimated a peak temperature at 750-825°C for the M1-D1 event. Maximum pressures estimates, based on preserved grossular content in garnet porphyroblasts, vary regionally perpendicular to the S1 trend, from 10 kbar in the northern part near the Cochrane River, down to 6 kbar in the southern part of the studied area near the Wolly-McClean drilling project. This M1-D1 event is interpreted as the consequence of the burial of the thinned Hearne margin, including the supracrustal Wollaston Group rocks, via southward thrusting, during the collision between the Hearne and the Reindeer zones, Sask craton and Superior Province.

The age of this M1-D1 burial event is constrained using monazite inclusions shielded in high pressure M1 garnet of sample 13W022c from the northern part of the studied area in the Cochrane River. This sample preserves the highest pressure recorded at ~10 kbar. The concordia date of 1813 ± 11 Ma is interpreted as the age of peak pressure M1-assemblage and the maximum burial depth of the Wollaston Group sediments related to the D1 phase of deformation (Fig. 14).

About 200 km to the south-west of our studied area, in the Frazer lakes zone, Mckechnie et al. (2012b) have dated, via U–Th–Pb EPMA dating, similar garnet-and melt-bearing metapelite that belong to the Wollaston Supergroup. Although this domain is far from our studied area, the Frazer lake zone is in a comparable finite lithological and structural position with respect to the Wollaston Lake area. Individual chemical U-Th-Pb monazite dates obtained on three pelitic gneisses show a large spread in age from 1813 ± 13 Ma down to 1295 ± 29 Ma with poorly defined clusters at ca. 1800 Ma and 1500-1600 Ma. This spread in age reflects, according to Mckechnie et al. (2012b), a partial resetting of the U-Th-Pb isotopic system. Thus these dates cannot be used to constrain the age of the M1 metamorphism. However, the oldest date of 1813 ± 13 Ma obtained on a monazite grain included within a large grain of garnet, is consistent with our concordant age obtained on monazite also included in garnet.

In the eastern Hearne Province, in an area close to Fraser Lakes (Fig.1), Schneider et al. (2007) have collected for U-Pb analysis of monazite three samples of metapelite from the Wollaston Group. These analyses yielded dates between 1822±1 Ma and 1811±3 Ma, which are consistent with our peak of M1-D1 event dated at 1813 ± 11 Ma.

The determination of the age of the D1 deformation event has also been attempted by dating leucocratic pegmatite layers that define the S1 foliation in the Archean basement (12W002a). All the zircon apparent ages obtained on this sample are Mesoarchean to Neoarchean. The oldest Mesoarchean date of ca 3100 Ma is interpreted as inherited. The youngest Neoarchean date of ca. 2750 Ma is interpreted as the age of crystallization of the pegmatite. The development of the gently dipping S1 foliation in the Archean basement can either be Neoarchean or younger than 2750 Ma (i.e. Paleoproterozoic) but we cannot conclude in this singular case.

Jeanneret et al. (2016) suggest that the M1-D1 tectono-metamorphic event is related to the burial of the thinned Hearne margin, that consists of the Archean basement and the overlying Paleoproterozoic Wollaston Group sediments, via southward thrusting during the north-south convergence of the Archean Hearne domain and the southern crustal domains: the juvenile Paleoproterozoic Reindeer zone with the Archean Sask craton and Archean Superior Province. The timing of this crustal thickening is consistent with the early stage of the Hearne-Sask craton collision at ca. 1840 Ma (Ansdell et Norman, 1995; Lewry and Collerson, 1990). This early collisional stage at ca. 1840 Ma correspond to the beginning of the M1-D1 event which is associated with prograde metamorphism, development of early leucosomes and emplacement of ca. 1840 Ma grey granite suite (Annesley et al., 1997b). This granite suite has been interpreted to represent lower crustal melts formed during crustal thickening (Peterson et al., 2002). Then, the burial of Wollaston Group metasediments continues to depths approaching peak pressures involving mafic magma underplating in the lower crust, initiation of large-scale crustal melting, and emplacement of 1835–1820 Ma tholeiitic to calc-alkaline intrusions (SIGC) (Annesley et al., 1997b; Annesley et al., 2005). All of these events are consistent with Sask Craton collision associated to subduction cessation and slab breakoff.

The maximum burial depth corresponding to a pressure of 10 kbar is recorded in the Cochrane River (northern part of the studied area; Fig.15). Annesley et al. (2005) suggested that the burial of the Wollaston Group sediments to depth equivalent to peak pressures of 6–9 kbar and peak temperatures of 750–825 °C occurred between 1835 and 1820 Ma (collision stage DP2a from Annesley et al., 2005). We rather suggest that the terminal collision phase of the Superior Province and peak metamorphism occurred 20 to 10 million years later, at ca. 1813 Ma (Fig.14). This tectonic phase is associated with magmatic emplacement of porphyritic calc-alkaline granites between 1824-1812 Ma, and more common peraluminous leucogranites and associated granitic pegmatite at ca. 1820–1800 Ma (Annesley et al., 1997c).

6.2 Timing of D2 sinistral transpressive deformation

The second regional tectono-metamorphic event M2-D2 is responsible for the exhumation of M1 rocks during an isothermal decompression event, which led to the formation of cordierite-bearing M2 assemblages at 5-6 kbar and 750-825°C. The whole studied area is equilibrated at these low pressure conditions during the M2-D2 event, which means that there is a differential exhumation across the studied area with a pressure drop of 4 to 5 kbar in the north (Cochrane river) and less than 1 kbar in the south (Wolly-McClean drilling project area) (Fig.14). This metamorphic event is coeval with upright F2 folding of the S1 foliation and the development of a penetrative steeply-dipping N40° S2 foliation and the N10° shear zones developed in a sinistral transpressional tectonic regime (Fig.2). Monazite U-Th-Pb dating of the four analyzed paragneisses, that show the development of a strong S2 foliation, yields very consistent ages of 1781± 11 Ma, 1779 ± 10 Ma, 1774 ± 8 Ma, and 1787 ± 10 Ma (Fig.12) with a weighted mean of 1779 ± 10 Ma. Furthermore, microtextural evidences, like the formation of euhedral monazite grains aligned with the S2 biotite - sillimanite foliation and containing euhedral micro-inclusions of sillimanite (Fig.7A and B), unequivocally show that this age of 1779 Ma corresponds to the timing of the peak of the second tectono-metamorphic event M2-D2 (Fig.14). Zircon dating of pegmatite in well-constrained D2 structural settings helps to confirm the previous data from monazite. The 13W042 pegmatite emplaced along a F2 axial plane yield an upper intercept age of 1783 ± 7 Ma while cores of zircon grains from the 12W002b pegmatite, structurally defined as post-S1 and pre to syn F2 folding, yield an upper intercept age of age of 1770 ± 9Ma. All these ages are interpreted as the timing of the D2 deformation and are consistent within uncertainties with the ages defined with monazite.

In conclusion, we suggest that the M2-D2 event, that correspond to the differential isothermal exhumation of previously buried rocks of the Hearne margin to a pressure of 4.5-6 corresponding to an approximate depth of 12 to 15 km occurred between ca. 1813 and 1770 Ma, with the 1770 Ma age being the timing of P-T equilibration at 4.5-6 kbar (Fig.15).

Jeanneret al. (2016) and Annesley et al. (2005) agree that this event (referred as DP2b in Annesley et al., 2005) occurred under a sinistral transpressive regime responsible for the development of the

penetrative NE-trending foliation of the WMTZ. However, our proposed age for this event (1813-1770 Ma) is over a longer period of time, than that proposed by Annesley et al. (2005) for the same event: 1820–1805 Ma. The M2-D2 event between ca. 1813-1770 Ma is consistent with the ca. 1770 Ma date, interpreted by Schneider et al. (2007) as timing a retrograde metamorphic event followed by exhumation and rapid cooling at the terminal stages of the THO. This 1770 Ma thermal event is here interpreted as the latter stage of THO exhumation and the beginning of the orogenic cooling event of wide regional significance (Chakungal et al., 2004; McKeough et al., 2013; Schneider et al., 2007).

6.3 A late retrogression event at ca. 1720 Ma

One paragneiss (MC15a) and one pegmatite (12W002b) samples show evidences for a later retrogression with the chloritization of biotite, breakdown of cordierite into phyllosilicate-bearing assemblage, crystallization of sulfur and dissolution/reprecipitation of both monazite and zircon, attesting for strong fluid-rock interactions. On this newly formed monazite we obtained an age of 1718±12 (Fig.12E). This age overlaps with a biotite Rb-Sr age of 1711 ± 8 Ma (Worden et al., 1985) and biotite $^{40}Ar/^{39}Ar$ age of ca. 1740-1720 Ma from the Southern part of the Wollaston Domain (Fig.1) (Schneider et al., 2007). Alexander et al. (2009) has also obtained by $^{40}Ar/^{39}Ar$ dating of muscovite from unaltered host rocks of the basement hosted deposits at McArthur River and Dawn Lake, a $^{40}Ar/^{39}Ar$ age of 1731±18 Ma (weighted mean). This ca. 1720 Ma event is interpreted as the final cooling below 350-400 °C (closure temperature of the Rb/Sr system in biotite, Dodson, 1973) and late fluid-rock interactions (Fig.14). This age is important as it suggests that there was a regional thermal event in the crystalline basement at around 1720-1710 Ma. Given that previous geochronological interpretations have suggested that the Athabasca sedimentation had started by this time, this age indicates that the time of initiation of sediment deposition should actually be at ca. 1710 Ma or later.

6.4 Pegmatite formation and U mobilization during the P-T-D-t evolution of the WMTZ

In the WMTZ, uranium-enriched granitic pegmatites are associated with many unconformity-related uranium deposits, such as Moore Lakes (Annesley et al., 2000), McLean Lake, and P-Patch (Key Lake: see Madore et al., 2000) and are considered to represent an important source of uranium for these deposits (Alexandre et al., 2005; Boiron et al., 2010; Cloutier et al., 2009; Derome et al., 2005; Hecht and Cuney, 2000; Jefferson et al., 2007a; Kotzer and Kyser, 1995; Madore et al., 2000; Mercadier et al., 2010; Richard et al., 2010).

Jeanneret et al. (2016) has revealed that the basement exposed to the north-east of the Athabasca Basin (ie. in the Wollaston Lake and Cochrane River study areas) and the uranium-enriched basement beneath the Athabasca Basin do not belong to the same structural level (up to 10-12 km of difference) during the M1-D1 event. Moreover, the occurrences of uranium-enriched granitic pegmatites reported throughout the D2 WMTZ basement around and beneath the Athabascan Group as well as in the basement exposed south-east of the Athabasca are almost unknown in the basement exposed just north-east of the Athabasca Basin along the D2 WMTZ trend where we have performed this study. This suggests a possible role of the M1-D1 peak pressure gradient (from 5 to 11-12 kbar towards the north-east) on the location of uranium-enriched lithologies.

Jeanneret et al. 2016 suggested a multistage genetic model for the studied granitic pegmatites.

The first stage represents the M1-D1 burial of Wollaston sediments to various depths at ca.1840-1813 Ma (equivalent to 12 to 5 kbar; Fig.15A). If we assume that monazite is the main carrier of uranium in the paragneiss, the enrichment in U of the melt will be controlled by the monazite solubility. Montel (1993) and Stepanov et al. (2012) have shown experimentally that monazite solubility is limited in pera-aluminous melt. Therefore, monazite saturation in the melt will be rapidly reached after a few percent of partial melting. We suggest that during the early stage of prograde and peak metamorphism the first batches of melt produced via low-degree fluid-present melting are the most likely enriched in uranium.

The second stage involved decompression to 5 kbar from ca. 1813 Ma to ca. 1770 Ma, accompanied with the development of crustal-scale steep S2 schistosity and vertical sinistral shear zones, that favor M1-D1 initially U-enriched melt segregation and transfer towards upper levels where they could differentiate and crystallize as uranium-enriched pegmatites (Fig. 15B).

The model presented here shares many similarities with the model proposed by McKechnie et al. (2013) for the formation and evolution of the granitic pegmatites at Fraser Lakes. The granitic pegmatites from this area are interpreted to be lower to middle crustal melts that were derived from a deeper partial melting zone similar to the Wollaston sediments exposed in this area (Annesley et al. 2010; McKechnie et al., 2013). The deeper parts of this transfer zone could be an analog of the basement exposed currently to the north-east of the Athabasca Basin (ie. in the Wollaston Lake and Cochrane River study areas), where the granitic melts are more restitic.

U–Pb geochronology of these uranium-enriched granitic pegmatites (McFarlane and McKeough, 2013; McKeough et al.,2013; McKechnie et al., 2012a, 2012b; Mercadier et al., 2013) and their relatively high-T partial melting conditions (~700-800 °C) constrain their melt-forming conditions between the M1-D1 event (ca. 1840-1813 Ma) and the M2-D2 event (ca. 1813-1770 Ma) of the THO (Fig.14). Furthermore, dating of uraninite from uranium-enriched granitic pegmatites and veins from the basement exposed south-east of the Athabasca suggest a primary crystallization event of uraninite at ca. 1805 Ma (Mckechnie et al., 2012b; Mercadier et al., 2013). Moreover, uranium-and thorium-enriched pegmatites from Fraser Lakes are considered as the products of earlier melts (Group-A pegmatites from Mckechnie et al., 2012b). This primary crystallization event of uraninite is consistent with the peak of M1-D1 event (ca. 1813 Ma) suggesting again that the first batches of melt are the most likely enriched in uranium (Fig.15A). Mercadier et al. (2013) suggested that the second event dated at 1774 Ma, is a probable high-temperature (HT) dissolution/precipitation event. This age is consistent with the M2-D2 event (ca. 1813-1770 Ma) event in which partial melting was still active (Fig.14, Fig.15B).

7. Conclusions

In this contribution, we have quantified the age of the two tectono-metamorphic events M1-D1 and M2-D2 defined by Jeanneret et al. (2016) in the Wollaston-Mudjatik Transition Zone (Fig.14). The stages of pegmatite formation, that are believed to be the proto-ore of the giant U unconformity-type deposits of the Athabasca basin, have been replaced in the P-T-D-t evolution of the basement and a geodynamic setting for this part of the THO (Fig. 15).

The early collision between the Hearne and Reindeer Zone, Sask Craton and Superior Province is characterized by the burial of the thinned Hearne margin via northward-underthrusting and corresponds to the M1-D1 event that occurred between ca.1840 and 1810 Ma (Fig.14, Fig.15). The latter stage of THO deformation characterized by a north-east-oriented sinistral transpressional tectonic regime and corresponding to the M2-D2 event occurred between ca. 1810 and 1770 Ma (Fig.14, Fig.15). The entire region has been re-equilibrated at 5-6 kbar and 750–825 °C at 1779 ± 10 Ma. Finally, the last cooling event at around 350-400 °C and late fluid-rock interactions occurred at ca. 1720 Ma (Fig.14). This age provides new insights to the time of initiation of Athabasca sedimentation that should actually be at ca. 1710 Ma old or younger.

The Wollaston Group metasedimentary rocks and D2 deformation of the WMTZ were important lithologie that controlled the location of uranium-enriched pegmatites and granites, but in addition we argue that the maximum depth of burial of the Wollaston Group sediments during D1 constitutes also another key parameter that should be taken into account for the formation of the uranium-enriched pegmatites.

With this in mind, we suggest a multistage genetic model for the studied pegmatites. Between ca. 1840 and 1813 Ma, during the M1-D1 event, the first batches of melt, that are associated with the prograde partial melting of Wollaston metasediments, are produced. At the same time the primary crystallization event of uraninite in uranium-enriched pegmatites occurred reinforcing the hypothesis that the first batches of melt are the most likely enriched in uranium. During the M2-D2 decompression and development of crustal scale D2 shear zones, partial melting was still active. Therefore, we suggest that previously produced melt could have been transferred upwards to the upper

crustal levels near the brittle/ductile transition at depth of about 15km, between the peak of the M1-D1 event at 1813 Ma and the peak of the M2-D2 event at 1770 Ma (Fig.14). However, we do not exclude the possibility that uranium-enriched pegmatites could have crystallized from different pulses and could represent the product of differentiation of M2-D2 melts that experienced contrasting crystal–liquid fractionation. From ca. 1720 Ma, the brittle reactivation of the D2 shear zones produced a permeable conduit system suitable for the migration of oxidizing basinal brines and basin-derived diagenetic-hydrothermal basement fluids that may have leached uranium from the basement lithologies, including uranium-enriched pegmatites and contributed to the formation of the unconformity-type deposits.

Acknowledgments

This research was funded and financially supported by AREVA. The project would not have been possible without the access to the drill core from the Wolly-McClean exploration project provided by AREVA Resources Canada. Particular mention should be made of the significant contributions of Jean-Louis Feybesse, Jean-Pierre Milési and Jean-Luc Lescuyer who gave birth to this project and participated in the sampling of drill-core. Sincere thanks to the Hatchet Lake Lodge for their assistance in the field and for their reliable floatplane service. This work was partly supported by the french RENATECH network and its FEMTO-ST technological facility. Didier Convert-Gaubier is thanked for preparing the thin sections and Maxime Mermet for his assistance for the sawing, milling, and sieving of the samples.

References

Alexandre, P., and Kyser, K., 2005. Effects of cationic substitutions and alteration in uraninite, and implications for the dating of uranium deposits. Can. Mineral. 43, 1005–1017. doi:10.2113/gscanmin.43.3.1005

Alexandre, P., Kyser, K., Thomas, D., Polito, P., and Marlatt, J., 2009. Geochronology of unconformity-related uranium deposits in the Athabasca Basin, Saskatchewan, Canada and their integration in the evolution of the basin. Miner. Depos. 44, 41–59. doi:10.1007/s00126-007-0153-3

Annesley, I.R., and Madore, C., 1994. A geological study of the Wollaston-Mudjatik domain boundary in the Wollaston Lake area, Hearne Province, Saskatchewan. Saskatchewan Research Council, Publication R-1230-6-C-94, 162 pp.

Annesley, I.R., and Madore, C., 1999. Leucogranites and pegmatites of the sub-Athabasca basement, Saskatchewan: U protore? In: Stanley C.J. et al. (Eds.), Mineral deposits: processes to processing. Balkema, Rotterdam, The Netherlands, Vo. 1, pp. 297– 300.

Annesley, I.R., Madore, C., Krogh, T.E.,1992. U–Pb geochronology of some granitoids from the Peter Lake Domain: a summary. In: Summary of Investigations 1992, Saskatchewan Geological Survey, Sask. Energy Mines, Misc. Rep. 92–4, pp 168–171.

Annesley, I.R., Madore, C., Chen, Y.D., and Krogh, T.E., 1995a. U/Pb geochronological studies on the gabbros from the Sandy Islands Gabbro Complex, Wollaston Domain, northern Saskatchewan. In: Geol. Asso. Can.-Mineral Asso. Can. Annual Meeting, Program with Abstracts, Vol. 20, A-3.

Annesley, I.R., Madore, C., and Shi, R., 1997a. Thermotectonic evolution of the Wollaston EAGLE Project Area. In: Thermotectonic and uranium metallogenic evolution of the Wollaston EAGLE Project area (Annesley, I.R., Madore, C., Shi, R., and Quirt, D.H.), Saskatchewan Research Council, Publication R-1420-2-C-97, Part 1, pp. 1–62.

Annesley, I.R., Madore, and C., Krogh, T.E., 1997b. U–Pb geochronology of thermotectonic events in the Wollaston Domain Lake area, Wollaston Domain: a summary of 1994–1996 results. In: Summary of Investigations 1997, Saskatchewan Geological Survey, Sask. Energy Mines, Misc. Rep. 97-4, pp. 162–176.

Annesley, I.R., Madore, C., and Krogh, T.E., 1997c. U–Pb geochronology of peraluminous pegmatites from the Wollaston Lake area, northern Saskatchewan. In: Geol. Asso. Can.-Mineral Asso. Can. Annual Meeting, Program with Abstracts, Vol. 22, A-4.

Annesley, I.R., Madore, C., Shi, R., and Krogh, T.E. 1999a. U–Pb geochronology and thermotectonic history of the Wollaston Domain in the Wollaston Lake area, Hearne Province, Saskatchewan. In: Geol. Asso. Can.-Mineral Asso. Can. Annual Meeting, Program with Abstracts, Vol. 21, A-4.

Annesley, I.R., Madore, C., Krogh, T.E., Kwok, Y.Y., and Kamo, S.L., 1999b. New U–Pb zircon and monazite geochronological results for Archean and Paleoproterozoic basement to the southeastern part of the Athabasca Basin, Saskatchewan. In: Summary of investigations 1999, Vol. 2, Saskatchewan Geological Survey, Sask. Energy Mines, Misc. Rep. 99-4.2, pp. 90–99.

Annesley, I.R., Madore, C., Kusmirski, R.T., and Bonli, T., 2000. Uraninite bearing granitic pegmatite, Moore Lakes, Saskatchewan: Petrology and UTh- Pb chemical ages. In: Summary of Investigations 2000, Saskatchewan Geological Survey, Sask. Energy Mines, Misc. Rep. 2000-4.2, pp. 201–211.

Annesley, I.R., Madore, C., Portella, P., 2005. Geology and thermotectonic evolution of the western margin of the Trans-Hudson Orogen: evidence from the eastern sub-Athabasca basement, Saskatchewan. Can. J. Earth Sci. 42, 573–597. doi:10.1139/e05-034

Annesley, I.R., Austman, C.L., Creighton, S., Mercadier, J., Ansdell, K., Gittings, F., Bogdan, T., and Billard, D., 2010. Fraser Lakes U-Th-REE mineralization, southeastern Athabasca basement: Composition and UTh- Pb chemical/isotopic ages, with implications for U protore and U/C type mineralization. In: Proceedings of Saskatchewan Geological Survey Open House Conference 2010, Saskatoon, Canada, p. 8.

Ansdell, K.M., 2005. Tectonic evolution of the Manitoba-Saskatchewan segment of the Paleoproterozoic Trans-Hudson Orogen, Canada. Can. J. Earth Sci. 42, 741–759. doi:10.1139/e05-035

Ansdell, K.M., Norman, A.R., 1995. UPb geochronology and tectonic development of the southern flank of the Kisseynew Domain, Trans-Hudson Orogen, Canada. Precambrian Res. 72, 147–167. doi:10.1016/0301-9268(94)00090-E

Ansdell, K.M., Mcneil, A., Delaney, G.D., Hamilton, M.A., 2000. Rifting and development of the Hearne Craton passive margin: age constraint from the Cook Lake area, Wollaston Domain, Trans-Hudson Orogen, Saskatchewan. In: GeoCanada 2000, The Millennium Geoscience Summit, Calgary, AB. Abstract Volume, Abstract #77 (CD-ROM).

Ashton, K. E., Lewry, J. F., Heaman, L. M., Hartlaub, R. P., Stauffer, M. R., Tran, H. T., 2005. The Pelican Thrust Zone: basal detachment between the Archean Sask Craton and Paleoproterozoic Flin Flon Glennie Complex, western Trans-Hudson Orogen. Can. J. of Earth Sci. 42, 685-706. doi: 10.1139/e04-035

Ballouard, C., Boulvais, P., Poujol, M., Gapais, D., Yamato, P., Tartèse, R., Cuney, M., 2015. Tectonic record, magmatic history and hydrothermal alteration in the Hercynian Guérande leucogranite, Armorican Massif, France. Lithos 220–223, 1–22. doi: 10.1016/j.lithos.2015.01.027

Beck, L.S., 1969. Uranium deposits of the Athabasca region; Saskatchewan Department of Mineral Resources, Rep.126, 140 p.

Bickford, M.E., Collerson, K.D., Lewry, J.F., Van Schmus, W.R., Chiarenzelli, J.R., 1990. Proterozoic collisional tectonism in the Trans-Hudson orogen, Saskatchewan. Geology 18, 14–18. doi:10.1130/0091-7613(1990)018<0014:PCTITT>2.3.CO;2

Bickford, M. E., Collerson, K. D., Lewry, J. F., 1994. Crustal histories of the Hearne and Rae provinces, southwestern Canadian Shield, Saskatchewan: constraints from geochronologic and isotopic data. Precambr. Res. 68, 1–21. doi.org/10.1016/0301-9268(94)90062-0

Bickford, M., Mock, T., Steinhart III, W., Collerson, K., and Lewry, J., 2005. Origin of the Archean Sask Craton and its extent within the Trans-Hudson Orogen: evidence from Pb and Nd isotopic compositions of basement rocks and post-orogenic intrusions. Can. J. of Earth Sci. 42, 659–684.

Boiron, M.C., Cathelineau, M., and Richard, A., 2010. Fluid flows and metal deposition near basement/cover unconformity: Lessons and analogies from Pb-Zn-F-Ba systems for the understanding of Proterozoic U deposits. Geofluids. 10, 270–292. doi: 10.1111/j.1468-8123.2010.00289.x

Braun, I., Montel, J. M., and Nicollet, C., 1998. Electron microprobe dating of monazites from high-grade gneisses and pegmatites of the Kerala Khondalite Belt, southern India. Chem. Geol.146, 65-85. doi :10.1016/S0009-2541(98)00005-9

Card, C.D., Harper, C.T., Barsi, N., Lesperance, J., and Smith, J.S., 2006a. Investigation of the Wollaston-Mudjatik Transition, Charcoal Lake and Cochrane River (Parts of NTS 64L-9,-10, -11,-14,-15 and -16). In: Summary of Investigations 2006, Volume 2, Saskatchewan Geological Survey, Sask. Industry and Resources, Misc. Rep. 2006-4.2.

Card, C.D., Harper, C.T., Barsi, N., Lesperance, J., and Smith, J.S., 2006b. Bedrock Geology of the Cochrane River area, Northeast Wollaston Domain (Parts of NTS 64L/10, /11, /14, /15); 1/ 50 000 scale preliminary map. In: Summary of Investigations 2006, Volume 2, Saskatchewan Geological Survey, Sask. Industry and Resources, Misc. Rep. 2006-4.2.

Card, C.D., Harper, C.T., Barsi, N., Lesperance J., and Smith, J.S., 2006c. Bedrock Geology of the Charcoal Lake area, Northeast Wollaston Domain (parts of NTS area 64L/ 9, /10, /15 and /16); 1:50 000 scale preliminary map. In Summary of Investigations 2006, Volume 2, Saskatchewan Geological Survey, Sask. Industry and Resources, Misc. Rep. 2006-4.2.

Chakungal, J., Reynolds, P., Jamieson, R., Corrigan, D., 2004. Slow post-orogenic cooling in a deeply eroded orogen: Reindeer Zone, Trans-Hudson orogen, Saskatchewan. Can. J. Earth Sci. 41, 867–880. doi: 10.1139/e04-023

Chandler, F.W., 1978. Geology of part of the Wollaston Lake fold belt, northern Wollaston Lake, Saskatchewan. Geological Survey of Canada Bulletin, v. 277, 57 p.

Chiarenzelli, J., 1989. Petrogenesis and tectonic significance of the Guncoat and Nistowiak gneisses, Glennie Lake Domain, northern Saskatchewan. Ph.D. dissertation. University of Kansas, Lawrence, Kansas, 229 pp.

Chiarenzelli, J., Aspler, L., Villeneuve, M., and Lewry, J., 1998. Early Proterozoic evolution of the Saskatchewan craton and its allochthonous cover, Trans-Hudson orogen. J. of Geol.. 106, 247–267. doi **:** 10.1086/516020

Cloutier, J., Kyser, K., Olivo, G.R., Alexandre, P., and Halaburda, J., 2009. The Millennium uranium deposit, Athabasca Basin, Saskatchewan, Canada: an atypical basement-hosted unconformity-related uranium deposit. Econ. Geol. 104, 815–840. doi: 10.2113/gsecongeo.104.6.81

Corrigan, D., 2012. Paleoproterozoic crustal evolution and tectonics processes: Insights from the LITHOPROBE program in the Trans-Hudson Orogen, Canada. Chapter 4 In: Percival, J.A., Cook, F.A., and Clowes, R.M. (Eds.), Tectonic Styles in Canada: The LITHOPROBE Perspective. Geological Association of Canada, Special Paper 49, pp. 237-284.

Corrigan, D., Hajnal, Z., Németh, B., and Lucas, S.B., 2005. Tectonic framework of a Paleoproterozoic arc–continent to continent–continent collisional zone, Trans-Hudson Orogen, from geological and seismic reflection studies. Can. J. Earth Sci. 42, 421–434. doi: 10.1139/e05-025

Corrigan, D., Pehrsson, S., Wodicka, N., De Kemp, E., 2009. The Paleoproterozoic Trans-Hudson Orogen: a prototype of modern accretionary processes. Geol. Soc. London, Spec. Publ. 327, 457–479. doi:10.1144/SP327.19

Creaser, R.A. and Stasiuk, L.D., 2007. Depositional age of the Douglas Formation, northern Saskatchewan, determined by Re-Os geochronology. Geological Survey of Canada Bulletin, vol. 588, p. 341.

Culshaw, N.G., and Clarke, D.B., 2009. Structural History and Granite Emplacement in the Rottenstone Domain during Closure of the Trans-Hudson Orogen, Davin Lake, Northern Saskatchewan. Can. J. of Earth Sci. 46, 287–306. doi: 10.1139/e09-021

Cumming, G.L., and Krstic, D., 1992. The age of unconformity-related uranium mineralization in the Athabasca Basin, northern Saskatchewan. Can. J. of Earth Sci.. 29,1623–1639. doi: 10.1139/e92-128

Cumming, G.L., Krstic, D., Wilson, J.A., 1987. Age of the Athabasca Group, Northern Alberta. In: Geol. Asso. Can.-Mineral Asso. Can. Annual Meeting, Program with Abstracts, Vol. 12, A-35.

Cuney, M., 2009. The extreme diversity of uranium deposits. Miner. Depos. 44, 3–9. doi: 10.1007/s00126-008-0223-1

Dodson, M.H., 1973, Closure temperature in cooling geochronological and petrological systems: Contrib. Mineral. Petrol. 40, 259–274. doi: 10.1007/BF00373790

Dumond, G., Goncalves, P., Williams, M. L., & Jercinovic, M. J., 2015. Monazite as a monitor of melting, garnet growth and feldspar recrystallization in continental lower crust. J. of Metamorph. Geol. 33, 735-762. doi:10.1111/jmg.12150

Durocher, K. E., Kyser, T. K., Delaney, G. D., 2001. Thermotectonic studies in the Paleoproterozoic Glennie domain, trans-Hudson orogen, Canada. Precambrian. Res. 109, 175-202. doi : 10.1016/S0301-9268(01)00144-9

Evans, M. E., and Bingham, D. K., 1973. Paleomagnetism of the Precambrian Martin Formation, Saskatchewan. Can. J. of Earth Sci.10, 1485-1493. doi :10.1139/e73-141

Fahrig, F. and West, T.D., 1986. Diabase dyke swarms of the Canadian Shield. Geological Survey of Canada. 1627A 1:4 873 900 scale map.

Fayek, M., and Kyser, T.K., 1997. Characterization of multiple fluid-flow events and rare-earth-element mobility associated with formation of unconformity-type uranium deposits in the Athabasca Basin, Saskatchewan. Canad. Mineral. 35, 627–658.

Fayek, M., Harrison, T.M., Ewing, R.C., Grove, M., and Coath, C.D., 2002a. O and Pb isotopic analyses of uranium minerals by ion microprobe and U-Pb ages from the Cigar Lake deposit. Chem. Geol. 185, 205–225. doi:10.1016/S0009-2541(01)00401-6.

Fayek, M., Kyser, T.K., and Riciputi, L.R., 2002b. U and Pb isotope analysis of uranium minerals by ion microprobe and the geochronology of McArthur River and Sue zone uranium deposits, Saskatchewan, Canada. Canad. Mineral. 40, 1553–1569. doi:10.2113/gscanmin.40.6.1553.

Foster, G., Kinny, P., Vance, D., Prince, C., & Harris, N. 2000. The significance of monazite U–Th–Pb age data in metamorphic assemblages; a combined study of monazite and garnet chronometry. Earth Planet. Sci. Lett. 181, 327-340. doi.org/10.1016/S0012-821X(00)00212-0

Fumerton, S. L., Stauffer, M. R. and Lewry, J. F., 1984. The Wathaman Batholith: largest known Precambrian pluton. Canad. J. of Earth Sci.21, 1082–1097. doi: 10.1139/e84-113

Gasquet, D., Bertrand, J. M., Paquette, J. L., Lehmann, J., Ratzov, G., Guedes, R. D. A., and Nomade, S., 2010. Miocene to Messinian deformation and hydrothermal activity in a pre-Alpine basement massif of the French western Alps: new U-Th-Pb and argon ages from the Lauzière massif. Bull. Soc. Géol. France. 181, 227-241. doi: 10.2113/gssgfbull.181.3.227

Goncalves, P., Nicollet, C., and Montel, J. M., 2004. Petrology and in situ U–Th–Pb monazite geochronology of ultrahigh-temperature metamorphism from the Andriamena mafic unit, north–central Madagascar. Significance of a petrographical P–T path in a polymetamorphic context. J. Petrol. 45, 1923-1957. doi : 10.1093/petrology/egh041

Gordon, T., Hunt, P., Bailes, A., Syme, E., 1990. U–Pb ages from the Flin Flon and Kisseynew belts, Manitoba: chronology of crust formation at an Early Proterozoic accretionary margin. In: Lewry, J., Stauffer,M. (Eds.), The Early ProterozoicTrans-Hudson Orogen of North America. Geol. Assoc. Can. Spec. Paper. 37, 177–199.

Hajnal, Z., Lewry, J., White, D., Ashton, K., Clowes, R., Stauffer, M., Gyorfi, I., and Takacs, E., 2005. The Sask Craton and Hearne Province margin: seismic reflection studies in the western Trans-Hudson Orogen. Canad. J. of Earth Sci. 42, 403–419. doi: 10.1139/E05-026

Hamilton, M. A., and Delaney, G., 2000. New U–Pb geochronological constraints on the age of basement and cover in the eastern Wollaston Domain, Saskatchewan, and evolution of the SE Hearne Province. In: GeoCanada Conference 2000, CD-ROM.

Harper C.T., 1987. Trace element geochemistry in the Waddy-Windrum Lakes area. In: Summary of investigations 1987. Saskatchewan Geological Survey, Sask. Energy and Mines, Misc. Rep.1987-4.

Harper, C.T., and Van Breemen, O., 2004. Progress report on U-Pb SHRIMP zircon geochronology and Sm-Nd isotope geochemistry of the Phelps Lake area, northeast Saskatchewan. In: Summary of Investigations 2004, Volume 2, Saskatchewan Geological Survey, Sask. Energy and Mines, Misc. Rep. 2004-4.2, CD-ROM, Paper A-6, 8p.

Harper, C.T., Ebel, C., Yeo, G., Card, C., and Nelson, C., 2005a. Wollaston Lake Project: Geology of the Wollaston Supergroup in the Rabbabou Bay–Wellbelove Bay area, northeast Wollaston Lake, Saskatchewan (parts of NTS 64L-6, -7, -10, and -11). In: Summary of Investigations 2005, Volume 2, Saskatchewan Geological Survey, Sask. Energy and Mines, Misc. Rep. 2005-4.2, CD-ROM, Paper A-6, 25 p.

Harper, C.T., Ebel, C., Yeo, G., Card, C., and Nelson, C., 2005b. Bedrock geology of the northeastern Wollaston Lake area; Shaganappie Island sheet, (parts of NTS 64L/6 and /7): 1:50 000 scale preliminary Map. In: Summary of Investigations 2005, Volume 2, Saskatchewan Geological Survey, Sask. Industry Resources, Misc. Rep. 2005-4.2.

Harper, C.T., Ebel, C., Yeo, G., Card, C., and Nelson, C., 2005c. Bedrock geology of the northeastern Wollaston Lake area; Usam Island sheet (parts of NTS 64L/10 and /11): 1:50 000 scale preliminary Map. In: Summary of Investigations 2005, Volume 2, Saskatchewan Geological Survey, Sask. Industry Resources, Misc. Rep. 2005-4.2.

Harper, C.T., Rayner, N., and Card, C., 2006. Preliminary U-Pb ages for Archean basement and Proterozoic intrusion from the northern Wollaston Lake area, Saskatchewan. In: Summary of Investigations 2006, Volume 2, Saskatchewan Geological Survey, Saskatchewan Industry Resources, Misc. Rep. 2006-4.2, CD-ROM, Paper A-7, 9p.

Hecht, L., and Cuney, M., 2000. Hydrothermal alteration of monazite in the Precambrian crystalline basement of the Athabasca Basin (Saskatchewan, Canada): implications for the formation of unconformity-related uranium deposits. Mineral. Depos. 35, 791–795. doi:10.1007/s001260050280

Hoeve, J., and Sibbald, T., 1978. On the genesis of Rabbit Lake and other unconformity-type uranium deposits in northern Saskatchewan, Canada. Econ. Geol.73, 1450–1473. doi:10.2113/gsecongeo.73.8.1450.

Hoeve, J., and Quirt, D., 1984. Mineralization and host rock alteration in relation to clay mineral diagenesis and evaluation of the Middle-Proterozoic Athabasca basin, northern Saskatchewan. Saskatchewan Research Council Technical Report, Vol. 187, 187 p.

Hoeve, J., Sibbald, T.I.I., Ramaekers, P., and Lewry, J.F., 1980. Athabasca Basin unconformity-type uranium deposits: A special class of sandstone- type deposits. In: Ferguson, J. and Goleby, A.B (Eds.), Uranium in the Pine Creek Geosyncline: Vienna. International Atomic Energy Agency. pp. 57- 594.

Hoffman, P.E., 1990. Subdivision of the Churchill Province and extent of the Trans- Hudson Orogen. In: Lewry, J.F., Stauffer, M.R. (Eds), The Early Proterozoic Trans- Hudson Orogen of North America. Geol. Assoc. Can. Spec. Paper.37, 15–40.

Horstwood, M.S.A., Foster, G.L., Parrish, R.R., Noble, S.R., Nowell, G.M., 2003. Common-Pb corrected in situ U-Pb accessory mineral geochronology by LA-MC-ICP-MS. J. of Anal. Atom. Spec, 19, 837-846.

Hulbert, L.J., and Grégoire, D.C., 1993. Re-Os isotope systematics of the Rankin Inlet Ni ores: An example of the application of ICP-MS to investigate Ni-Cu-PGE mineralization, and the potential use of Os isotopes in mineral exploration. Canad. Mineral. 31, 861–876.

Jackson, S.E., Pearson, N.J., Griffin, W.L., Belousova, E.A., 2004. The application of laser ablation-inductively coupled plasma-mass spectrometry to in situ U–Pb zircon geochronology.
Chem. Geol. 211, 47–69. doi: 10.1016/j.chemgeo.2004.06.017

Jeanneret, P., Goncalves, P., Durand, C., Trap, P., Marquer, D., Quirt, D., and Ledru, P., 2016. Tectono-metamorphic evolution of the pre-Athabasca basement within the Wollaston-Mudjatik Transition Zone, Saskatchewan. Canad. J. of Earth Sci. 53,231-259. doi: 10.1139/cjes-2015-0136

Jefferson, C.W., Thomas, D.J., Gandhi, S.S., Ramaekers, P., Delaney, G., Brisbin, D., Cutts, C., Portella, P., and Olson, R.A., 2007a. Unconformity-associated uranium deposits of the Athabasca Basin, Saskatchewan and Alberta. In: Jefferson, C.W and Delaney, G. (Eds.), EXTECH IV: Geology and Uranium EXploration TECHnology of the Proterozoic Athabasca Basin. Geological Survey of Canada, Bulletin 588, pp. 23–68.

Jefferson, C.W., Thomas, D.J., Gandhi, S.S., Ramaekers, P., Delaney, G., Brisbin, Cutts, C., Quirt, D., Portella, P., and Olson, R.A., 2007b. Unconformity-associated uranium deposits of the Athabasca Basin, Saskatchewan and Alberta. In: Goodfellow WD Mineral Deposits of Canada: A synthesis of Major Deposit-types, District Metallogeny, the Evolution of Geological Provinces, and Exploration Methods. Geological Association of Canada, Mineral deposits division, pp 273-305.

Jefferson, C.W., Thomas, D., Quirt, D., Mwenifumbo, C.J., and Brisbin, D., 2007c. Empirical models for Canadian unconformity-associated uranium deposits. In: Milkereit, B. (Ed.) Proceedings of Exploration 07: Fifth Decennial International Conference on Mineral Exploration, pp. 741-769.

Kotzer, T.G., and Kyser, T.K., 1995. Petrogenesis of the Proterozoic Athabasca Basin, northern Saskatchewan, Canada, and its relation to diagenesis, hydrothermal uranium mineralization and paleohydrogeology. Chem. Geol. 120, 45–89. doi : 10.1016/0009-2541(94)00114-N

Krogh, T.E., and Clark, L.A., 1987. Zircon dating of sub-Athabasca granitoid rocks, Saskatchewan. In: Geol. Asso. Can.-Mineral Asso. Can. Annual Meeting, Program with Abstracts, Vol. 12, 64.

Kydonakis, K., Brun, J-P, Poujol, M., Monié , P., and Chatzitheodoridis, E., 2016. Inferences on the Mesozoic evolution of the North Aegean from the isotopic record of the Chalkidiki block. Tectonophysics. 682, 65–84. doi : 10.1016/j.tecto.2016.06.006

Kyser, T.K., and Stauffer, M., 1995. Petrogenesis and ages of plutons in the Central Metavolcanic Belt, La Ronge Domain. In Trans-Hudson Orogen Transect. Hajnal, Z. and Lewry. J. (Eds). Lithoprobe Report. 48, 122–130.

Kyser, T.K., Hiatt, E.E., Renac, C., Durocher, K., Holk, G.J., Deckart, K., 2000, Diagenetic fluids in paleo- and meso-Proterozoic sedimentary basins and their implications for long protracted fluid histories: p. 225-262. In: Kyser, K., (ed.), Fluids and Basin Evolution, Mineralogical Association of Canada, Ottawa, Canada, 262 p.

LeCheminant, A.N., and Heaman, L.M., 1989. Mackenzie igneous events, Canada: Middle Proterozoic hotspot magmatism associated with ocean opening. Earth Planet. Sci. Lett. 96, 38–48. doi : 10.1016/0012-821X(89)90122-2

Lewry, J.F, and Collerson, K.D., 1990. Trans-Hudson Orogen: extent, subdivision, and problems. In: Lewry, J.F. and Stauffer, M.R. (Eds.), The Early Proterozoic Trans- Hudson Orogen of North America. Geological Association of Canada Special Publication Paper 37, pp 1–14.

Lewry, J.F., and Sibbald, T.I.I., 1977. Variation in lithology and tectonometamorphic relationships in the Precambrian basement of northern Saskatchewan. Canad. J. of Earth Sci.14, 1453–1467.doi: 10.1139/e77-126

Lewry, J.F., and Sibbald, T.I.I., 1980. Thermotectonic evolution of the Churchill province in northern Saskatchewan. Tectonophysics.68, 45–82. doi : 10.1016/0040-1951(80)90008-6

Lewry, J., Hajnal, Z., Green, A., Lucas, S., White, D., Stauffer, M., Aston, K., Weber, W., and Clowes, R., 1994. Structure of Paleoproterozoic continent-continent collision zone: LITHOPROBE seismic reflection profiles across the Trans-Hudson orogen. Tectonophysics. 232,143–160. doi : 10.1016/0040-1951(94)90081-7

Ludwig, K. R., 2008. User's manual for Isoplot 3.70, a geolocronological toolkit for Microsoft Excel. Berkeley: Berkeley Geochronology Center Special Publication.4, 25-32.

MacDougall, D. G., and Heaman, L. M., 2002. Diabase sill complexes in Northern Saskatchewan: Analogues for the Lithoprobe Trans-Hudson Orogen Transect (THOT) Wollaston Lake S2b reflector. In: Geological Association of Canada Annual Meeting, Saskatoon, Saskatchewan, p. 70.

Machado, N., Zwanzig, H., Parent, M., 1999. U–Pb ages of plutonism, sedimentation, and metamorphism, of the Paleoproterozoic Kisseynew metasedimentary belt, Trans-Hudson orogen (Manitoba, Canada). Can. J. Earth Sci. 36, 1829–1842. doi: 10.1139/e99-012

Madore, C., and Annesley, I.R., 1993. Metamorphic pressure temperature conditions of the basal Aphebian Wollaston Group, Hearne Province, Saskatchewan. In: Geol. Asso. Can.-Mineral Asso. Can. Annual Meeting, Program with Abstracts, Vol. 18, A-65.

Madore, C., Annesley, I.R., Kwok, K.K., and Krogh, T.E., 1999a. Petrography, geochemistry, and age of granitic pegmatites from the Close Lake and Epp Lake areas, Mudjatik Domain, Saskatchewan. In: Geol. Asso. Can.-Mineral Asso. Can. Annual Meeting, Program with Abstracts, Vol. 23, A-77.

Madore, C., Annesley, I.R., and Tran, H.T., 1999b. Petrology and geochemistry of Paleoproterozoic Wollaston Group metasediments from the eastern Keller Lake–Siemens Lake area, Saskatchewan: A preliminary interpretation. In: Summary of investigations 1999, Vol. 2. Saskatchewan Geological Survey, Sask.Energy and Mines, Misc. Rep. 99-4.2, pp. 80–89.

Madore, C., Annesley, I.R., and Wheatley, K., 2000. Petrogenesis, age, and uranium fertility of peraluminous leucogranites and pegmatites of the Mc- Clean Lake / Sue and Key Lake / P-Patch deposit areas, Saskatchewan. In: Proceedings of The Millennium Geoscience Summit, University of Calgary, GeoCanada, Canada, p. 1041.

McFarlane, C.R.M, McKeough, M.A., 2013. Petrogenesis of the Kulyk Lake monazite–apatite– Fe(Ti)-oxide occurrence revealed using in-situ LA-(MC)-ICP-MS trace element mapping, U–Pb dating, and Sm–Nd isotope systematics on monazite. Amer. Miner. 98, 1644–1659. doi: 10.2138/am.2013.4368

McGill, B.D., Marlat, J.L., Matthews, R.B., Sopuck, V.J., Homeniuk, L.A., Hubregtse, J.J., 1993. The P2 North uranium deposit, Saskatchewan, Canada. Exploration and Mining Geology. 2, 321–331.

McKechnie, C.L., Annesley, I.R., and Ansdell, K.M., 2012a. Radioactive abyssal granitic pegmatites and leucogranites in the Wollaston Domain, northern Saskatchewan, Canada: Mineral compositions and conditions of emplacement in the Fraser Lakes area. Canad. Mineral. 50, 1637–1667. doi: 10.3749/canmin.50.6.1637

McKechnie, C.L., Annesley, I.R., and Ansdell, K.M., 2012b. Medium- to low-pressure politic gneisses of Fraser Lakes zone B, Wollaston Domain, northern Saskatchewan, Canada: Mineral compositions, metamorphic P-T-t path, and implications for the genesis of radioactive abyssal granitic pegmatites. Canad. Mineral. 50, 1669–1694. doi: 10.3749/canmin.50.6.1669

McKechnie, C.L., Annesley, I.R., and Ansdell, K.M., 2013. Geological setting, petrology, and geochemistry of granitic pegmatites and leucogranites hosting U-Th-REE mineralization at Fraser Lakes zone B, Wollaston Domain, northern Saskatchewan, Canada. Exploration and Mining Geology. 21, 1–26.

McKeough, M.A., and Lentz, D.R., 2011. Paleoproterozoic latetectonic granitic pegmatite-hosted U–Th ± REE–Y–Nb mineralization, northern Saskatchewan: products of assimilation, fractional crystallization, and hybridization processes. In: Summary of Investigations 2011, Volume 2. Saskatchewan Geological Survey and Sask. Ministry of Energy and Resources, Misc. Rep. 2011–4.2 Paper A-6, pp 1–21

McKeough, M.A., Lentz, D.R.., Brown, J.A., 2010. Geology and associated pegmatite- and vein-hosted uranium mineralization of the Kulyk, Eagle, and Karin lakes regions, Wollaston Domain, northern Saskatchewan. In: Summary of Investigations 2010 Volume 2. Saskatchewan Geological Survey and Sask. Ministry of Energy and Resources, Misc. Rep. 2010–4.2 Paper A-6, pp 1–23

McKeough M.A., Lentz D.R., McFarlane C.R.M., Brown J., 2013. Geology and evolution of pegmatite-hosted U-Th ± REE-Y-Nb Mineralization, Kulyk, Eagle, and Karin Lakes region, Wollaston Domain, northern Saskatchewan, Canada: examples of the dual role of extreme fractionation and hybridization processes. J. Geosci. 58.4, 321 – 346

Mercadier, J., Richard, A., Boiron, M.-C., Cathelineau, M., and Cuney, M., 2010. Migration of brines in the basement rocks of the Athabasca Basin through microfracture networks (P-Patch U deposit, Canada). Lithos, 115, 121–136.doi: 10.1016/j.lithos.2009.11.010

Mercadier, J., Cuney, M., Cathelineau, M., and Lacorde, M., 2011a. U redox fronts and kaolinisation in basement-hosted unconformity-related U ores of the Athabasca Basin, Canada: Late U remobilisation by meteoric fluids. Miner. Depos. 46, 105–135. doi:10.1007/s00126-010-0314-7

Mercadier, J., Annesley, I.R., McKechnie, C.L., Bogdan, T.S., and Creighton, S., 2013. Magmatic and Metamorphic Uraninite Mineralization in the Western Margin of the Trans-Hudson Orogen (Saskatchewan, Canada): A Uranium Source for Unconformity-Related Uranium Deposits? Econ. Geol. 108, 1037–1065. doi:10.2113/econgeo.108.5.1037

Montel, J.-M., 1993. A model for monazite/melt equilibrium and application to the generation of granitic magmas. Chem. Geol. 110, 127–146. doi: 10.1016/0009-2541(93)90250-M

Montel, J. M., Kornprobst, J., and Vielzeuf, D., 2000. Preservation of old U-Th-Pb ages in shielded monazite: example from the Beni Bousera Hercynian kinzigites, Morocco. J. Metamorph. Geol. 18.3, 335-342. doi: 10.1046/j.1525-1314.2000.00261.x

Norman, A.R., Williams, P.F., and Ansdell, K.M., 1995. Early Proterozoic deformation along the southern margin of the Kisseynew gneiss belt, Trans-Hudson orogen: 30 million year progressive deformation. Canad. J. of Earth Sci. 32, 875–894. Doi: 10.1139/e95-073

Orrell, S.E., Bickford, M.E., and Lewry, J.F., 1999. Crustal evolution and age of thermotectonic reworking in the western hinterland of the Trans-Hudson Orogen, northern Saskatchewan. Precambr.Res. 95, 187–223. Doi: 10.1016/S0301-9268(98)00117-X

Paquette, J.L., Tiepolo, M., 2007. High-resolution (5 mm) U-Th-Pb isotopes dating of monazite with excimer laser ablation (ELA)-ICPMS. Chem. Geol. 240, 222–237. doi: 10.1016/j.chemgeo.2007.02.014

Peterson, T. D., van Breemen, O., Sandeman, H. A., and Rainbird, R. H., 2000. Proterozoic (1.85–1.75 Ga) granitoid plutonism and tectonics of the western Churchill Province. In: Geol. Asso. Can.-Mineral Asso. Can. Annual Joint Meeting.

Peterson, T. D., Van Breemen, O., Sandeman, H., and Cousens, B., 2002. Proterozoic (1.85–1.75 Ga) igneous suites of the Western Churchill Province: granitoid and ultrapotassic magmatism in a reworked Archean hinterland. Precambr. Res. 119, 73-100. doi: 10.1016/S0301-9268(02)00118-3

Peterson, T. D., Scott, J. M., LeCheminant, A. N., Jefferson, C. W., & Pehrsson, S. J., 2015. The Kivalliq igneous suite: anorogenic bimodal magmatism at 1.75 Ga in the western Churchill Province, Canada. Precambr. Res.262, 101-119. doi: 10.1016/j.precamres.2015.02.019

Quirt, D.H., 1993. Petrology and geochemistry of the Helikian Athabasca diabase dykes, Saskatchewan. In Summary of Investigations 1993, Saskatchewan geological Survey, Sask. Energy and Mines, Misc.Rep. 93-4, pp. 174–182.

Quirt, D.H., 1997. Geochemistry, host-rock alteration, mineralization, and uranium metallogenesis of the Wollaston EAGLE project area. In: Thermotectonic and uranium metallogenic evolution of the Wollaston

EAGLE Project area (Annesley, I.R., Madore, C., Shi, R., and Quirt, D.H.), Saskatchewan Research Council, Publication No. R-1420-2-C-97, Part 2, pp. 1–98.

Quirt, D.H., 2003. Athabasca unconformity-type uranium deposits: one deposit type with many variations. In: Proceedings of International Conference on uranium Geochemistry, Nancy, France, pp. 309-312.

Rainbird, R.H., Hadlari, T., Aspler, L.B., Donaldson, J.A., LeCheminant, A.N., and Peterson, T.D., 2003b. Sequence stratigraphy and evolution of the Paleoproterozoic intracontinental Baker Lake and Thelon basins, western Churchill Province, Nunavut, Canada. Precambr. Res.125, 21–53. doi: 10.1016/S0301-9268(03)00076-7

Rainbird, R.H., Stern, R.A., Rayner, N., and Jefferson, C.W., 2007. Age, provenance, and regional correlation of the Athabasca Group, Saskatchewan and Alberta, constrained by igneous and detrital zircon geochronology. In: Jefferson, C.W, Delaney, D. (Eds.), EXTECH IV Geology and Uranium EXploration TECHnology of the Proterozoic Athabasca Basin, Saskatchewan and Alberta. Geological Survey of Canada, Bulletin 588 (also Saskatchewan Geological Society, Special Publication 17; Geological Association of Canada, Mineral Deposits Division, Special Publication 4), p. 193.

Rand, M.H., Mompean, F.J., Perrone, J., and Illemassène, M., 2009. Chemical thermodynamics of thorium: Paris, Organization for Economic Co-operation and Development (OECD), 900 p.

Ray, G.E., 1975. Foster Lake (NE)–Geikie River (SE) area: Reconnaissance geological mapping of 74A-15(E), -16 and 74H-1 and -2. In: Summary of Investigations 1975, Saskatchewan Geological Survey, Sask. Department of Mineral Resources, p13-18.

Ray, G.E and Wanless, R.K., 1980. The age and geological history of the Wollaston, Peter Lake, and Rottenstone domains in northern Saskatchewan; Canad. J. of Earth Sci. 17, p.333-347.

Rayner, N., Rainbird, R., Stern, R., 2003. SHRIMP U–Pb detrital zircon geochronology of Athabasca Group sandstones, northern Saskatchewan and Alberta. Current Research—Geol. Surv. Can.0704-2884; 2003-F2, 20 p.

Rayner, N.M., Stern, R.A., Bickford, M.E., 2005. Tectonic implications of new SHRIMP and TIMS U–Pb geochronology of rocks from the Sask Craton, Peter Lake Domain, and Hearne margin, Trans-Hudson Orogen, Saskatchewan. Canad. J. Earth Sci. 42, 635–657. doi: 10.1139/e04-045

Richard, A., Pettke, T., Cathelineau, M., Boiron, M.-C., Mercadier, J., Cuney, M., and Derome, D. 2010. Brine-rock interaction in the Athabasca basement (McArthur River U deposit, Canada): Consequences for fluid chemistry and uranium uptake. Terra Nova. 22, 303–308. doi: 10.1111/j.1365-3121.2010.00947.x

Schneider, D.A, Heizler, M. T., Bickford, M. E., Wortman, G. L., Condie, K. C. and Perilli, S. 2007. Timing constraints of orogeny to cratonization: thermochronology of the Paleoproterozoic Trans- Hudson orogen, Manitoba and Saskatchewan, Canada. Precambr Res. 153, 65–95. doi: 10.1016/j.precamres.2006.11.007

Sibbald, T.I.I.,1983. Economic geology investigation. In: Summary of Investigations 1983. Saskatchewan Geological Survey, Misc. Rep. 1983–4.

Simpson, R. L., Parrish, R. R., Searle, M. P., and Waters, D. J. 2000. Two episodes of monazite crystallization during metamorphism and crustal melting in the Everest region of the Nepalese Himalaya. Geology. 28(5), 403-406. doi: 10.1130/0091-7613(2000)28<403:TEOMCD>2.0.CO;2

Sláma, J., Košler, J., Condon, D. J., Crowley, J. L., Gerdes, A., Hanchar, J. M., and Schaltegger, U. 2008. Plešovice zircon—a new natural reference material for U–Pb and Hf isotopic microanalysis. Chem Geol. 249(1), 1-35. doi: 10.1016/j.chemgeo.2007.11.005

Stepanov, A. S., Hermann, J., Rubatto, D., and Rapp, R. P. 2012. Experimental study of monazite/melt partitioning with implications for the REE, Th and U geochemistry of crustal rocks. Chem Geol. 300: 200-220. doi: 10.1016/j.chemgeo.2012.01.007

Stern, R. A., and Berman, R. G. 2001. Monazite U–Pb and Th–Pb geochronology by ion microprobe, with an application to in situ dating of an Archean metasedimentary rock. Chem Geol. 172(1), 113-130. doi: 10.1016/S0009-2541(00)00239-4

Terry, M. P., Robinson, P., Hamilton, A., and Jercinovic, M. J. 2000. Monazite geochronology of UHP and HP metamorphism, deformation, and exhumation, Nordøyane, Western Gneiss Region, Norway. Am Mineral. 85(11-12), 1651-1664. doi: 10.2138/am-2000-11-1208

Thériault, R. J., St-Onge, M. R., & Scott, D. J. 2001. Nd isotopic and geochemical signature of the Paleoproterozoic Trans-Hudson Orogen, southern Baffin Island, Canada: implications for the evolution of eastern Laurentia. Precambr Res. 108(1), 113-138. doi: 10.1016/S0301-9268(00)00159-5

Thomas, D.J., 1978. Uranium Metallogenic Studies: Charlebois Lake and Cup Lake. In: Christopher J.E., Macdonald. R.(Eds.), Summary of investigations 1978. Saskatchewan Geological Survey, pp. 66–73.

Thomas, D.J., 1979. Uranium Metallogenic Studies: "Pegmatite" Project Geology. In: Christopher J.E., Macdonald. R.(Eds.), Summary of investigations 1979. Saskatchewan Geological Survey, pp. 86–95.

Thomas, D.J., 1980. Uranium Metallogenic Studies: Uraniferous Pegmatite Project Geology. In: Christopher J.E., Macdonald. R.(Eds.), Summary of investigations 1980. Saskatchewan Geological Survey, pp. 49–53.

Tran, H.T. 2001. Tectonic evolution of the Paleoproterozoic Wollaston Group in the Cree Lake Zone, Northern Saskatchewan, Canada. Ph.D. Thesis, University of Regina, Regina, Canada.

Tran, H.T., Ansdell, K.M., Bethune, K.M, Ashton, K.E., and Hamilton, M.A. 2008. Provenance and tectonic setting of Paleoproterozoic metasedimentary rocks along the eastern margin of Hearne craton: Constraints from SHRIMP geochronology, Wollaston Group, Saskatchewan, Canada. Precambr Res. 167, 171-185. Doi: 10.1016/j.precamres.2008.08.003

Van Achterbergh, E., Ryan, C.G., Jackson, S.E., Griffin, W.L., 2001. Data reduction software for LA-ICPMS: appendix. In: Sylvester, P.J. (Ed.), Laser Ablation-ICP Mass Spectrometry in the Earth Sciences: Principles and Applications. Mineral. Assoc. Canada (MAC) Short Courses Ser., Ottawa, Ontario, Canada, 29, 239–243.

Van Breemen, O., Peterson, T.D., Sandeman, H.A., 2005. U–Pb zircon geochronology and Nd isotope geochemistry of proterozoic granitoids in the western Churchill Province; intrusive age pattern and Archean source domains. Can J Earth Sci. 42, 339–377. doi: 10.1139/e05-007

Van Schmus, W.R., Bickford, M., Lewry, J., Macdonald, R., 1987. U–Pb geochronology in the Trans-Hudson orogen, northern Saskatchewan. Can J Earth Sci 24, 407– 424. doi: 10.1139/e87-043

Williams, M. L., Jercinovic, M. J., Goncalves, P., and Mahan, K. 2006. Format and philosophy for collecting, compiling, and reporting microprobe monazite ages. Chem Geol. 225, 1-15. doi: 10.1016/j.chemgeo.2005.07.024

Worden, J.M., Cumming, G.L., and Baadsgaard, H., 1985: Geochronology of host rocks and mineralization of the Midwest uranium deposit, northern Saskatchewan. In: Sibbald, T.I., Petruk, W. (Eds.), Geology of Uranium Deposits. Canadian Institute of Mining and Metallurgy. 32, 67-72.

Yeo, G.M., and Delaney, G., 2007. The Wollaston Supergroup, stratigraphy and metallogeny of a Paleoproterozoic Wilson cycle in the Trans-Hudson Orogen, Saskatchewan. In: Jefferson, C.W., Delaney, D. (Eds.), EXTECH IV: Geology and Uranium Exploration Technology of the Proterozoic Athabasca Basin, Saskatchewan and Alberta. Geology Survey of Canada, Bulletin 588, (also Geological Association of Canada, Mineral Deposits Division, Special Publication 4; Saskatchewan Geological Society, Special Publication 18), pp.89 -11

Figure captions

Fig.1: A) Simplified geological map of the Canadian Shield, with extension of western Precambrian terranes shown beneath Phanerozoic cover. The area affected by Trans–Hudson Orogen is delimited by the thick red hashed line (modified after Corrigan et al. 2009). Paleo- to Mesoproterozoic basins within the Canadian Shield that contain unconformity-associated uranium deposits (e.g. Athabasca (A)) or are considered to have potential for them (e.g. Thelon (T)) are plotted, as well as the major tectonic elements of the northwestern Canadian Shield. B) Lithotectonic domains of the exposed portion of the Hearne Province in northern Saskatchewan, encompassing parts of the Mudjatik and Wollaston Domains, and the Reindeer Zone. The locations of several unconformity-type uranium deposits within the Athabasca Basin, including McClean Lake, are plotted. The study area is outlined by the black rectangle and shown in more detail in Fig 2. Abbreviations: WMTZ-Wollaston-Mudjatik Transition Zone; TFZ – Tabbernor Fault Zone. The shaded region corresponds to the location of the WMTZ.

Fig. 2: Summary diagram of the finite strain pattern and the thermobarometric estimates of the studied area. The three main study areas, Wolly-McClean exploration project area, Wollaston Lake, and Cochrane River, are outlined and studied samples are located. Abbreviations: WMTZ-Wollaston-Mudjatik Transition Zone.

Fig.3: Compilation of previous geochronological results from the Wollaston-Mudjatik Transition Zone.

Fig. 4: (A) Thin section in natural light of the sample 13W022C. It is composed by an assemblage of garnet-cordierite-sillimanite-biotite-quartz, oriented parallel to the penetrative S2 foliation. (B), (C) & (D) SEM-BSE images of monazites grains occurring as minutes inclusions in garnet porphyroblasts, localized by black rectangles in (A).

Fig. 5: SEM-based X-Ray elementary map of Yttrium, Uranium and Thorium distribution in three monazites that form minute inclusions in the 13W022C sample. (A) Monazite grain Mnz a located in Fig. 5D. (B) Monazite grain Mnz d located in Fig. 5C. (C) Monazite grain Mnz g located in Fig. 5B.

All grains are small, rounded to sub-rounded and exhibits complex chemical patterns. Ellipses mark analysis spots labeled with measured $^{208}Pb/^{232}Th$ ages and associated 2σ errors.

Fig. 6: Outcrop and drill-core photos. A) Grt-crd-bearing pelitic gneiss, from the western part of the Wollaston Lake area. Garnet occurs as pluri-millimeter-size porphyroclats in a quartzo-feldspathic leucosome. B and C) Garnet-cordierite-bearing paragneiss, from drill core sample from the northern part of Wolly-McClean exploration project area, consists of porphyroblasts of garnet, cordierite, and feldspar, with biotite-sillimanite-rich layers interpreted as a M1 assemblage. D) Vertical pink pegmatite emplaced along F2 axial plane, from the north shore of the Cochrane River. E) Three generations of pegmatite have been distinguished. (*a*) leucocratic pegmatite syn-S1 foliation; (*b*) pink pegmatite that cross-cut slightly the first generation, suggesting that this pegmatite is post-S1 and pre-F2 folding; (*c*) pink pegmatite parallel to the axial plane of F2 folds that affect the two previous generations.

Fig. 7: (A) Thin section in natural light of the 12W008 sample. It consists of a very penetrative S2 foliation composed by sillimanite and biotite wrapping around garnet porphyroblasts and cordierite. Monazites grains are located in the matrix. (B) & (C) SEM-BSE images of monazites grains located in sillimanite – biotite S2 foliation band. Tiny inclusions of euhedral sillimanite in the monazite grains indicate a coeval crystallization. (D) Thin section in natural light of the TC34 sample. In this sample, the foliation is less penetrative and consists in a sillimanite – biotite layer containing accessory phases like ilmenite and pyrite. This sample contains abundant monazite grains compared to sample 12W008. (E) Highly corroded monazite grain located near a S2 deformation band. (F) Monazite grain in a low-strain domain of the sample.

Fig. 8: (A) SEM-BSE, X-ray elemental map of Yttrium and Thorium distribution images of a TC34 monazite grain (Mnz 34). It exhibits a slightly richer Yttrium outer rim but no thorium variation. (B) SEM-BSE, X-ray elemental map of Yttrium and Thorium distribution images of a LS70 monazite grain (Mnz 42). The yttrium distribution is more complex but consists of a Yttrium-depleted core compared to the rim. (C) SEM-BSE, X-ray elementary map of Yttrium and Thorium distribution images of a MC15A monazite grain (Mnz 8). Contrary to the previous monazite grains, this monazite

exhibits an Yttrium-rich and a Thorium-rich core, whose boundaries do not match. Ellipses mark analysis spots labeled with measured $^{208}Pb/^{232}Th$ ages and associated 2σ errors.

Fig. 9: (A) Thin section in natural light of the LS70 sample. It consists in a high-strain domain composed of a sillimanite-biotite-cordierite assemblage relatively poor in monazite grains compared to the low-strain domain which is composed of a garnet-cordierite-biotite assemblage. (B) a smaller monazite grain within the foliation of the high-strain domain. (C) A large monazite grain from a low-strain domain containing minute sillimanite inclusions. (D) Thin section in natural light of the MCS15A sample. This sample is deeply affected by the S2 foliation and is enriched in sulfides (Pyrite & Chalcopyrite – Ccp). Garnet is affected by retrogression and replaced by cordierite and chlorite-sericite. (E) An anhedral monazite grain contains inclusions of chlorite and apatite, suggesting crystallization during retrogression. (F) Monazite grain embedded in the retrogressed biotite-chlorite matrix. A small grain of chalcopyrite crystallized in the pressure shadow of the monazite grain.

Fig. 10: (A) Optical microscope image in natural light of the 13W042 pegmatite sample with location of (B). (B) Enlarged optical microscope image in polarized and analyzed light of the 13W042 pegmatite sample. It consists of a quartz-K-feldspar-plagioclase-biotite assemblage. (C) & (D) Optical microscope images in polarized and analyzed light of, respectively, the 12W002a and 12W002b pegmatite samples. They contain a quartz-K-feldspar-plagioclase-biotite assemblage

Fig. 11: SEM-BSE image of zircon grains in pegmatites samples described in Fig. 10. (A) Zircon grains from sample 13W042 are elongated exhibiting cores and rims zonation. Some cores preserved magmatic oscillatory zoning (Zr 19) while patchy zoning is associated with minute inclusions of monazite (Zr 23, 16). (B) Zircon crystals in sample12W002a. They are less elongated and more sub-rounded (Zr 11) and they show a large core with relatively uniform zonation, that is presumably inherited, surrounded by a large band exhibiting oscillatory zoning, corresponding to a magmatic stage. Sometimes, a uniform outer overgrowth cross-cuts the oscillatory-zoning band and corresponds to a metamorphic stage (Zr 7, 11). (C) Zircon grains from sample12W002b. These grains are euhedral to rounded and show more complex patterns. They contain a core, that can be oscillatory zoned (Zr 26) surrounded by a rim that exhibit a complex zonation. This rim is the result of a fluid-mediated alteration phase, which can alter the core and create embayments (Zr 1). Zr 19 exhibits a simpler

zoning pattern, quite uniform, which can be related to a later crystallization after the fluid-mediated alteration. Ellipses mark analysis spots labeled with measured $^{207}Pb/^{206}Pb$ ages and associated 2σ errors.

Fig. 12: (A) to (E) U-Th-Pb Concordia diagrams for the analyzed monazite grains. Diagrams created with the Isoplot v.3.7 program (Ludwig, 2008). Ellipses represent 1σ error. A large part of the analyses is concordant and allows calculation of a Concordia age. (E) Two ages can be calculated from sample MCS15A. See discussion in the text.

Fig. 13: U-Pb Concordia diagrams and Age spectra reporting the $^{207}Pb/^{206}Pb$ dates obtained on zircon grains. A) Sample 13W042 provides a group of concordant to discordant data with an upper intercept age of 1783±7 Ma, probably linked to the development of the S2 foliation (B) The $^{207}Pb/^{206}Pb$ dates yield a single age peak at 1784±13 Ma. (C) Sample 12W002a, situated in the S1 foliation exhibits a large range of dates demonstrating the important contribution of inheritance (D). (E) Zircon crystals in sample 12W002b show a group of data with an upper intercept date of a 1770±9 Ma. (F) Analyses of altered zircon grains in sample 12W002a show a strong discordance and cannot be used to calculate an age.

Fig. 14: P-T-D-t diagram summarizing the results of the thermobarometry and geochronology studies, and integrating other results from the Athabasca basin region (modified after Mercadier et al., 2013).

Fig. 15: Simplified crustal-scale cross-sections showing the evolution of the WMTZ and the multistage genetic model for studied granitic pegmatite. (A) M1-D1 event: thickening of the Hearne margin by burial and underthrusting of the thinned margin after the docking of the Reindeer Zone with the Hearne Craton. The M1-D1 burial of Wollaston sediments to various depths occurred between ca.1840 and 1813 Ma (equivalent to 12 to 5 kbar). During this stage of prograde and peak metamorphism, the first batches of melt produced via low-degree fluid-present melting are the most likely enriched in uranium. Part of these silicate-melts was segregated, transferred, and collected in the middle crust (at ca. 5 kbar, U red arrows). (B) M2-D2 event: exhumation and decompression (to ~5 kbar) from ca. 1813 Ma to ca. 1770 Ma in response to isostatic re-equilibration and development of D2 vertical shear zone during a sinistral transpression. The development of crustal-scale steep S2schistosity and shear zones favors melt segregation and transfer of melt towards upper levels where

they could differentiate and crystallize as uranium-enriched pegmatites (U vertical red arrows). The pink, orange, and green round symbols show the inferred locations of the studied areas during the initial stage, M1-D1 event, and M2-D2 event. At M2-D2, the symbols with transparent backgrounds represent the location of the studied areas during D1. The thick black line in (A) and (B) marks the suture between the Reindeer Zone and the Hearne Craton. In all figures, the White line marks the present erosional level.

Figures

Fig.1:

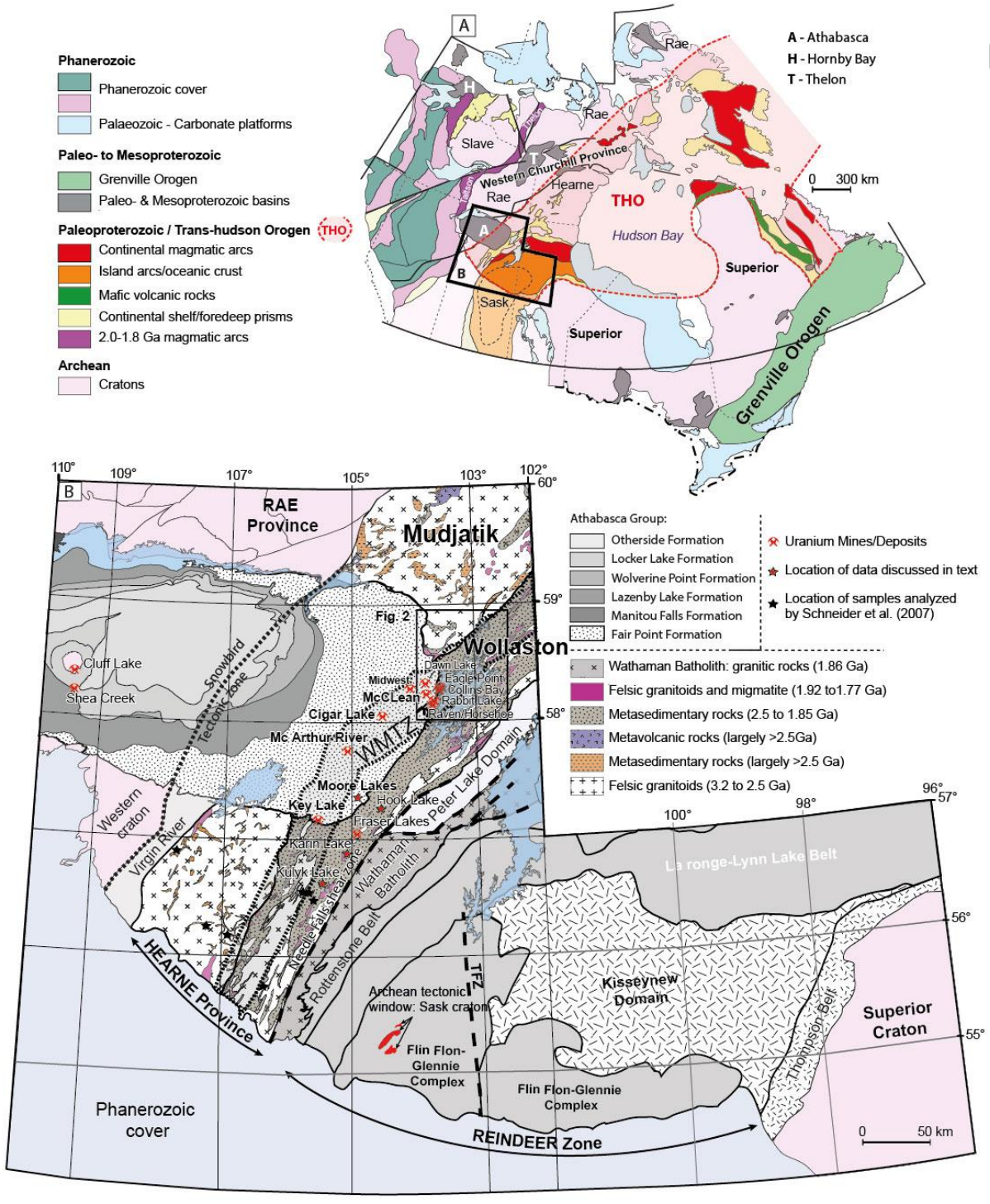

Fig.2:

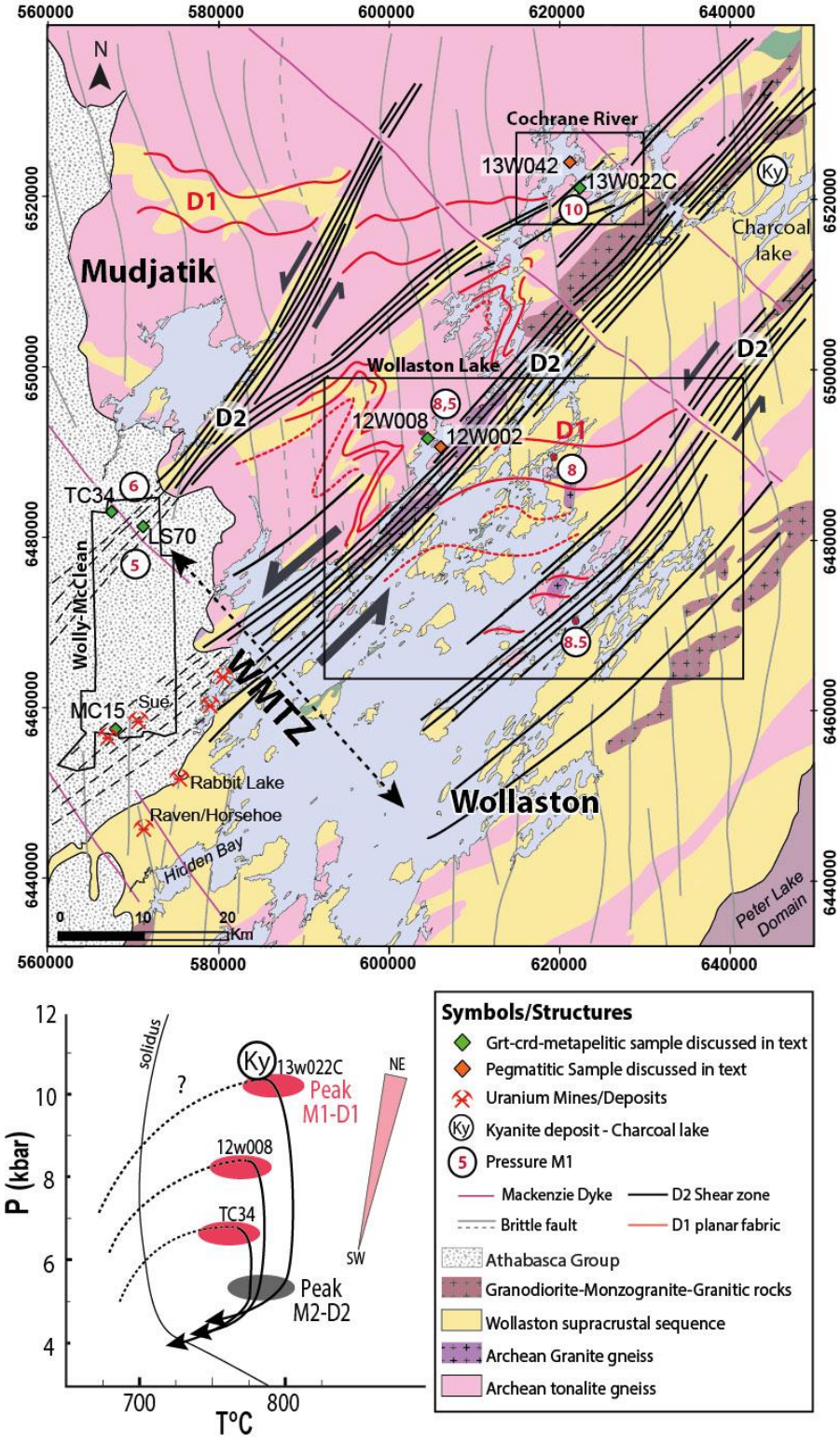

Fig.3:

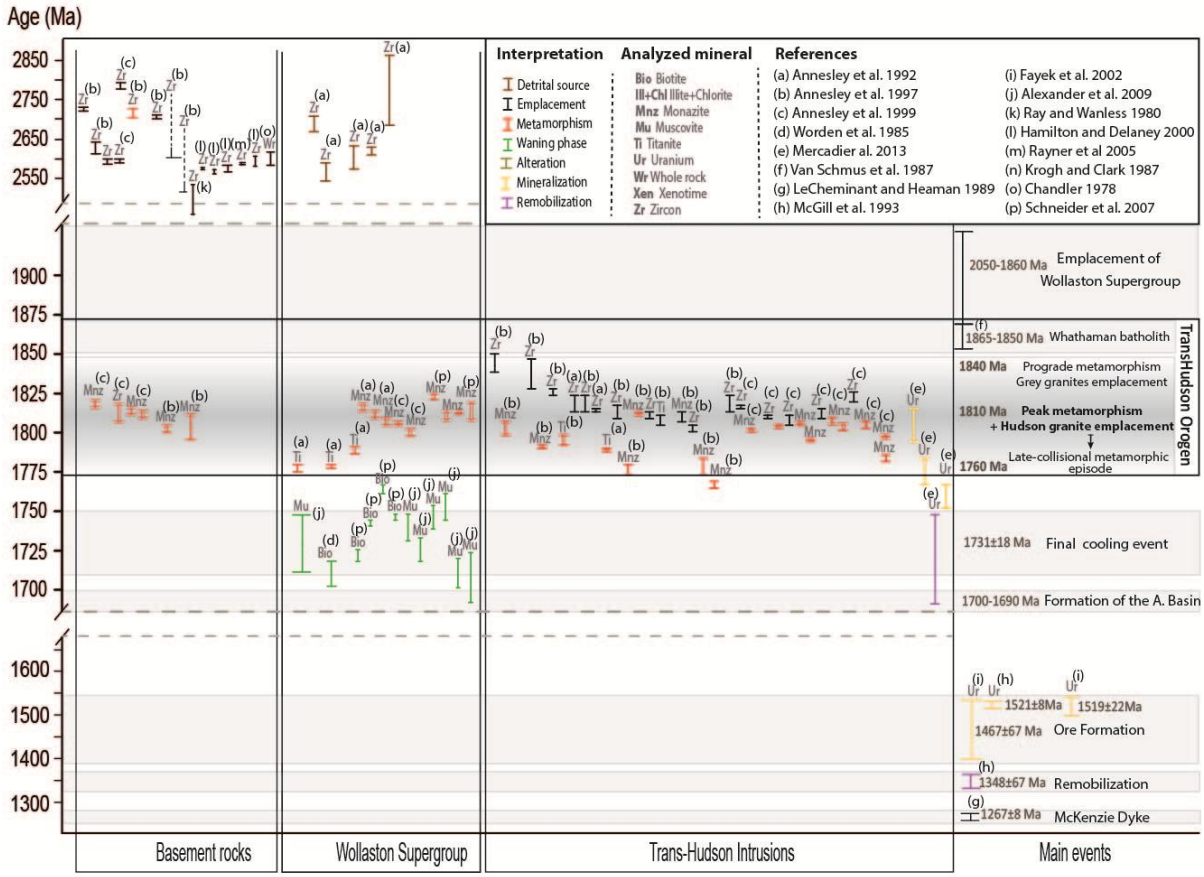

Fig.4:

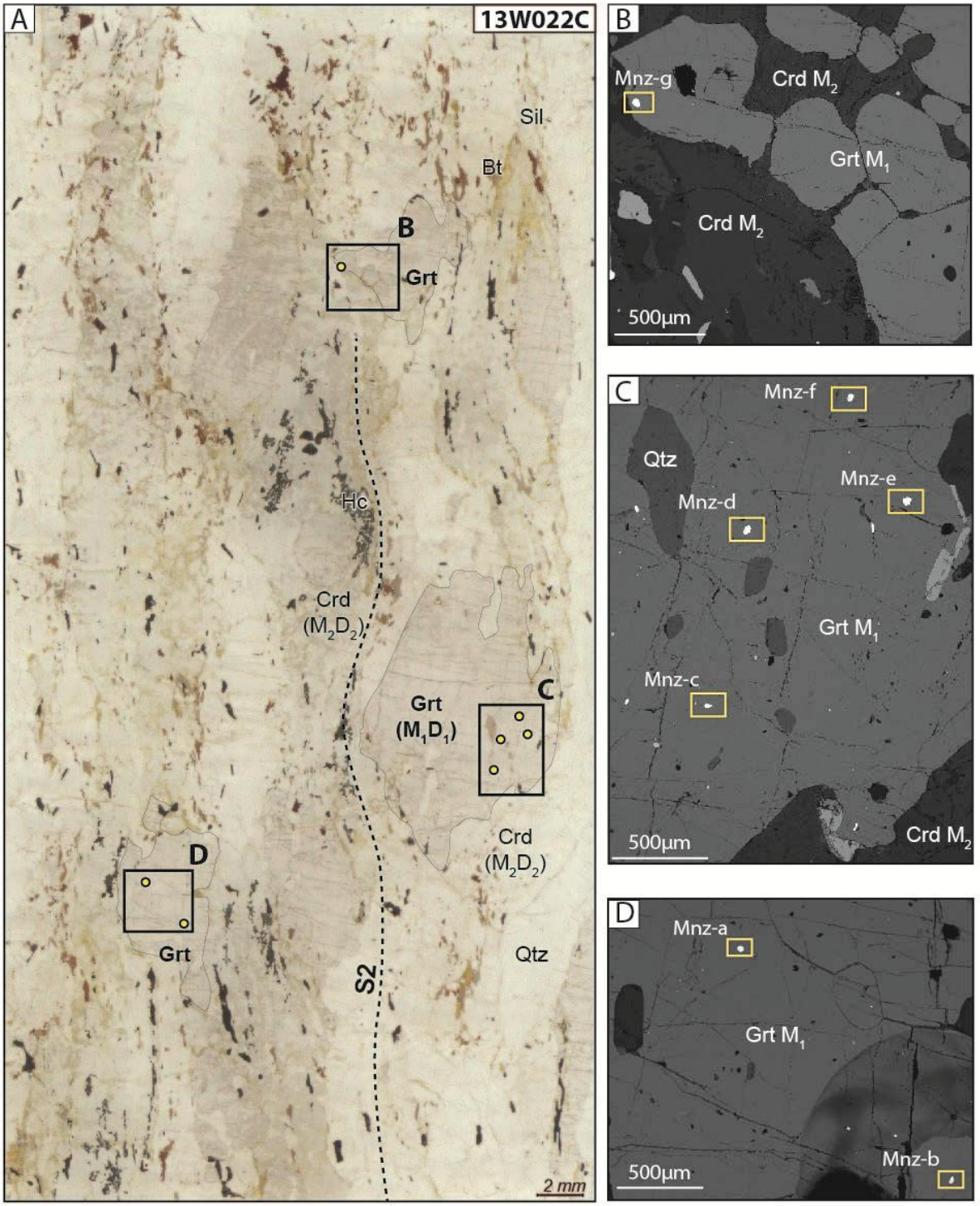

Fig.5:

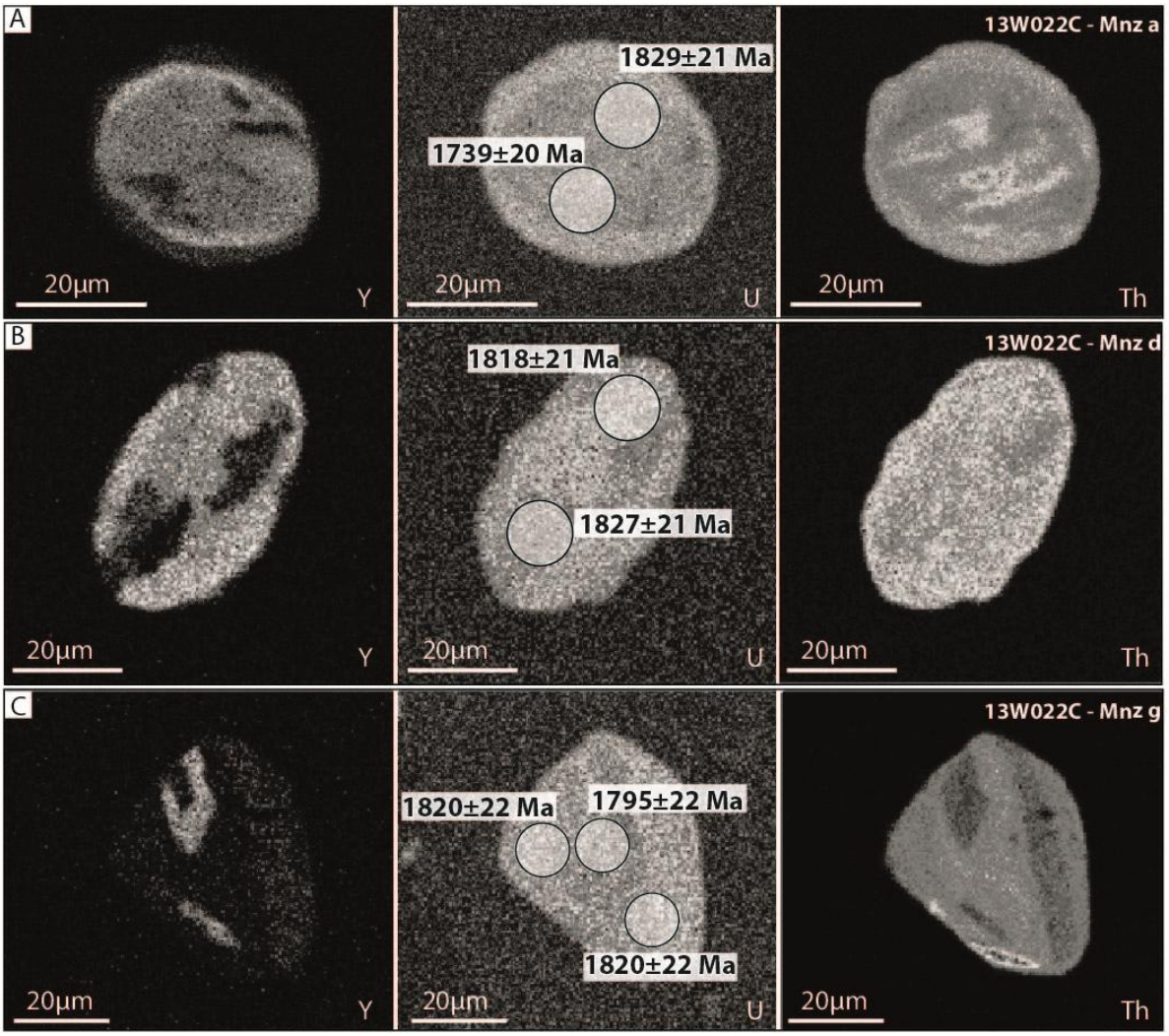
A
20µm
Y
1829±21 Ma
1739±20 Ma
20µm
U
13W022C - Mnz a
20µm
Th
B
20µm
Y
1818±21 Ma
1827±21 Ma
20µm
U
13W022C - Mnz d
20µm
Th
C
20µm
Y
1820±22 Ma
1795±22 Ma
1820±22 Ma
20µm
U
13W022C - Mnz g
20µm
Th

Fig.6:

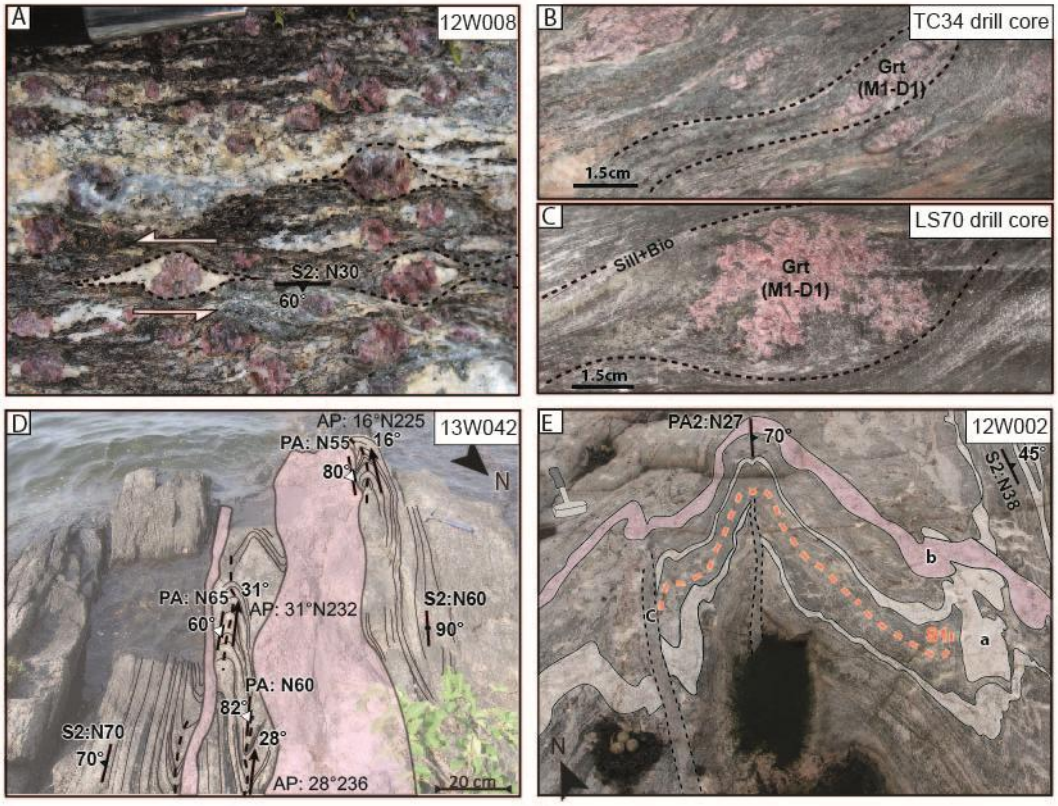

Fig.7:

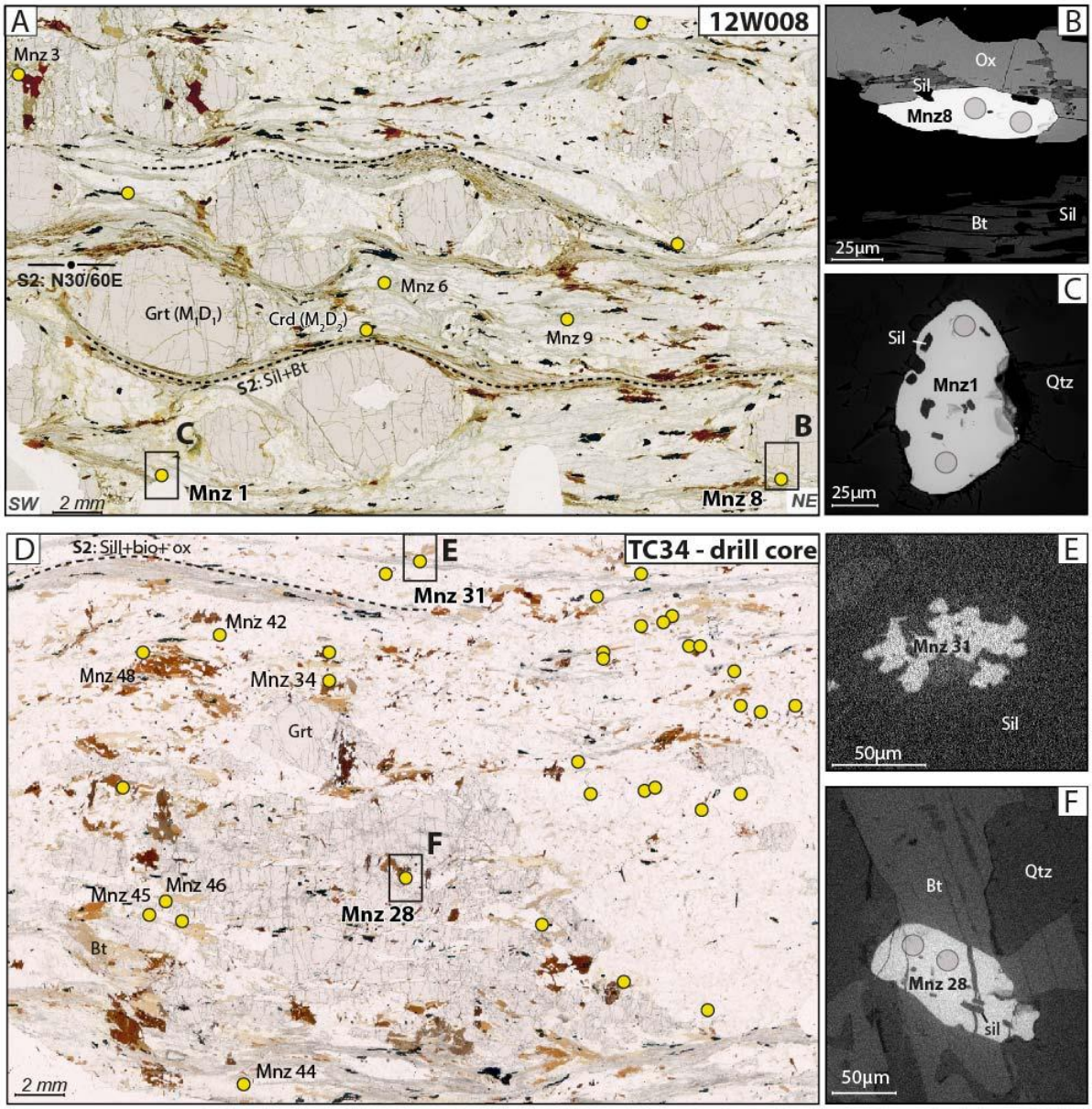

Fig.8:

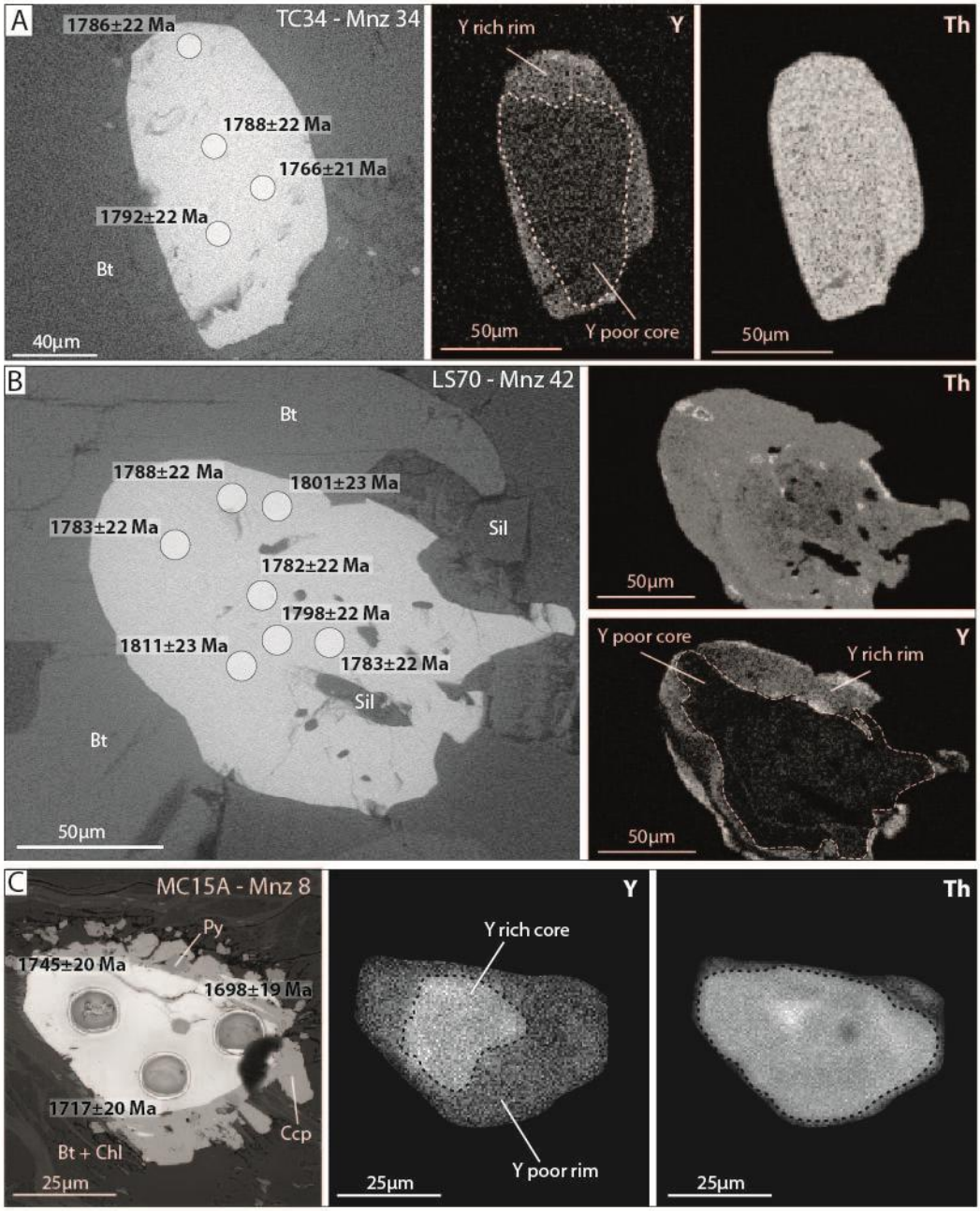

Fig.9:

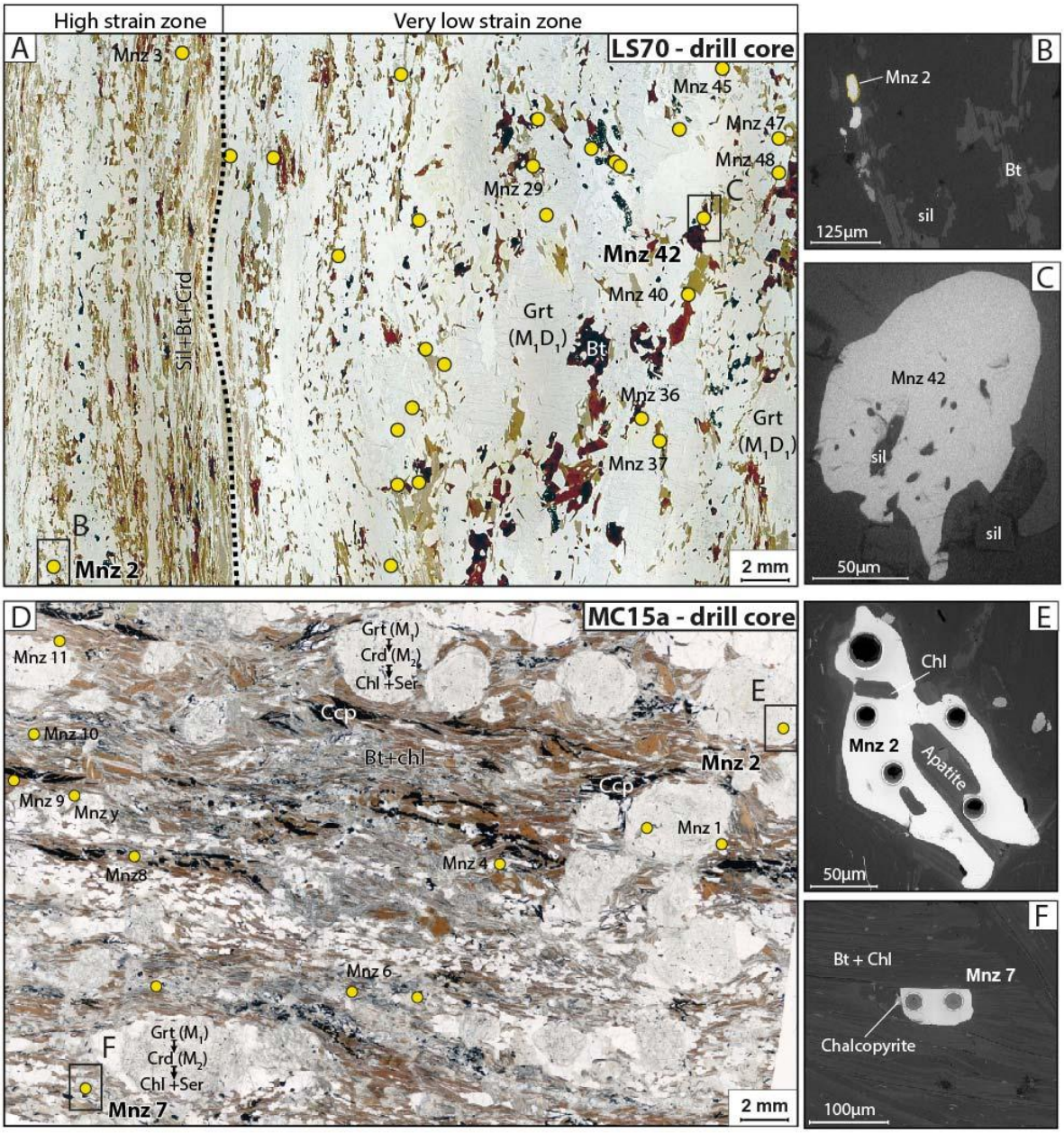

Fig.10:

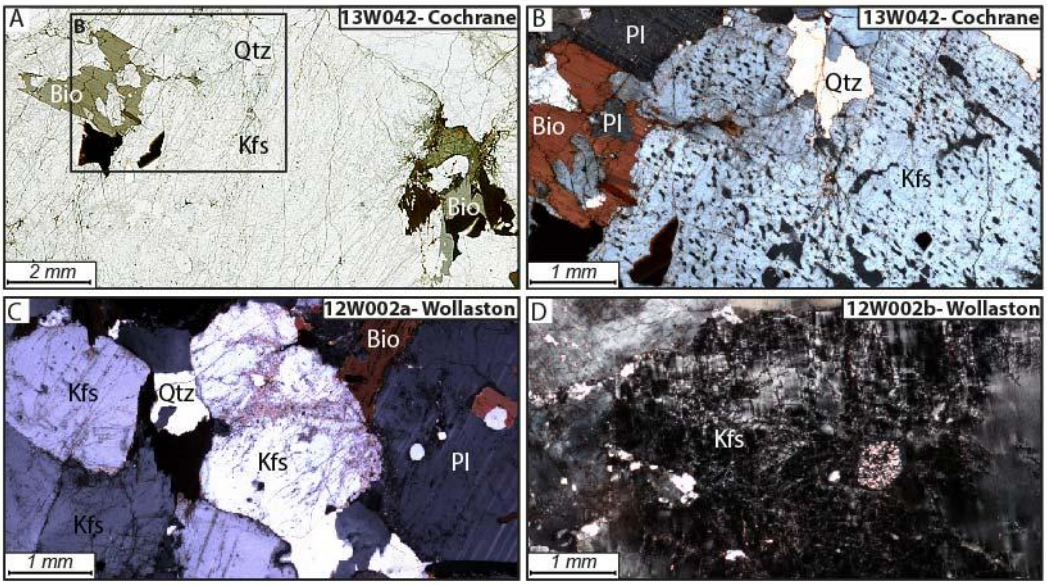

Fig.11:

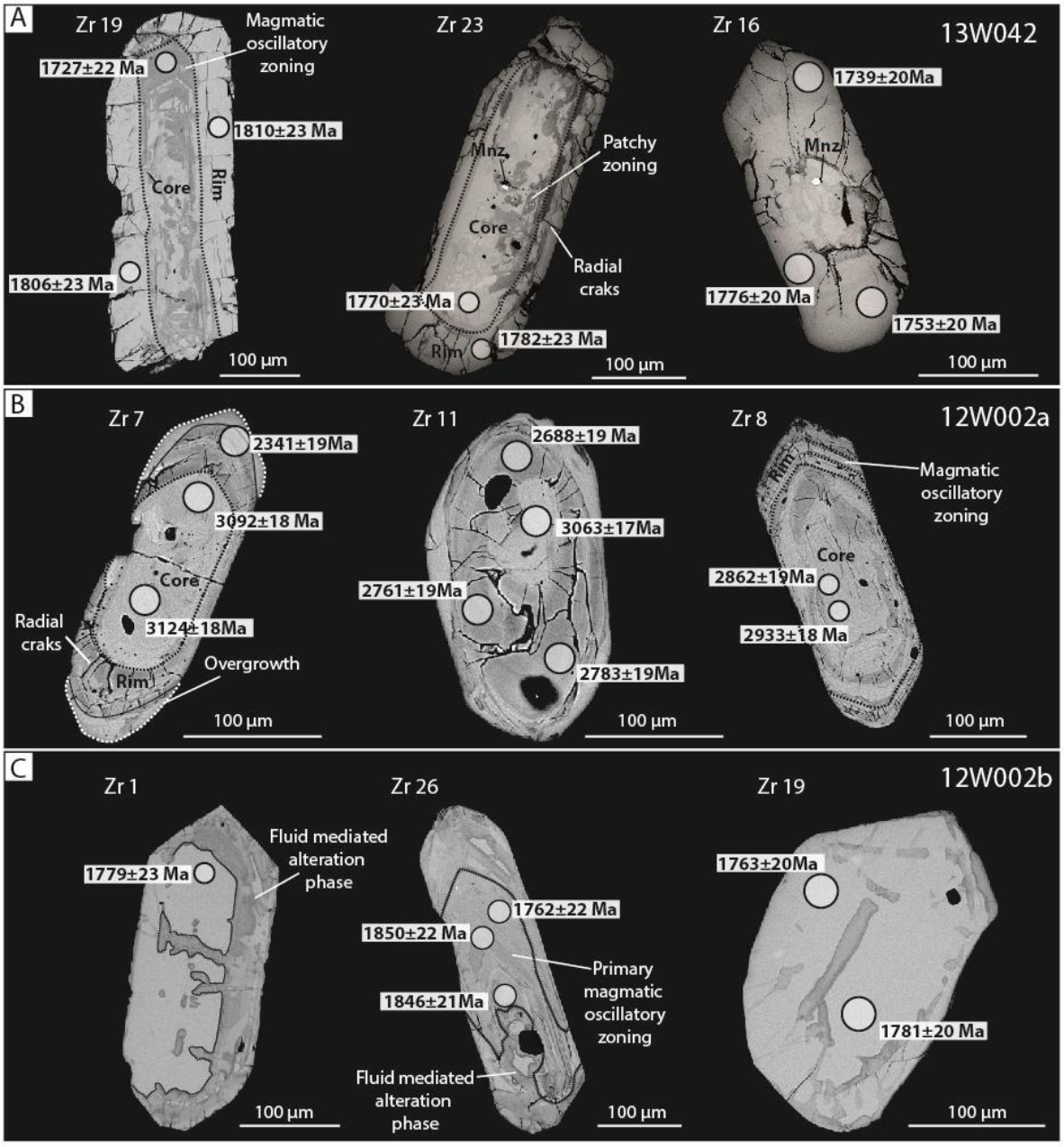

Fig.12:

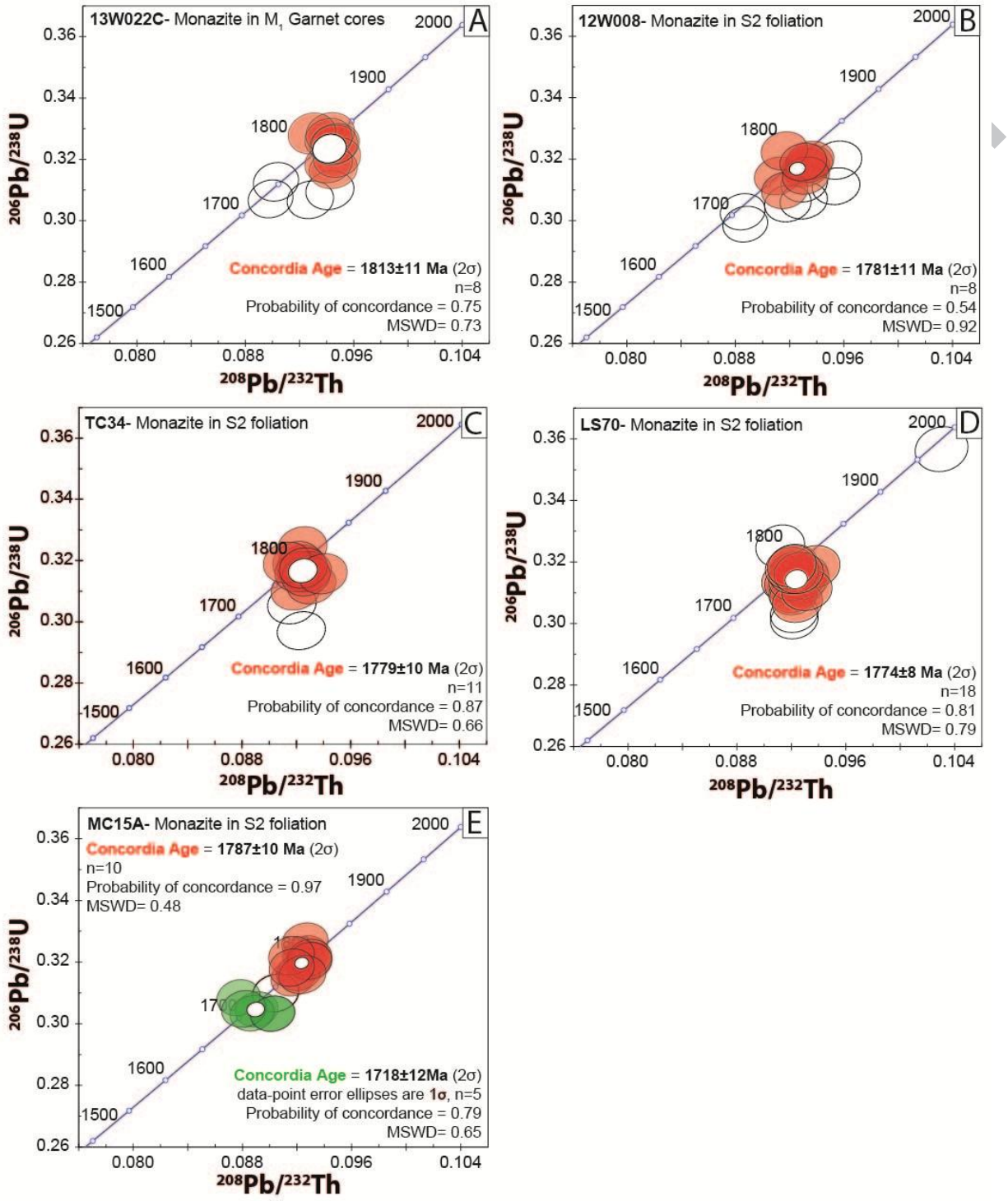

Fig.13:

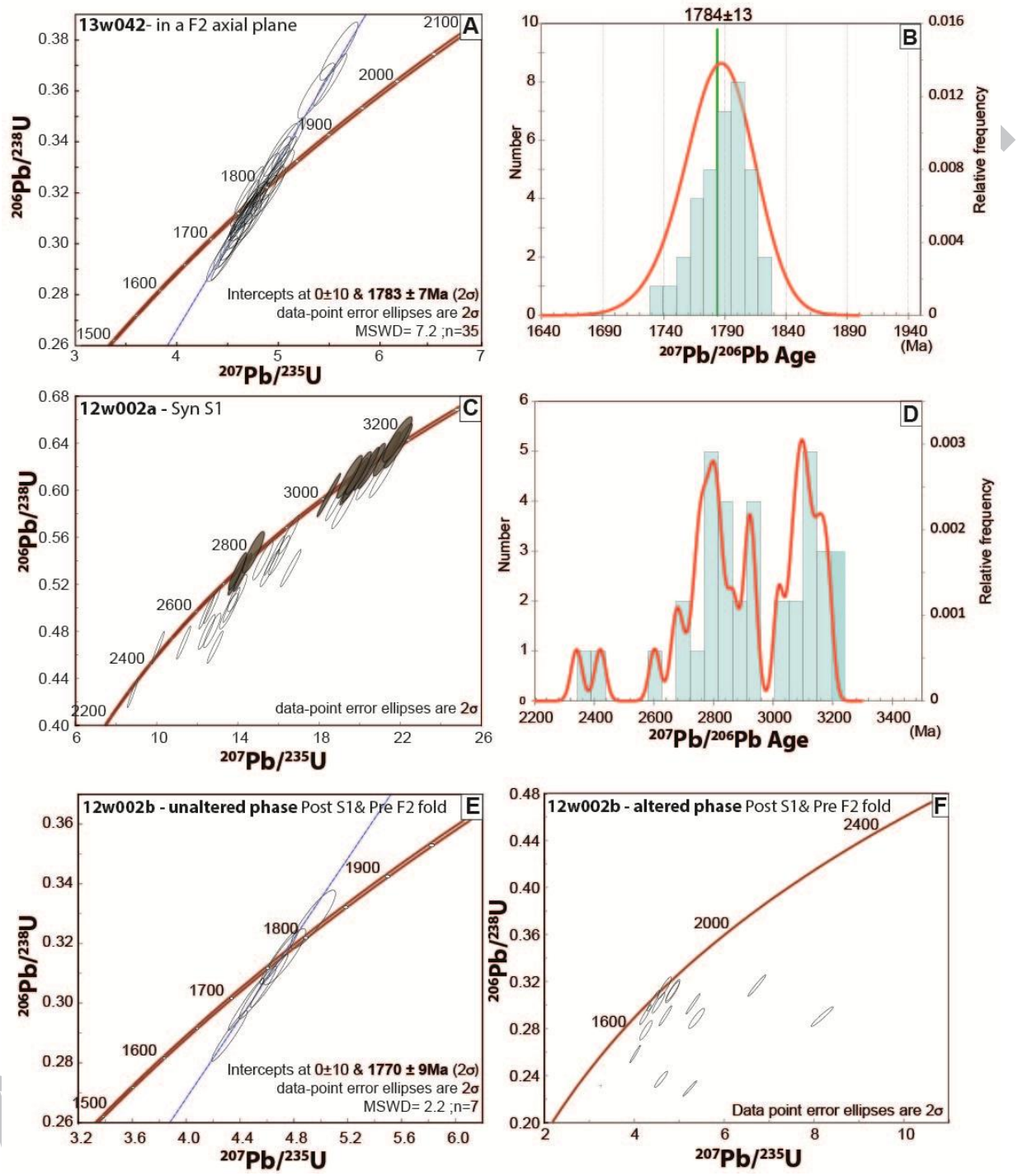

Fig.14:

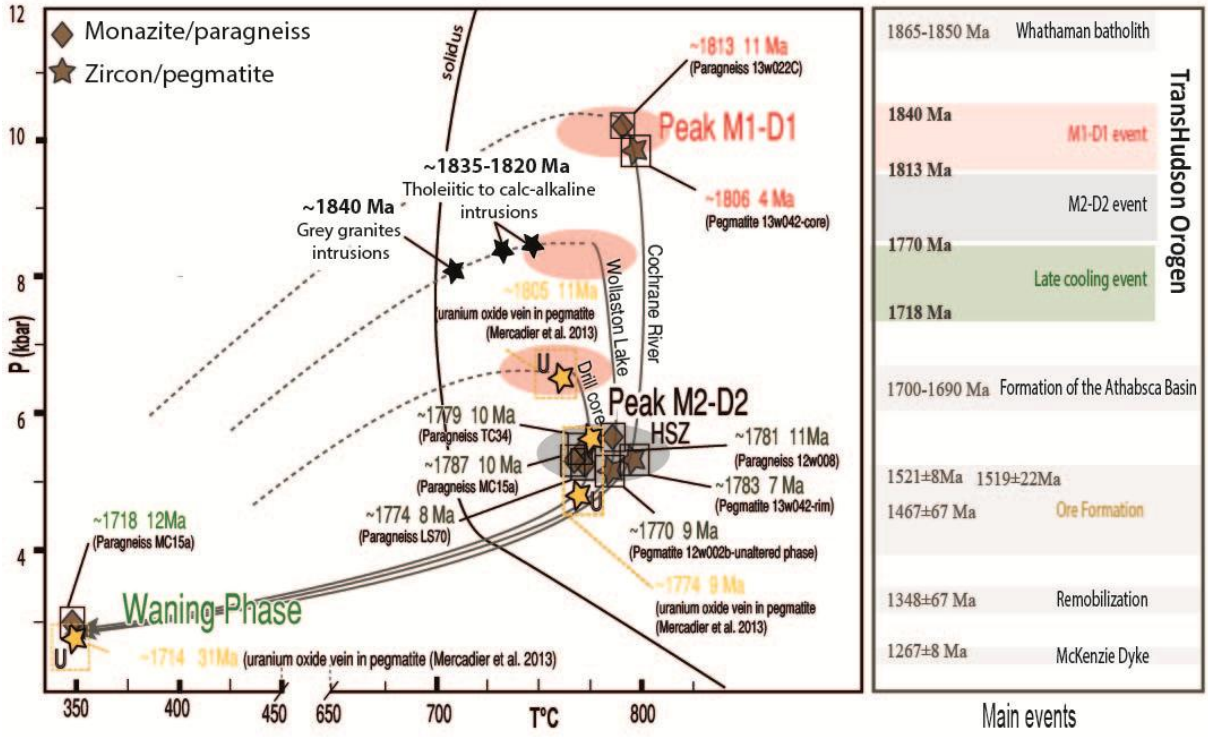

Fig.15:

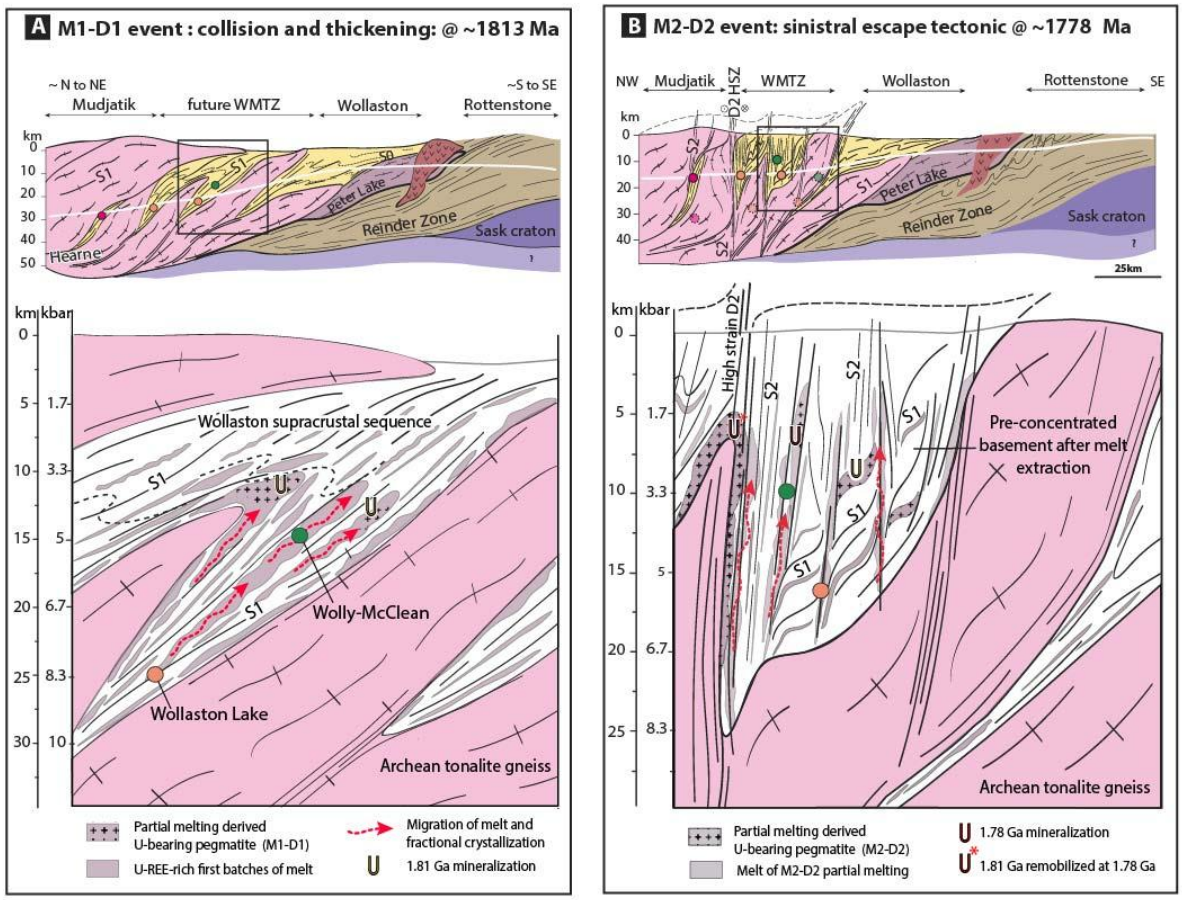

Tables

Table 1: Localities of samples discussed in text.

Area	samples	GPS coordinates X	GPS coordinates Y	description
Wolly-McClean	TC34	567413	6483274	grt-crd-metapelitic sample
	LS70	571103	6481524	grt-crd-metapelitic sample
	MCS15	567882	6457811	grt-crd-metapelitic sample
Wollaston Lake	12W008	604458	6491874	grt-crd-metapelitic sample
	12W002A	605890	6490759	pegmatitic sample
	12W002B	605890	6490759	pegmatitic sample
Cochrane River	13W042	621105	6524309	pegmatitic sample
	13W022C	622330	6521232	grt-crd-metapelitic sample

Table 2: U-Th/Pb monazite data from garnet-cordierite-bearing pelitic gneiss samples obtained using in-situ isotopic analysis by LA-ICP-MS

												Ages (Ma)					Pb	U	Th	
Samples	**Grains**		**Analysis_#**	**$^{207}Pb/^{235}U$**	**±1σ**	**$^{208}Pb/^{232}Th$**	**±1σ**	**$^{206}Pb/^{238}U$**	**±1σ**	**Rho**	**$^{207}Pb/^{235}U$**		**$^{208}Pb/^{232}Th$**		**$^{206}Pb/^{238}U$**		(ppm)	(ppm)	(ppm)	Th/U
13W022C	a	1	6030415	4.609	0.060	0.0947	0.0012	0.3207	0.0043	0.1	1751	11	1829	21	1793	21	2000	2622	14634	5.6
		2	7030415	4.425	0.058	0.0899	0.0011	0.3071	0.0041	0.1	1717	11	1739	20	1727	20	2314	2854	18832	6.6
	b	1	4030415	4.390	0.057	0.0928	0.0011	0.3068	0.0041	0.1	1710	11	1794	20	1725	21	4280	6575	29782	4.5
	c	1	8030415	4.529	0.059	0.0903	0.0011	0.3127	0.0042	0.1	1736	11	1747	20	1754	20	4278	3483	39943	11.5
	d	1	9030415	4.577	0.060	0.0941	0.0012	0.3189	0.0042	0.1	1745	11	1818	21	1784	21	3534	4760	25856	5.4
		2	10030415	4.692	0.061	0.0946	0.0012	0.3253	0.0043	0.1	1766	11	1827	21	1816	21	3120	3963	23224	5.9
	e	1	11030415	4.615	0.061	0.0945	0.0012	0.3170	0.0042	0.1	1752	11	1824	21	1775	21	4538	3424	41311	12.1
	f	1	12030415	4.691	0.062	0.0945	0.0012	0.3249	0.0043	0.1	1766	11	1825	21	1814	21	3827	3128	33942	10.8
		2	13030415	4.722	0.063	0.0941	0.0012	0.3269	0.0044	0.1	1771	11	1818	21	1823	21	3629	3230	31498	9.8
	g	1	18030415	4.641	0.063	0.0929	0.0012	0.3285	0.0045	0.1	1757	11	1795	22	1831	21	2344	894	24509	27.4
		2	19030415	4.382	0.059	0.0942	0.0012	0.3099	0.0042	0.1	1709	11	1820	21	1740	22	2498	2174	22361	10.3
		3	20030415	4.713	0.065	0.0942	0.0012	0.3286	0.0045	0.1	1770	11	1820	22	1832	22	2067	894	21029	23.5
12W008	6	a	4121113	4.226	0.050	0.0931	0.0011	0.3122	0.0040	0.1	1679	10	1799	21	1752	19	3372	4706	39439	8.4
		b	5121113	4.183	0.049	0.0916	0.0011	0.3098	0.0039	0.1	1671	10	1771	21	1740	19	3068	4380	36306	8.3
		c	6121113	4.249	0.050	0.0932	0.0011	0.3147	0.0040	0.1	1684	10	1800	21	1764	20	3043	4239	35558	8.4
	9	a	7121113	4.231	0.050	0.0954	0.0012	0.3114	0.0040	0.1	1680	10	1842	21	1747	19	3784	7585	36450	4.8
		b	8121113	4.328	0.051	0.0934	0.0011	0.3187	0.0041	0.1	1699	10	1804	21	1783	20	3652	7478	34976	4.7
		c	9121113	4.265	0.051	0.0932	0.0011	0.3173	0.0040	0.1	1687	10	1801	21	1776	20	3846	7779	37398	4.8
	8	a	11121113	4.242	0.051	0.0916	0.0011	0.3227	0.0041	0.1	1682	10	1771	21	1803	20	2983	2731	39923	14.6
		b	12121113	4.339	0.052	0.0930	0.0011	0.3191	0.0041	0.1	1701	10	1797	21	1785	20	3051	2154	42328	19.7
	7		17121113	4.065	0.049	0.0887	0.0011	0.2988	0.0038	0.1	1647	10	1718	20	1686	19	3321	4161	43358	10.4
			18121113	4.143	0.050	0.0885	0.0011	0.3029	0.0039	0.1	1663	10	1715	20	1706	19	3227	4168	41695	10.0
	3	a	19121113	4.599	0.056	0.0955	0.0012	0.3198	0.0041	0.1	1749	10	1844	22	1789	20	2282	6331	16349	2.6
		b	20121113	4.216	0.051	0.0931	0.0012	0.3067	0.0039	0.1	1677	10	1798	21	1724	19	2790	9034	17759	2.0
		c	21121113	4.162	0.051	0.0911	0.0011	0.3146	0.0041	0.1	1667	10	1762	21	1763	20	2863	7815	22615	2.9
	1		22121113	4.099	0.050	0.0919	0.0011	0.3057	0.0039	0.1	1654	10	1777	21	1720	19	3099	4720	36448	7.7
			23121113	4.319	0.053	0.0935	0.0012	0.3197	0.0041	0.1	1697	10	1807	21	1788	20	3334	5368	36944	6.9
TC34	44	a	22020415	4.569	0.064	0.0924	0.0012	0.3239	0.0045	0.1	1744	12	1787	22	1809	22	3668	2311	35996	15.6
		b	23020415	4.534	0.066	0.0924	0.0012	0.3180	0.0045	0.1	1737	12	1785	22	1780	22	1285	1028	11978	11.7
	46		25020415	4.367	0.092	0.0917	0.0012	0.3058	0.0043	0.1	1706	12	1773	22	1720	21	3852	3089	36411	11.8
	45	a	26020415	4.416	0.092	0.0919	0.0012	0.3099	0.0043	0.1	1715	12	1778	22	1740	21	3664	3539	32567	9.2
		b	27020415	4.507	0.092	0.0920	0.0012	0.3192	0.0044	0.1	1732	12	1780	22	1786	22	3534	3377	31154	9.2
	48		28020415	4.510	0.093	0.0931	0.0012	0.3121	0.0043	0.1	1733	12	1799	22	1751	21	5621	6216	46714	7.5
	42	a	33020415	4.456	0.093	0.0928	0.0012	0.3160	0.0044	0.1	1723	12	1793	22	1770	21	2389	2835	19093	6.7
		b	34020415	4.443	0.092	0.0922	0.0012	0.3160	0.0044	0.1	1721	12	1783	22	1770	21	2545	2465	22125	9.0
	34	a	35020415	4.460	0.093	0.0927	0.0012	0.3147	0.0044	0.1	1724	12	1792	22	1764	21	3654	1465	37840	25.8
		b	36020415	4.471	0.091	0.0913	0.0012	0.3191	0.0044	0.1	1726	12	1766	21	1785	22	3340	1356	34968	25.8
		c	37020415	4.432	0.093	0.0925	0.0012	0.3173	0.0044	0.1	1718	12	1788	22	1777	22	3398	1253	35475	28.3
		d	38020415	4.169	0.092	0.0924	0.0012	0.2971	0.0041	0.1	1668	12	1786	22	1677	20	4586	7367	31999	4.3
	28	a	39020415	4.472	0.094	0.0939	0.0012	0.3153	0.0044	0.1	1726	12	1815	22	1767	21	3746	1795	37206	20.7

Table 2: ***(Continued)***

Samples	Grains		Analysis_#	$^{207}Pb/^{235}U$	$\pm1\sigma$	$^{208}Pb/^{232}Th$	$\pm1\sigma$	$^{206}Pb/^{238}U$	$\pm1\sigma$	Rho	Ages (Ma) $^{207}Pb/^{235}U$		$^{208}Pb/^{232}Th$		$^{206}Pb/^{238}U$		Pb (ppm)	U (ppm)	Th (ppm)	Th/U
LS70	2	a	7020415a	4.429	0.069	0.0915	0.0011	0.3137	0.0042	0.1	1718	13	1770	20	1759	21	5328	6552	43546	6.6
		b	8020415a	4.442	0.070	0.0924	0.0011	0.3160	0.0043	0.1	1720	13	1786	20	1770	21	5048	7178	37774	5.3
		c	9020415a	4.371	0.070	0.0929	0.0011	0.3126	0.0042	0.1	1707	13	1795	20	1754	21	5788	9038	40879	4.5
	3	b	11020415a	4.402	0.073	0.0921	0.0011	0.3160	0.0043	0.1	1713	14	1780	20	1770	21	5167	6748	40473	6.0
	29	a	5020415b	4.597	0.063	0.0918	0.0011	0.3130	0.0042	0.1	1749	11	1775	21	1756	21	3285	3325	28759	8.6
		b	7020415b	5.153	0.071	0.1030	0.0013	0.3567	0.0048	0.1	1845	12	1982	24	1966	23	3535	3471	26610	7.7
	36	b	9020415b	4.400	0.062	0.0922	0.0012	0.3033	0.0041	0.1	1712	12	1783	21	1708	20	2861	4678	20087	4.3
	37	a	10020415	4.598	0.065	0.0930	0.0012	0.3156	0.0043	0.1	1749	12	1798	21	1768	21	3018	2861	26686	9.3
		b	11020415	4.291	0.061	0.0922	0.0012	0.3012	0.0041	0.1	1692	12	1783	21	1697	20	3891	6099	28274	4.6
	39		12020415b	4.536	0.066	0.0921	0.0012	0.3098	0.0042	0.1	1738	12	1781	21	1740	21	2603	3442	20487	6.0
	40		13020415b	4.365	0.064	0.0922	0.0012	0.3090	0.0042	0.1	1706	12	1783	21	1736	21	5145	4920	46223	9.4
	42	a	14020415b	4.586	0.068	0.0930	0.0012	0.3144	0.0043	0.1	1747	12	1798	22	1762	21	3404	6027	21759	3.6
		b	5020415c	4.715	0.067	0.0922	0.0012	0.3187	0.0046	0.1	1770	12	1782	22	1784	22	4114	3560	38600	10.8
		c	6020415c	4.672	0.065	0.0938	0.0012	0.3183	0.0045	0.1	1762	12	1811	23	1782	22	3611	3667	31636	8.6
		d	7020415c	4.557	0.064	0.0922	0.0012	0.3141	0.0045	0.1	1741	12	1783	22	1761	22	4484	9433	25378	2.7
		e	8020415c	4.415	0.061	0.0925	0.0012	0.3068	0.0043	0.1	1715	12	1788	22	1725	21	4424	5027	38119	7.6
		f	9020415c	4.399	0.061	0.0932	0.0012	0.3108	0.0044	0.1	1712	11	1801	23	1745	22	5016	4887	45039	9.2
		g	10020415c	4.632	0.067	0.0922	0.0012	0.3164	0.0045	0.1	1755	12	1783	22	1772	22	3839	1204	42249	35.1
	45	b	13020415c	4.593	0.065	0.0920	0.0012	0.3178	0.0045	0.1	1748	12	1778	22	1779	22	2526	1090	26838	24.6
	47	a	19020415c	4.699	0.066	0.0912	0.0012	0.3252	0.0046	0.1	1767	12	1764	22	1815	22	3003	1928	29850	15.5
		b	20020415c	4.554	0.064	0.0926	0.0012	0.3163	0.0044	0.1	1741	12	1790	22	1772	22	3058	2140	29526	13.8
	48		21020415c	4.647	0.066	0.0921	0.0012	0.3185	0.0045	0.1	1758	12	1780	22	1783	22	2526	1853	24175	13.0
MC15A	2	a	8121113	4.368	0.051	0.0916	0.0011	0.3150	0.0039	0.1	1706	10	1772	20	1765	19	4502	3423	41100	12.0
		b	9121113	4.422	0.052	0.0921	0.0011	0.3167	0.0039	0.1	1717	10	1780	20	1774	19	3779	2673	34988	13.1
		c	10121113	4.650	0.055	0.0929	0.0011	0.3215	0.0040	0.1	1758	10	1795	20	1797	19	3842	2734	35142	12.9
		d	11121113	4.477	0.053	0.0929	0.0011	0.3205	0.0040	0.1	1727	10	1795	20	1792	19	4232	3151	38440	12.2
	4		14121113	4.104	0.049	0.0890	0.0010	0.3047	0.0038	0.1	1655	10	1723	19	1715	19	4205	3597	39249	10.9
	6		21121113	4.422	0.054	0.0926	0.0011	0.3225	0.0041	0.1	1717	10	1790	20	1802	20	4486	5129	36190	7.1
	8	a	22121113	4.190	0.051	0.0877	0.0010	0.3085	0.0039	0.1	1672	10	1698	19	1733	19	5137	2799	54549	19.5
		b	24121113	4.187	0.052	0.0886	0.0011	0.3034	0.0038	0.1	1671	10	1717	20	1708	19	4515	4194	42364	10.1
		c	23121113	4.208	0.052	0.0902	0.0011	0.3033	0.0038	0.1	1676	10	1745	20	1708	19	5972	6530	51956	8.0
	7		25121113	4.367	0.054	0.0916	0.0011	0.3183	0.0040	0.1	1781	20	1706	10	1771	20	3586	1619	37576	23.2
	9		29121113	4.561	0.058	0.0925	0.0011	0.3266	0.0042	0.1	1742	11	1789	21	1822	20	3986	3661	35577	9.7
	11		38121113	4.481	0.060	0.0928	0.0011	0.3203	0.0042	0.1	1727	11	1794	21	1791	20	4855	4265	45139	10.6
	10	a	30121113	4.475	0.057	0.0916	0.0011	0.3222	0.0041	0.1	1726	11	1771	21	1800	20	4290	2398	43919	18.3
		b	34121113	4.304	0.056	0.0924	0.0011	0.3161	0.0041	0.1	1694	11	1785	21	1771	20	4246	2609	42935	16.5
		c	35121113	4.258	0.056	0.0904	0.0011	0.3101	0.0040	0.1	1685	11	1750	21	1741	20	3944	2397	41059	17.1
	11		36121113	4.218	0.056	0.0881	0.0011	0.3048	0.0040	0.1	1678	11	1706	20	1715	20	4396	3662	44115	12.0

Table 3: U-Pb zircon data from pegmatitic samples obtained using in-situ isotopic analysis by LA-ICP-MS

Sample: 13W042		Spot	Pb	Th	U									Age (Ma)						
Analysis_#	zircon	location	(ppm)	(ppm)	(ppm)	Th/U	$^{207}Pb/^{206}Pb$	1σ	$^{207}Pb/^{235}U$	1σ	$^{206}Pb/^{238}U$	1 σ	Rho	$^{207}Pb/^{235}U$		$^{206}Pb/^{238}U$		$^{207}Pb/^{206}Pb$		% Conc.
30190514	14a	core	-	-	-	-	0.1084	0.0013	4.958	0.066	0.3320	0.0041	0.9321	1812	11	1848	20	1772	21	102.3
31190514	14b	rim	-	-	-	-	0.1080	0.0013	4.848	0.066	0.3256	0.0041	0.9227	1793	11	1817	20	1766	22	101,5
32190514	14c	rim	-	-	-	-	0.1092	0.0013	4.949	0.067	0.3287	0.0041	0.9241	1811	11	1832	20	1786	22	101.4
33190514	14d	core	-	-	-	-	0.1091	0.0013	5.101	0.068	0.3392	0.0042	0.9244	1836	11	1883	20	1784	22	102.9
34190514	9a	rim	-	-	-	-	0.1081	0.0013	5.021	0.069	0.3369	0.0042	0.9126	1823	12	1872	20	1768	23	103.1
35190514	9b	rim	-	-	-	-	0.1094	0.0014	4.514	0.063	0.2992	0.0038	0.9070	1734	12	1688	19	1790	23	96.8
38190514	17a	rim	-	-	-	-	0.1081	0.0013	5.596	0.076	0.3756	0.0047	0.9115	1916	12	2056	22	1767	22	108.4
39190514	19a	core	-	-	-	-	0.1057	0.0013	3.147	0.043	0.2159	0.0027	0.9133	1444	10	1260	14	1727	22	83.6
43190514	19b	rim	-	-	-	-	0.1106	0.0014	4.987	0.069	0.3270	0.0041	0.8996	1817	12	1824	20	1810	23	100.4
44190514	19c	rim	-	-	-	-	0.1104	0.0014	4.828	0.067	0.3173	0.0039	0.8977	1790	12	1776	19	1806	23	99.1
45190514	23a	rim	-	-	-	-	0.1090	0.0014	4.730	0.066	0.3149	0.0039	0.8913	1773	12	1765	19	1782	23	99.5
47190514	23c	core	-	-	-	-	0.1083	0.0014	5.373	0.075	0.3600	0.0045	0.8916	1881	12	1982	21	1770	23	106.2
48190514	1a	rim	-	-	-	-	0.1097	0.0014	4.448	0.063	0.2942	0.0037	0.8839	1721	12	1662	18	1794	24	95.9
49190514	1b	rim	-	-	-	-	0.1109	0.0014	4.899	0.069	0.3205	0.0040	0.8858	1802	12	1792	19	1814	23	99.3
50190514	1c	core	-	-	-	-	0.1095	0.0014	4.629	0.065	0.3068	0.0038	0.8820	1755	12	1725	19	1790	24	98.0
51190514	4a	-	-	-	-	-	0.1102	0.0015	4.672	0.066	0.3076	0.0038	0.8801	1762	12	1729	19	1803	24	97.8
52190514	4b	-	-	-	-	-	0.1096	0.0015	4.691	0.066	0.3105	0.0038	0.8755	1766	12	1743	19	1793	24	98.5
53190514	5a	-	-	-	-	-	0.1098	0.0015	4.583	0.065	0.3028	0.0038	0.8726	1746	12	1705	19	1796	24	97.2
5200514a	5b	-	133	88	444	0.20	0.1103	0.0012	4.470	0.054	0.2940	0.0034	0.9713	1725	10	1662	17	1804	19	95.6
8200514a	6c	-	134	108	1505	0.07	0.1101	0.0012	4.543	0.055	0.2994	0.0035	0.9698	1739	10	1688	17	1801	19	96.6
11200514a	11a	-	146	161	3904	0.04	0.1090	0.0012	4.661	0.056	0.3101	0.0036	0.9690	1760	10	1741	18	1783	19	98.7
12200514a	11b	-	131	278	445	0.63	0.1085	0.0012	4.641	0.056	0.3102	0.0036	0.9690	1757	10	1742	18	1775	20	99.0
13200514a	11c	-	136	155	360	0.43	0.1088	0.0012	4.699	0.056	0.3132	0.0037	0.9703	1767	10	1757	18	1780	19	99.3
14200514a	12a	-	99	175	407	0.43	0.1081	0.0012	4.657	0.056	0.3125	0.0037	0.9670	1760	10	1753	18	1768	20	99.5
18200514a	12b	-	92	146	261	0.56	0.1090	0.0012	4.764	0.058	0.3170	0.0037	0.9623	1779	10	1775	18	1783	20	99.8
19200514a	12c	-	89	154	247	0.62	0.1096	0.0012	4.889	0.059	0.3235	0.0038	0.9621	1800	10	1807	18	1793	20	100.4
21200514a	15b	core	647	83	2064	0.04	0.1106	0.0012	4.910	0.059	0.3220	0.0037	0.9672	1804	10	1799	18	1810	19	99.7
22200514a	16a	rim	141	213	407	0.53	0.1072	0.0012	4.670	0.057	0.3160	0.0037	0.9542	1762	10	1770	18	1753	20	100.5
23200514a	16b	rim	90	164	248	0.66	0.1064	0.0012	4.711	0.058	0.3212	0.0038	0.9527	1769	10	1796	18	1739	20	101.8
25200514a	16d	rim	142	127	440	0.29	0.1086	0.0012	4.662	0.056	0.3114	0.0036	0.9608	1760	10	1748	18	1776	20	99.1
31200514a	18c	-	1675	231	7844	0.03	0.1075	0.0012	3.285	0.039	0.2216	0.0026	0.9625	1477	9	1290	13	1758	20	84.0
34200514a	24b	core	910	94	2837	0.03	0.1097	0.0012	5.031	0.061	0.3327	0.0038	0.9571	1825	10	1851	19	1795	20	101.7
35200514a	24d	rim	168	226	508	0.45	0.1113	0.0013	4.761	0.059	0.3104	0.0036	0.9405	1778	10	1743	18	1820	21	97.7

37200514a	29b	core	3882	228	11062	0.02	0.1097	0.0012	5.511	0.067	0.3644	0.0042	0.9533	1902	10	2003	20	1795	20	106.0
39200514a	31b	-	1545	111	5077	0.02	0.1098	0.0012	4.770	0.058	0.3153	0.0036	0.9509	1780	10	1767	18	1795	20	99.1

Table 3: ***(Continued)***

Sample: 12W002a																				
		Spot	Pb	Th	U									Age (Ma)						
Analysis_#	zircon	location	(ppm)	(ppm)	(ppm)	Th/U	$^{207}Pb/^{206}Pb$	1σ	$^{207}Pb/^{235}U$	1σ	$^{206}Pb/^{238}U$	1 σ	Rho	$^{207}Pb/^{235}U$		$^{206}Pb/^{238}U$		$^{207}Pb/^{206}Pb$		% Conc.
5190514a	1a	core	247	61	371	0.16	0.2249	0.0024	18.480	0.237	0.5959	0.0075	0.9855	3015	12	3013	30	3016	17	100
6190514a	1b	core	623	644	929	0.69	0.2104	0.0022	15.794	0.203	0.5444	0.0069	0.9811	2864	12	2802	29	2909	17	98.5
8190514a	2b	core	396	305	532	0.57	0.2351	0.0025	19.648	0.255	0.6063	0.0077	0.9737	3074	13	3055	31	3087	17	99.6
5190514b	2c	rim	92	18	192	0.09	0.1567	0.0017	10.067	0.127	0.4661	0.0057	0.9724	2441	12	2466	25	2420	18	100.9
6190514b	5c	core	234	127	383	0.33	0.2257	0.0025	16.603	0.209	0.5338	0.0065	0.9740	2912	12	2757	27	3022	17	96.4
11190514a	7a	core	344	283	459	0.62	0.2358	0.0026	19.787	0.261	0.6088	0.0077	0.9570	3081	13	3065	31	3092	18	99.7
12190514a	7b	core	236	118	323	0.36	0.2406	0.0027	20.587	0.274	0.6207	0.0079	0.9506	3119	13	3113	31	3124	18	99.9
7190514b	7c	rim	126	13	288	0.04	0.1496	0.0016	8.820	0.111	0.4278	0.0052	0.9718	2320	11	2296	24	2341	19	99.1
13190514a	8a	core	387	195	621	0.31	0.2136	0.0024	16.035	0.215	0.5447	0.0069	0.9452	2879	13	2803	29	2933	18	98.2
14190514a	8b	core	358	210	577	0.36	0.2045	0.0024	15.233	0.206	0.5404	0.0068	0.9380	2830	13	2785	29	2862	19	98.9
9190514b	11a	core	36	51	55	0.93	0.1839	0.0021	12.724	0.166	0.5020	0.0063	0.9606	2659	12	2622	27	2688	19	98.9
10190514b	11b	core	441	303	622	0.49	0.2316	0.0025	18.889	0.235	0.5916	0.0072	0.9743	3036	12	2996	29	3063	17	99.1
11190514b	11c	core	47	57	72	0.79	0.1922	0.0023	13.966	0.185	0.5272	0.0067	0.9568	2747	13	2730	28	2761	19	99.5
12190514b	11d	core	32	40	49	0.82	0.1948	0.0023	14.236	0.185	0.5302	0.0066	0.9605	2766	12	2742	28	2783	19	99.4
13190514b	12a	rim	81	11	154	0.07	0.1819	0.0020	12.456	0.157	0.4967	0.0061	0.9675	2639	12	2600	26	2671	18	98.8
14190514b	12b	rim	125	51	247	0.21	0.1747	0.0019	11.326	0.143	0.4704	0.0057	0.9668	2550	12	2485	25	2603	18	98.0
18190514b	12c	core	400	318	526	0.60	0.2386	0.0026	20.337	0.255	0.6183	0.0075	0.9659	3108	12	3103	30	3111	17	99.9
19190514b	12d	core	353	101	693	0.14	0.2002	0.0022	12.874	0.162	0.4665	0.0057	0.9632	2671	12	2468	25	2828	18	94.4
21190514b	13a	core	427	407	546	0.75	0.2505	0.0028	21.120	0.266	0.6117	0.0074	0.9620	3144	12	3077	30	3188	17	98.6
22190514b	13b	core	209	58	383	0.15	0.1975	0.0022	13.680	0.173	0.5025	0.0061	0.9599	2728	12	2624	26	2806	18	97.2
23190514b	13c	core	313	224	421	0.53	0.2434	0.0027	20.460	0.259	0.6098	0.0074	0.9583	3113	12	3069	30	3142	18	99.1
24190514b	13d	core	518	426	723	0.59	0.2385	0.0027	19.213	0.243	0.5845	0.0071	0.9576	3053	12	2967	29	3110	18	98.2
25190514b	13e	rim	35	18	66	0.27	0.1886	0.0023	12.465	0.168	0.4795	0.0061	0.9390	2640	13	2525	26	2730	20	96.7
26190514b	14a	core	634	466	1009	0.46	0.2117	0.0024	15.575	0.198	0.5337	0.0065	0.9534	2851	12	2757	27	2919	18	97.7
27190514b	14b	core	585	393	889	0.44	0.2131	0.0024	16.515	0.210	0.5622	0.0068	0.9511	2907	12	2876	28	2929	18	99.2
31190514b	15a	core	262	56	682	0.08	0.2052	0.0024	10.281	0.133	0.3635	0.0044	0.9434	2460	12	1999	21	2868	19	85.8
33190514b	16a	core	153	96	202	0.48	0.2490	0.0029	21.892	0.283	0.6378	0.0078	0.9390	3179	13	3181	31	3178	18	100.0
34190514b	16b	core	275	218	361	0.60	0.2455	0.0028	21.351	0.276	0.6308	0.0077	0.9370	3155	13	3153	30	3156	18	100.0
35190514b	17a	core	258	53	386	0.14	0.2353	0.0027	19.939	0.259	0.6146	0.0075	0.9354	3088	13	3088	30	3089	18	100.0
36190514b	17b	core	279	105	411	0.25	0.2313	0.0027	19.497	0.254	0.6114	0.0074	0.9333	3067	13	3076	30	3061	19	100.2
38190514b	21b	rim	505	286	858	0.33	0.1911	0.0023	13.988	0.183	0.5311	0.0065	0.9280	2749	12	2746	27	2751	19	99.9
44190514b	23a	rim	30	44	47	0.94	0.1977	0.0025	13.550	0.186	0.4972	0.0062	0.9070	2719	13	2602	27	2807	21	96.8
45190514b	23b	rim	36	53	59	0.91	0.1922	0.0025	12.733	0.175	0.4807	0.0060	0.9043	2660	13	2530	26	2761	21	96.4
46190514b	25a	core	176	116	225	0.52	0.2465	0.0030	21.859	0.294	0.6432	0.0079	0.9077	3178	13	3201	31	3163	19	100.5
47190514b	25b	rim	28	62	34	1.82	0.1957	0.0028	14.762	0.218	0.5472	0.0072	0.8910	2800	14	2813	30	2791	23	100.3
48190514b	25c	rim	27	66	35	1.89	0.1976	0.0026	13.964	0.197	0.5126	0.0065	0.8959	2747	13	2668	28	2807	21	97.9

Table 3: ***(Continued)***

Sample: 12W002b		Pb	Th	U										Age (Ma)					
Analysis_#	**zircon**	**(ppm)**	**(ppm)**	**(ppm)**	**Th/U**	**$^{207}Pb/^{206}Pb$**	**1σ**	**$^{207}Pb/^{235}U$**	**1σ**	**$^{206}Pb/^{238}U$**	**1 σ**	**Rho**	**$^{207}Pb/^{235}U$**		**$^{206}Pb/^{238}U$**		**$^{207}Pb/^{206}Pb$**		**% Conc.**
Unaltered phase (core – Fig. 13E)																			
50190514b	1b	711	216	2276	0.09	0.1088	0.0014	4.731	0.064	0.3156	0.0038	0.8969	1773	11	1768	19	1779	23	99.7
53190514b	4a	514	158	1578	0.10	0.1093	0.0014	4.943	0.068	0.3281	0.0040	0.8862	1810	12	1829	19	1788	23	101.2
12190514c	17a	662	183	2257	0.08	0.1076	0.0012	4.444	0.054	0.2996	0.0036	0.9748	1721	10	1690	18	1759	19	97.8
20190514c	19a	662	179	2191	0.08	0.1089	0.0012	4.616	0.057	0.3075	0.0037	0.9656	1752	10	1729	18	1781	20	98.4
22190514c	19c	604	154	1951	0.08	0.1078	0.0012	4.692	0.058	0.3156	0.0038	0.9629	1766	10	1768	18	1763	20	100.1
23190514c	25a	503	164	1768	0.09	0.1085	0.0012	4.322	0.054	0.2890	0.0035	0.9560	1698	10	1637	17	1774	20	95.7
24190514c	25b	516	159	1726	0.09	0.1083	0.0012	4.532	0.057	0.3036	0.0036	0.9558	1737	10	1709	18	1771	20	98.1
Altered phase (rim– Fig. 13F)																			
6190514c	4c	948	339	3451	0.10	0.1660	0.0018	5.237	0.063	0.2289	0.0027	0.9812	1859	10	1329	14	2517	18	73.8
7190514c	4d	484	129	1344	0.10	0.1542	0.0017	6.729	0.082	0.3165	0.0038	0.9768	2076	11	1773	18	2393	18	86.8
36190514c	9a	342	96	1137	0.08	0.1091	0.0013	4.541	0.059	0.3018	0.0036	0.9304	1739	11	1700	18	1785	21	97.4
8190514c	11a	1035	385	3948	0.10	0.1129	0.0012	4.020	0.049	0.2582	0.0031	0.9800	1638	10	1481	16	1847	19	88.7
10190514c	11c	310	79	1055	0.07	0.1171	0.0013	4.694	0.058	0.2909	0.0035	0.9671	1766	10	1646	17	1912	20	92.4
11190514c	11d	884	213	2790	0.08	0.1279	0.0014	5.308	0.064	0.3010	0.0036	0.9784	1870	10	1696	18	2070	19	90.4
37190514c	13	1230	601	4608	0.13	0.1409	0.0016	4.597	0.060	0.2367	0.0029	0.9301	1749	11	1370	15	2238	20	78.1
38190514c	15	512	190	9839	0.02	0.0848	0.0010	0.621	0.008	0.0531	0.0006	0.9277	490	5	333	4	1312	23	37.4
39190514c	16	1533	103	11322	0.01	0.4477	0.0053	3.976	0.052	0.0644	0.0008	0.9288	1629	11	403	5	4078	17	40.0
19190514c	17e	939	214	2490	0.09	0.2046	0.0022	8.183	0.101	0.2901	0.0035	0.9673	2252	11	1642	17	2863	18	78.6
40190514c	21	292	251	12080	0.02	0.0597	0.0008	0.213	0.003	0.0259	0.0003	0.8754	196	3	165	2	594	28	33.1
25190514c	25c	584	409	3249	0.13	0.0915	0.0010	2.246	0.028	0.1780	0.0021	0.9558	1196	9	1056	12	1458	21	82.0
41190514c	26a	1300	228	4210.1	0.05	0.1128	0.0013	4.861	0.064	0.3125	0.0038	0.9198	1796	11	1753	19	1846	21	97.3
45190514c	26b	1262	220	4299	0.05	0.1131	0.0014	4.850	0.065	0.3110	0.0038	0.9104	1794	11	1746	19	1850	22	96.9
46190514c	26c	1660	150	5695	0.03	0.1078	0.0013	4.673	0.062	0.3146	0.0038	0.9063	1763	11	1763	19	1762	22	100.0
47190514c	32a	891	235	2997	0.08	0.1354	0.0017	5.389	0.072	0.2886	0.0035	0.9053	1883	12	1635	18	2170	21	86.8
48190514c	32b	866	260	3259	0.08	0.1110	0.0014	4.261	0.058	0.2785	0.0034	0.9002	1686	11	1584	17	1815	22	92.9
49190514c	36	362	497	15453	0.03	0.0646	0.0008	0.228	0.003	0.0256	0.0003	0.8764	208	3	163	2	761	27	27.4
32190514c	39a	1008	336	3485	0.10	0.1057	0.0012	4.251	0.054	0.2918	0.0035	0.9441	1684	10	1651	17	1726	21	97.6
33190514c	39b	1063	409	3524	0.12	0.1058	0.0012	4.429	0.056	0.3036	0.0036	0.9407	1718	11	1709	18	1729	21	99.4

Supplementary Table 1. Operating conditions for the LA-ICP-MS equipment

Laboratory & Sample Preparation	
Laboratory name	Géosciences Rennes, UMR CNRS 6118, Rennes, France
Sample type/mineral	Monazite and zircon
Sample preparation	Polished thin sections (Mnz) or epoxy resin mount (Zrn)
Imaging	Back-scattered electron imaging (MIMENTO platform in Besançon and University of Lille 1)
Laser ablation system	
Make, Model & type	ESI NWR193UC, Excimer
Ablation cell	ESI NWR TwoVol2
Laser wavelength	193 nm
Pulse width	< 5 ns
Fluence	6 – 6.55 J/cm-2
Repetition rate	3 Hz (Mnz) and 4 Hz (Zrn)
Spot size	10 µm (Mnz) and 25 µm (Zrn)
Sampling mode / pattern	Single spot
Carrier gas	100% He, Ar make-up gas and N_2 (3 ml/mn) combined using in-house smoothing device
Background collection	20 seconds
Ablation duration	60 seconds
Wash-out delay	15 seconds
Cell carrier gas flow (He)	0.75 l/min
ICP-MS Instrument	
Make, Model & type	Agilent 7700x, Q-ICP-MS
Sample introduction	Via conventional tubing
RF power	1350W
Sampler, skimmer cones	Ni
Extraction lenses	X type
Make-up gas flow (Ar)	0.87 l/min
Detection system	Single collector secondary electron multiplier
Data acquisition protocol	Time-resolved analysis
Scanning mode	Peak hopping, one point per peak
Detector mode	Pulse counting, dead time correction applied, and analog mode when signal intensity > ~ 10^6 cps
Masses measured	^{204}(Hg + Pb), ^{206}Pb, ^{207}Pb, ^{208}Pb, ^{232}Th, ^{238}U
Integration time per peak	10-30 ms
Sensitivity / Efficiency	27000 cps/ppm Pb (50µm, 10Hz)

Data Processing

Gas blank	20 seconds on-peak
Calibration strategy	Moacyr monazite and GJ1 zircon used as primary reference materials, Manangoutry monazite and Plešovice zircon used as secondary reference material (quality control)
Reference Material info	Moacyr Monazite (Gasquet et al., 2010, Fletcher et al., 2010) GJ1 zircon (Jackson et al., 2004) Manangoutry monazite (Paquette and Tiepolo, 2007) Plešovice zircon (Sláma et al., 2008)
Data processing package used	Glitter ((Van Achterbergh et al., 2001)
Uncertainty level & propagation	Propagation is by quadratic addition according to Horstwood et al. (2003). Reproducibility and age uncertainty of reference material are propagated.
Quality control / Validation	Manangoutry: 557.5 ± 2.4 Ma (N=18, MSWD = 0.90) Plešovice: 337.8 ± 1.9 Ma (N=18, MSWD = 0.85)